U.PORTO

FEUP FACULDADE DE ENGENHARIA
UNIVERSIDADE DO PORTO

TREATMENT, PROCESSING AND INTERPRETATION OF GPR DATA ACQUIRED FROM THE ARCHAEOLOGICAL SITE OF CASTRO DE UL, NORTHERN PORTUGAL

DOUGLAS JOSTER NINJE

Dissertation submitted in partial fulfilment of the requirements for the degree of

MASTER IN MINING AND GEO-ENVIRONMENTAL ENGINEERING

Supervisor: Prof. Jorge Manuel Cabral Machado de Carvalho

President of the Jury: Prof. José Manuel Soutelo Soeiro de Carvalho

Examiner: Prof. Maria Manuela Martins De Carvalho

OCTOBER 2017

MASTER IN MINING AND GEO-ENVIRONMENTAL ENGINEERING 2016/2017

DEPARTMENT OF MINING ENGINEERING

Tel. +351 22 041 3163 / +351 22 041 31634

Edited by;

FACULDADE DE ENGENHARIA DA UNIVERSIDADE DO PORTO

Rua Dr. Roberto Frias

4200-465 Porto

Portugal

Tel. +351 22 508 1400

Fax +351 22 508 1440

Email feup@fe.up.pt

URL http://www.fe.up.pt

Our God reigns!

ACKNOWLEDGEMENTS

"Imagination is more important than knowledge. Knowledge is limited. Imagination encircles the world"

-Albert Einstein-

I would like to thank my supervisor Prof. Jorge Manuel Cabral Machado de Carvalho for guiding me throughout this research project, for his advice and corrections, which helped me in developing this work. Also to Mr. João Tiago Tavares for all the supporting documents and information provided about the study site, on-going projects and any related information deemed helpful for this work.

I would also like to thank all academic and support staff from the Mining Engineering Department, who, through their classroom and administration support, imparted in me with very vital knowledge in mining engineering, the knowledge that was so essential for the project and any other related works after. The works of these notable people will not only benefit me, but also Malawi will benefit from it together with my future prospective employers elsewhere.

Special thanks to the Erasmus Mundus through its DREAM Project, coordinated by the University of Porto for sponsoring and supporting all my studies, my friends: Andreas Salom, Simplício Roseiro and Rebbah Rania whom we worked as an African team tirelessly in the library, supporting and sharing knowledge in the field of mining.

Lastly, but not the least, a very big appreciation to my dear wife Lusungu for all her support and love throughout my study period.

OBRIGADO!

ABSTRACT

Castro de Ul, an archaeological site located in the municipality of Oliveira de Azeméis is considered to have been of military value as evidenced by the vestiges dating back to the early Roman settlers around 2000 A.C. The municipality has an on-going project of investigating the musealisation potential of the site. A Ground Penetrating Radar, GPR survey was conducted on the site in the year 2013 and this paper used the same data to map and interpret the anomalies as being possible archaeological remains. The main objective of this work was to organize, analyze, process and interpret the GPR profiles by integrating 2D radargrams into 3D blocks.

The acquired data was integrated, analysed and processed, with the help of videos and horizontal and vertical 2D slices to investigate the existence of anomalies from all orientations, employing knowledge to interpret these anomalies and evaluate if they would be potential archaeological remains. The analysis extended along adjacent blocks to test for the continuity of the anomalies detected. The work revealed the existence of some features that would be the walls of old buildings, and in most parts, the existence of rubbles from old buildings. This was evidenced by the two excavations made on the site, but still, more excavation would be suggested to ascertain the findings.

The work achieved the purpose despite the limitations incurred: not much data were acquired due to physical obstacles, and the data was not accompanied by GPS coordinates.

Key words: GPR, archaeology, Castro de UL, radargram, reflexW.

Table of Contents

LIST OF FIGURES

LIST OF TABLES

ABBREVIATIONS

2D: Two Dimension

3D: Three Dimension

A.C.: After Christ (Antes de Cristo)

CMP: Common Mid-Point

EDXRF: Energy Dispersive X-ray Fluorescence

EM wave: Electromagnetic wave

EMI: Electromagnetic Induction

ERT: Electrical Resistivity Tomography

FDEM: Frequency Domain Electro Magnetic

GPR: Ground Penetrating Radar

GPS: Global Positioning System

GSSI: Geophysical Survey System Inco

IR: Infra-Red

MHz: Mega Hertz

NRM: Natural Remanent Magnetization

SAR: Synthetic Aperture Radar

SEM-EDS: Scanning Electron Microscopy with Energy Dispersive Spectroscopy

SNR: Signal to Noise Ratio

TRM: Thermoremanent Magnetization

TWT: Two Way Time

WARR: Wide Angle Reflections and Refractions

XRD: X-ray Diffraction

XRF: X-ray Fluorescence

1

INTRODUCTION

"*We cannot teach people anything; we can only help them discover it within themselves.*"

Galileo Galilei

1.1. Background

Ground Penetrating Radar (GPR) is a non-invasive geophysical method which uses wide band non-sinusoidal electromagnetic waves and has a capability of producing high-resolution images to characterize a shallow subsurface target[1, 2]. Over recent years, characterization of shallow subsurface (0.25 to 10m) using GPR is becoming very useful in engineering, environmental and archeological investigations. GPR is an appropriate technique in archaeological investigations considering the range in depth of the interested targets, and again that the method is nondestructive, orienting archaeological excavations, thereby optimizing time and costs related to archeological surveys and excavations. GPR presents a high resolution and does not alter the surface of the archeological sites [3, 4].

GPR is applied in a variety of environments, including rock, soil, ice, freshwater, pavements, walls and so on. This makes the method to have a widespread application and use in civil engineering to detect subsurface objects, changes in material properties, and voids and cracks[5]. GPR is also used in geological studies, environmental contamination, geotechnical, sedimentology, hydrology, glaciology and biomonitoring. It has been widely applied in archeological studies to map the special extent of buried features. The application of GPR in archaeology is most suitable since it is non-invasive, thereby preventing destruction of essential archaeological evidence [1].

GPR maps the archeological features and changes in the soil, identifying the size, shape and depth, and location of the buried remains and related stratigraphy. This can be displayed in 2D

profiles with high resolution[6]. These 2D profiles can be correlated between each other throughout the grids to portray a better understanding of the spatial extent of the obtained target. It is still possible to arrange these into 3D volume blocks, which can be analyzed and visualized in many ways [1].

The study in this report is mainly focused on the treatment of data acquired on the archeological site of Castro de Ul in the municipality of Oliveira de Azeméis in the northern part of Portugal. The data used were acquired from the site in the year 2013 by a GPR equipment that used two antennas with center frequencies 270 MHz and 900 MHz depending on the target depths and resolutions. In an initial exploratory phase, the data acquired were processed using software Radan, by GSSI and the interpretation applied identified some targeted points as being possible features of buried remains of old structures. In this study, the same data was further and more consistently processed in an integrated way, using a different software, ReflexW by Sandmeier.

1.2. Study area

1.2.1. Location

Castro de Ul is an archaeological site located on a hilltop [7] near modern Oliveira de Azeméis, a Portuguese city in the district of Aveiro. The municipality of Oliveira de Azeméis is bordered with Arouca to the northeast, Vale de Cambra and Sever de Vouga to the east, to the south of the municipality is Albegaria-a-Velha, Estarreja to the southwest and Ovar to the west. *Figure A.1* in *Appendix A* is the map of Oliveira de Azeméis showing the location of Castro de Ul. It is well-known by the castros (hillforts) of Ul and Ossela which have vestiges dating back to early settlers in around 2000 a.c. [8].

1.2.2. Geology

The geology of Oliveira de Azeméis and that of the north of Portugal mainly comprises the granite and granodiorite gneiss. The general geology comprises the Arouca quartzdiorite which is an early late-tectonic granitoid and two other older alkaline granite; Freita and Arose [9].

Arouca quartzdiorite is normally formed in the initial stages of crystallization of tectonic granitoids and therefore is younger. Its composition is mainly calcosodic plagioclase, quarts and biotite. Freita and Aroes granites are composed of quartz, potassic feldspar, plagioclase with muscovite and biotite. *Figure 1.1* shows the schematic granitoids outcrops existing in Oliveira de Azeméis.

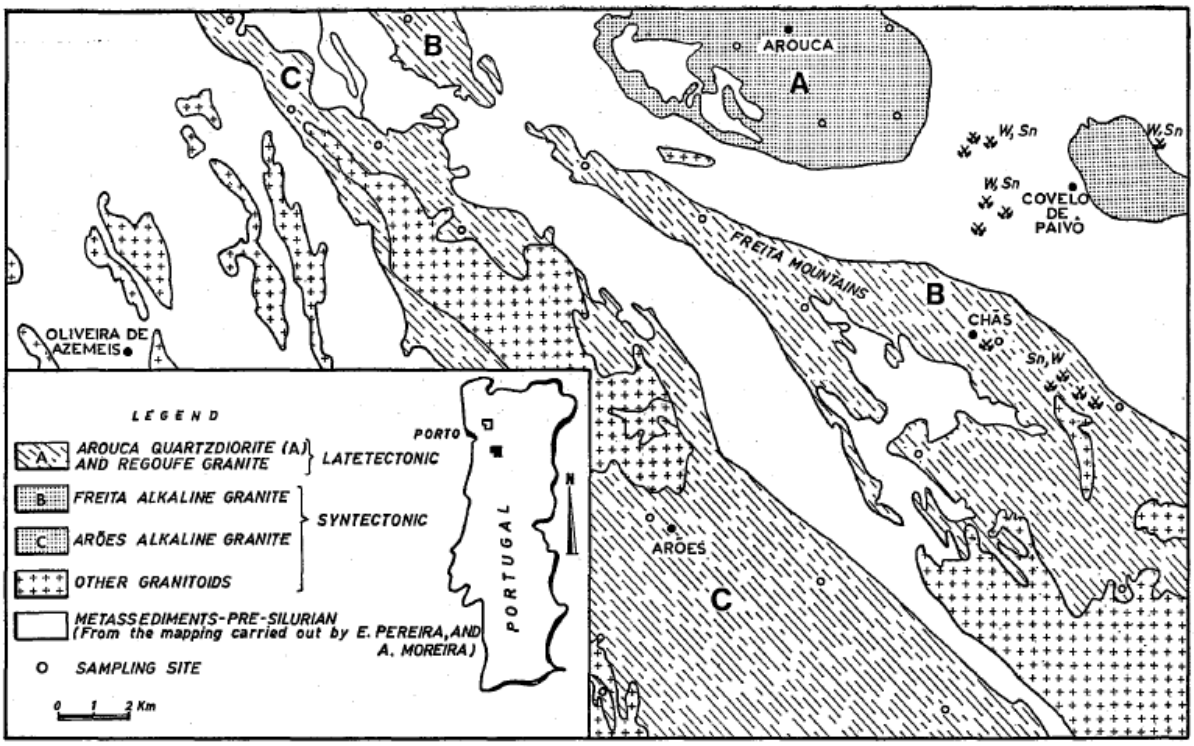

Figure 1. 1: General geology of the Oliveira de Azeméis area

Source: Santos and Pereira [9]

1.2.3. Heritage

Castro de Ul lies on a hilltop, bounded by two confluent rivers: the Ul to the west and the Antuã that flows to the southeast part of the hilltop. Ancient hilltops in the Iberian Peninsula are usually associated with the Roman and medieval defensive structures like watchtowers and small castles [7]. According to Azeméis no Passado [10], Castro de Ul lies on a top of a hill, 98m high and has some traces of an ancient fortress. The place is regarded to be of military value during the Roman time as is evidenced by the vestiges found on the site. Among the vestiges are the remnants of ceramics of Roman construction. This leads to a belief that the

origin of this place might be the Lusitanian fort, a flourishing oppidum at the arrival of the Romans.

De Man et al [7] report that the site has been settled for quite a long time starting from the Bronze Age, and now exists a small parish with many scattered houses and a church lying against and around the Northern slope towards the modern village and its connections to many water mills.

1.2.4. Archaeological history

The hilltop of Ul attracted attention of some 20th century historians with the first known excavation reported to be done in the years between 1941 and 1949 by a local priest [7]. A lot of pottery, glass, metals and millstones were assembled and stored in the church building and his residence. This assemblage was dispersed before 1980s.

Another project followed in the 1980s and identifies three occupation phases: the Chalcolithic and Bronze Age characterized by the recovery of silex pieces and polished stones; the Iron Age attested by indigenous pottery; and lastly the period linked to built structures which was characterized by Roman coins, coarse ware and glass. This last one was well defined whilst the previous were scattered elements in Roman layers and surface findings.

There have been other recent investigations that were led to excavating the site partly to ascertain the findings from the non-invasive surveys using GPR. These investigations were supported by the Universities of Porto and Aveiro. These works were mainly interested in the built structure which might be a narrow wall seemed to separate the area, but not yet confirmed. This survey detected many anomalies comprising several man-made structures [7].

Several works have been carried out on the site employing both physical and geochemical methods. In 2015 was conducted an Electromagnetic Induction survey and combined with the 2013 GPR survey which detected anomalies that would be linked to the early settlement of the site by the Romans [7].

1.3. Research objectives

The ongoing project that is taking place at Castro de Ul in the municipality of Oliveira de Azeméis aims at the assessment of the musealisation potential of the site. Several researches have been conducted along recent years employing various types of geophysical methods of site investigations and archaeological excavations.

The main objective of this research project was to prepare, analyze, integrate process and interpret the GPR data previously acquired from the archeological site, in order to identify promising targets for posterior excavations. The software ReflexW by Sandmeier Geophysical Research was used in analyzing and processing of raw data.

1.4. Project methodology

The methodology employed to the project in order to achieve the objectives stated above includes bibliographical research on similar works conducted in the archeological sites mainly in the Iberian Peninsula, data processing and interpretation using appropriate methods. The paragraphs below explain the works involved in each stage in brief.

Bibliographic research of previous works conducted on hillforts (castros) of the Iberian Peninsula using GPR and/or related methods applied for archeological studies was conducted. This involved the study using GPR as a geophysical method employed in archeological studies, how the method works and the review of previous works conducted in various archeological sites. Other studies include the study of the processing procedures and the use of specific computer applications to process and interpret data and findings.

Data treatment and processing: involved importing the field data acquired from the site in the year 2013. This data was used as input data in the processing using ReflexW software, a Sandmeier Geophysical Research product. The computer application ReflexW returns 2D processed radargrams and 3D blocks that map anomalies, which could be possible features of buried remains. The 2D profiles were integrated into 3D blocks in order to give a meaningful interpretation of the possibilities from the site.

Interpretation: This involved the critical analysis of the integration of the squares developed initially and the corresponding points of the model developed. The interpretations try to identify all the possible features related to buried archeological remains.

Conclusion and recommendations: the conclusion of the study was based on the results obtained from the interpretations. This suggested some recommendations to be done for further studies on the site.

1.5. Project structure

The dissertation is organized in the following way:

Chapter 1 is the introductory chapter. It introduces the work under study in general considering the application of GPR in archeological studies. It discusses the objectives of the project and the methodology employed in the development of the work.

Chapter 2 discusses the literature review. This includes previous researches on archeological studies conducted in the Iberian Peninsula. It discusses the successes developed from the different methods employed in the fieldwork and data processing.

Chapter 3 discusses the method of GPR in general and then specifically its applicability in archeological studies. The chapter explores the method, equipment and the general principle governing how it works. It also tackles the field procedures employed in data acquisition, data processing using different tools and interpretation of the results. Lastly, the chapter talks about the pitfalls encountered during data acquisition and interpretation.

Chapter 4 talks about the data collection procedures in the field. It tackles the directions to which data were collected, squares demarcated for the field work and the number of data collected in each square.

Chapter 5 discusses the detailed procedure in data treatment and processing. The treatment applied to the data during processing using ReflexW is clearly highlighted in this chapter. It also integrates the processed radar grams into 3D blocks ready for interpretation.

Chapter 6 discusses the interpretation of the processed profiles in both 2D, 3D and the integrated adjacent squares developed. It shows the anomalies identified and the possible interpretation.

Chapter 7 is the chapter of conclusion and recommendations. It draws the conclusion based on the results from the interpretations of the outcome of the work.

2

LITERATURE REVIEW

"*If I have seen further than others, it is by standing upon the shoulders of giants*."

Sir Isaac Newton

2.1. Introduction

It was traditionally regarded that aerial imaging was the best technique to be applied in the exploration of large areas until the 1980s when the first generation of geophysical survey instruments were introduced. These instruments became the best to be used for archaeological investigations[11]. Ever since, geophysical imaging techniques have been applied in the archeological investigations.

The techniques applied involve the imaging and mapping of archaeological objects without contact (non-invasive). This enables the archaeologists to explore large areas and have a wider understanding of the possible archaeological features. The information obtained allows the archaeologist to make the right decision on where to excavate thereby optimizing time, cost and resources [2, 3, 11]. These techniques are normally employed to estimate the distribution of cultural relics before digging. Results from the application of these geophysical methods provide useful qualitative and quantitative information of the form, size and orientation of specific features of investigated structures[12], hence increased effectiveness of excavations.

Geophysical methods such as ground penetrating radar, GPR have been applied in archaeological studies for the past 40 years [1] to map the spatial extent of buried cultural heritage. Cultural heritage must be preserved from any kind of destruction, therefore,

penetrating investigation tools such as boreholes should be avoided, or their impact be reduced to the minimum [13, 14]; they might destroy essential archaeological evidence [15-17].

GPR finds itself in a wide range of applications over the past 20 years. Its applications include sedimentology, groundwater contamination, glaciology, archaeology, civil and geotechnical engineering, geological exploration, forensic, demining and many more[18].

2.2. Geophysical methods applied in Archaeological investigations

Since 1946, various geophysical methods have been applied in archaeological investigations[19]. The most common amongst these several geophysical methods include electrical resistivity, magnetic and electromagnetic methods namely ground probing radar.

Historically, aerial photographs were employed in the prospection of archaeological sites since the end of First World War, and in the middle of 1940's, many geophysical methods began to be employed. The initial efforts were focused on the application of resistivity method followed later in the 1980s with the high resolution magnetic methods, geo-radar and infra-red imagery. The vast growth of the methods employed in archaeological investigations is attributable to its extremely rapid[20] and possibility of integrating the results into 3D volume blocks which helps in the clear visualization of the study site [21].

2.2.1. Resistivity

The electrical resistivity method is the active geophysical method that measures the apparent resistivity of soil. The method is based on the variation of electric resistivity of the soil, the sediment and the rock[22]. It is widely applied in archaeological investigations since the variations in resistivity due to buried archaeological features gives precise and geometrically consistent maps of these features[20].

Electrical Resistivity Tomography (ERT) is a form of electrical resistivity which comprises a multiple of electrodes in a line to generate a single section of the properties of the soil[11]. The method increases the resolution of soundings and is fast since it has several channels that allow

simultaneous measurements of potential difference from several detector lines[23]. The ERT profiles can be combined to generate a 3D model of earth resistivity.

2.2.2. Magnetometry

This method measures the local variation of the earth's magnetic field in order to describe the subsoil of an area[11]. The measure of this variation is based on the enrichment of the magnetic materials or the Natural Remanent (NRM) and Thermo Remanent (TRM) magnetization of the soil and archaeological features [22].

The principle behind the method is the inhomogeneity of the magnetic properties of the features under study. The geological structure of the earth contains iron materials, these attribute different magnetic behaviors in the subsoil as they can be magnetized either by natural or human factors. In archaeology, the magnetic anomalies created by alteration of a sedimentary structure or by an intruding object used in the construction of a buried structure can be detected and measured. This totally depends on the contrast between the magnetic behavior of the intruding feature and that of the medium.

The method is cheap, and therefore, finds itself widely employed in archaeological prospection [22].

2.2.3. Ground Penetrating Radar

This is an electromagnetic method of surveying that transmits electromagnetic signal into the ground by the emitting antenna. The signal is reflected by the propagation media and recorded by the receiving antenna. The readings of the amplitude values, taken in time lapses in different positions are recorded and stored in the GPR. Knowing the velocity of the pulses, it is possible to compute the depth of the object under target at a recorded time [11].

The results of GPR measurements are presented in radargrams, which represent the direction of antenna motion in the horizontal axis and that of the increase in time in the vertical axis. This can be converted into depth. The radagram files can be integrated to each other to form a 3D volume block that can be examined in three axes. This integration is a powerful tool to

explain the results in archaeological investigations since it represents buried structures in a way archaeologist express their work. Much about this method is fully explained in the next chapter.

2.2.4. Electromagnetic Induction (EMI)

Electromagnetic Induction methods are a family of geophysical methods that are based on the inducing of the magnetic fields by a coil into the ground and then measure the ground's response by the receiving coil. The induced magnetic field generates electric currents into the ground objects in varying intensity depending on the electric properties. These are measured by the receiver and give an apparent conductivity which can later be interpreted as possible features of buried archaeological remains [11].

EMI is widely applied in archaeological investigation because it is fast and has a capability to survey a large area. The apparent conductivity maps can give relevant information of buried remains of archaeological structures. However, due to the complexity in data interpretation, other methods of geophysical prospection are preferred.

2.3. Review of archaeological researches in the Iberian Peninsula

Various investigations involving archaeological studies have been conducted in the southwestern part of Europe referred to as the Iberian Peninsula, employing different techniques for different purposes. Archaeological investigations have been conducted to identify and characterize ancient settlement types [24-26], environmental and landscape evolution [27-29], and in archaeological prospection [30, 31] and discovery[32]. In all these, various methods ranging from geophysical prospecting methods to geochemical laboratory methods.

2.3.1. Archaeological investigations of the ancient settlements

Investigations were conducted to determine the ancient settlements; their types and patterns. Vaz et al [24] studied the wood remains found in the ovens and hearths of the iron age period at the hilltop of Quinta de Crestelos, Sabor Valley, North-East of Portugal. The aim of this investigation was to identify the main firewood species so that they can define the patterns of the fuel used. This would help them identify the characterization of the people living in this area and their settlement pattern. In another scenario, over 100 samples of storage structures were collected from As Laias (a hilltop), and analyzed in the laboratory using stereoscope microscope to study the archaeobotanical materials[26]. The results revealed the existing of the cereal remains in the storage facilities. This from the archaeologist point of view might be a possibility of a communal settlement. However, the interpretation of the As Laias together with other sites with storage areas in the Iberia might give a misinformed understanding of the social and economic practices of the Iron Age inhabitants within the peninsula.

Other laboratory methods such as optical microscopy, micro-EDXRF, SEM-EDS and XRD were employed on the artefact fragments collected from Late Bronze Age habitat site of Castro da Senhora da Guia de Baiões[25]. Results from this work proved that the iron smelting and recycling was the most common activity in the site. This supported the earlier suggestion to explore the Western Iberian tin resources during this Late Bronze Age period.

2.3.2. Environmental transformation and landscape evolution

Climatic and anthropogenic factors have caused a wide spread environmental and landscape changes as per documented in the Iberian Peninsula between the third and second millennia BC[28]. These factors might have included erosion, deforestation and valley infilling. 29 samples of ovicaprid mandibles and maxillae from an archaeological site of Zambujal in Torres Vedras, Portugal were analyzed in the laboratory using stable isotope analysis. The method was chosen because of its ability to provide a record of dietary pattern from historic humans and animals. This helps archaeologists to interpret the climatic, environmental and cultural practices in the past populations. Results from the 29 samples indicated a significant change

and therefore suggests the impacts of environmental and cultural changes related to animal husbandry in Portugal.

In the Alto Ribatejo, artefacts and regolith from passage tombs, pitfalls, stone scatter and clay structures were analyzed using optically simulated luminescence, neutral activation analysis and XRD [29]. The results revealed different phases in landscape formation and stability from late 6 millennia to the Roman conquest. Chester[27] suggested a chronological framework for Pleistocene and Holocene geomorphology and landscape evolution in Algarve.

2.3.3. Geophysical prospection and discoveries

Various geophysical methods have been applied in the investigations and interpretations of archaeological sites. In some cases, the works results in significant historic discoveries. It is estimated that several people died during and after the Spanish civil war between 1936 and 1939. A GPR survey was conducted in the mountainous terrain in the Asturias region of Northern Spain [32] in search for an unmarked mass grave during the war. The results from the survey indicated some clear geophysical anomalies on 2D radagrams. A further intrusive forensic archaeological investigation revealed the existing of human remains. Arias et al [30] applied geophysical survey methods to Mesolithic sites of Sado valley in southern Portugal. These surveys resulted in the production of magnetic gradiometry maps, which showed targeted points for excavations. The excavations confirmed the results from the geophysical surveys, and ascertain the methods as being efficient tools for delimitation of the sites and identification of Mesolithic and Neolithic structures.

Ranieri et al [31] integrated several geophysical methods to interpret the archaeological findings at the Roman city of Pollentia, in the Island of Mallorca in Spain. They applied magnetic survey, Electromagnetic (FDEM), ERT, GPR and 3D virtual visualization methods. The integrating of the methods helps confirming the anomalies identified and the 3D visualization provides promising results for the excavation targets.

2.4. Conclusion

GPR as a geophysical method has been applied in several areas ranging from archaeology, environmental and landscape evolution, prospection and discoveries. The method, together with other methods such as geochemical and archeobotanical methods have been employed to study the archaeological remains in the Iberian Peninsula and several other methods accompanied by excavation confirmed the results obtained.

3

GROUND PENETRATING RADAR

'Never give up. I invented algebra and the laws of electricity, and never learned how to count to 100.'

Carl Friedrich Gauss

3.1. Introduction

Ground Penetrating Radar (GPR), ground-probing radar, sub-surface radar or surface penetrating radar [33] as others may call it refers to a range of electromagnetic methods with high resolution frequency band ranging between 10 MHz-2600 MHz [34], that has a capability to locate features or interfaces either buried beneath the earth's surface or lying within visually opaque structures.

Signals of short wavelengths are emitted and propagated into the ground to detect the anomalous variations in the dielectric properties of the targeted material. The basic principle behind GPR system is that it measures energy reflected or scattered from the targeted features; the amplitudes are recorded as functions of travel time [34]. The application, and design principles of GPR depend on the target features under investigations and its environment [33]. It has wide applications in geotechnical engineering [35-37], geology[38], environmental [28, 39], construction [2, 5, 38, 40], archaeology [6, 21, 41-47] and several more areas as will be discussed in the next sub-chapter.

3.2. Applications of Ground Penetrating Radar

GPR is applied in almost every type of engineering and geotechnical problems [48]. From locating small voids [5, 49] and reinforcing bars [38, 50] in foundations and walls [51],

determining deep geologic features, buried archaeological features [6, 42] and many more. The following paragraphs describe brief applications of GPR in archaeology, civil engineering, forensic applications, geophysics, mine detection, utilities and remote sensing.

3.2.1. Archaeology

GPR is one of the most useful geophysical methods used to estimate the distribution of cultural relics in a site before a strategic excavation is implemented. The method provides qualitative and quantitative information of the form, size, shape, depth and spatial orientation of buried features [12]. The application of GPR in archaeological investigations helps to optimize time and cost[3] as it directs to the strategic points of targeted anomalies for future excavation. It is also possible to integrate the 2D profiles into 3D volume blocks, which can easily identify anomalies for further investigations [16, 44, 52, 53].

3.2.2. Engineering applications

GPR is applied in several engineering problems. Grandjean [54] performed different tests using different GPR techniques on a site characterized by underground heterogeneities such as pipes, small voids and so on to ascertain the performance and reliability of the method when applied in civil engineering problems. The work consisted on the measurement with monostatic and bistatic antennas above various buried heterogeneities and performing different processing technics such as 2D and 3D migration, velocity analysis and some numerical simulations. The results proved a need for further testing such as geotechnical or laboratory testing to confirm the findings.

GPR has also been employed in concrete works [55, 56] to determine the depth-amplitude effects in concrete bridge deck and to characterize and monitor water ingress during absorption in concrete curing. It has also been applied in railway ballast [57] and in pavement investigations to map and characterize different pavement layers, thickness and pavement conditions [58]. In the ballast investigation, GPR was employed to assess the railway ballast, which was progressively polluted with a fine-grained silty soil material.

GPR can also be applied in hydrogeology. In Arboz province in Iran, GPR survey was conducted in the developing residential area to identify the depth of ground water table and the probable cavities. This was necessary for the design of foundations for the construction of buildings on the site. The survey detected the presence of water table at 12 m and no occurrence of cavities. This helped the engineers to concentrate on remediating water flows and not wasting time and efforts on the cavity fillings on the site [59].

It was also applied to identify small-scale fractures of a waste disposal in a tunnel. The GPR 3D visualization helped to reconstruct the spatial distribution and interconnectivity within the tunnel walls[60]. Benedetto [61] and Lopez [62] applied GPR in tunneling and road pavement inspection and detected the major causes of structural failure at traffic speed.

In geotechnics, it can be used to evaluate the quality of soil consolidation [63] and soil formation lithology [64]. Cui [63] characterized the distribution of sandy loam soils with varying values of compactness and different moisture content using GPR surveys. Integrated geophysical methods, including GPR were used to characterize and reconstruct the internal structure and longtime evolution of hazardous sinkholes in Fluvia, North East of Spain [65].

In dense urban areas, it is necessary to map the subsurface utility facilities such as electric and telephone cables, water and gas pipes, sewage pipes and any other infrastructures. The subsurface utility survey is very important prior to excavation particularly in urban sites where the misdetection of any of the utilities may be hazardous [40]. A GPR survey with 200MHz antennae was done in the city of São Paulo, Brazil to map the utilities or existing infrastructures in the subsurface in order to orient the construction of the Line 4 (yellow line) subway tunnel [66]. The survey produced the utility placements, which was used as a basis for planning for the geotechnical excavation of the line, thereby minimizing problems that would rise if the preexisting utility facilities in the subsurface were damaged.

GPR and Infrared photography (IR) were applied in the city of Doha in Qatar to detect water leakages in the city. 23 GPR and 115 IR images were acquired for this purpose. The GPR was used to locate the buried pipes and the IR was for the simulation of the leakages. The methods proved to be efficient and accurate in the detection of the simulated and actual leakages with small margin of error of 2.9-5.6% [67]. The method is reliable and can help city engineers to detect and locate water leaks with accuracy.

3.2.3. Forensic applications

GPR was applied in the searching of the unmarked and clandestine graves [68-70]. GPR proved to be the best method amongst several geophysical methods as it is not labor intensive and time consuming unlike the actual work might be when involving excavations [68]. However, the interpretation might lead to incorrect information. Fiedler [71] recommended confirmation with other methods such as tachymetric and botanic surveys. The GPR survey was conducted in separate Viking age and Medieval churchyards to map the skeletal remains in Northern Iceland [72].

Salsarola [73] experimented the application of GPR by burying 11 pig carcasses in a wooded area for a period ranging 2 to 111 weeks and employed the survey to identify the anomalies and exhumed the remains. The method proved useful but weaker with time.

3.2.4. Mine detection

GPR is also widely used in mine detection. Landmine is an explosive buried in the ground purposely to explode when a person or vehicle passes over [74]. GPR is a powerful and non-destructive geophysical approach with a wide range of advantages in landmine inspection. The GPR images [75] integrated with the other global positioning devices such as GPS [76] helps in the improvement of the accuracy of the buried-object location. This makes the method a suitable one in mine detection. Khan et al [75], introduced a cepstral approach for the detection of landmines. The approach involved the extraction of cepstral features from the GPR images and transforming them into a 1D signal. The experimental results confirmed the landmine detection from the GPR images at low as well as high signal to noise ratio (SNRs).

Synthetic GPR method was successfully employed for buried landmine classification. 1D temporal signatures were employed as reference waveforms for efficient clutter suppression [77]. This improved the target detection. The classification helped to substantially reduce the number of false alarms and speed up clearance labor.

3.2.5. Remote sensing

GPR techniques are used in remote sensing to penetrate the vegetation and dry soil of the earth. Airborne GPR, processed using synthetic aperture techniques has been used to detect buried metallic mines from a height of several hundred meters in synthetic aperture radar (SAR) mode [33]. Remote sensing involves the collection of raw data by a sensor (without direct contact) such as a Ground Penetrating Radar (GPR) and inverting it to form an image of the subsurface area [78].

3.3. Why GPR is suitably applied in archaeological investigation?

GPR is a very powerful tool in geophysical exploration due to its high resolution imaging [6] and ability to map the size, shape and orientation [3, 4] of the targeted features in 2D images which can be integrated into 3D for easy visual analysis. This makes the method to be widely recommended in archaeological studies. It is non-invasive [1, 2] and non-destructive [6] thereby avoid to destroy the archaeological evidence [1].

GPR has a capability to take images at a depth range of 0.25 to 10 meters where most of the archaeological remains lie and can provide the qualitative and quantitative information of the form, size and orientation of specific features of investigated structures [12].

The work of archaeological investigations would be more hectic and exorbitant with more labor and time [2, 3]. It would involve actual excavations in the field of research. The use of GPR helps the researchers to identify points of interesting anomalies without excavations, and a proper plan for excavations can be made and this makes it time and cost efficient [11].

3.4. Basic principles of GPR

Ground Penetrating Radar uses the electromagnetic signals to probe lossy dielectric materials below the earth surface and detect the changes in material properties within them. The technique employs propagating, reflecting and receiving of the signal from the antennae to the ground and back into the antennae. Its applications are to both the natural geological materials

and man-made composite materials such as concrete, asphalt and other construction materials [79].

3.4.1. The GPR System

The GPR system briefly comprises the antennas (transmitter and receiver) connected to a control unit and a signal display with a recording system [80]. *Figure 3.1* shows a schematic illustration of the GPR system. The transmitting antennae emits an electromagnetic wave field into the ground and the receiving antennae records this field and its reflections from the ground [4]. The control unit generates the pulse radar energy that are propagated into the subsurface through the antennae. It basically comprises the power source which can be an internal rechargeable or external battery, the built-in computer with a storage device and a display [81].

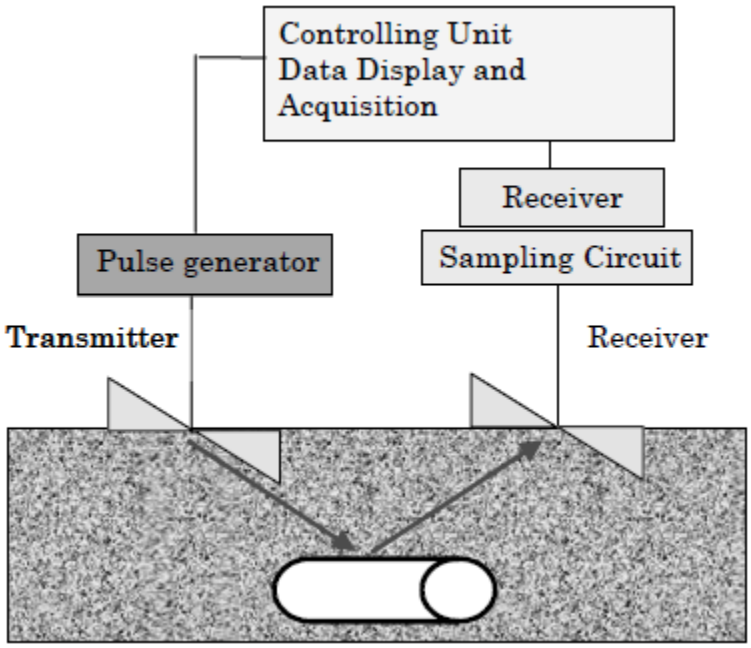

Figure 3. 1: A schematic diagram of a GPR system

Source: Sato, M, 2009

3.4.2. Wave propagation in the soil

GPR uses electromagnetic waves in its measurements. The transmitting antennae propagates the wave into the ground. As the wave strikes the structure, it is reflected from the subsurface. The receiving antennae measures this reflected wave [80].

The acquired GPR data are provided in a 2D profile comprising the horizontal survey distance against the vertical two-way-time (TWT). The travel time, commonly referred to as the TWT is defined as the time taken between transmission and reception [82]. The TWT is converted into depth if the velocity of propagation is known. The depth is expressed as in equation 3.1:

$$d = \frac{v\tau}{2} \tag{3.1}$$

Where: v is the velocity of propagation (m/s)

τ is the TWT measured in nanoseconds (ns)

The velocity v and reflectivity of the wave signal is characterized by the dielectric constant, also called relative permittivity. The wave velocity is given by:

$$v = \frac{c}{\sqrt{\varepsilon_r}} = \frac{3x10^8}{\sqrt{\varepsilon_r}} \tag{3.2}$$

Where: c is the speed of light (300mm/ns) and

ε_r is the relative dielectric constant.

The electromagnetic wave propagation through a media is affected by several material properties. Some of these are the dielectric constant and the electrical conductivity. Dielectric constant or dielectric permittivity is a property that strongly depends on the water content of the material. *Figure 3.2* shows the relationship between the dielectric constant of soil and its water content. the dielectric constant of rock and soil materials in dry conditions lies between 3 and 5 [80]. On another hand, electrical conductivity is the measure of charge transport through a medium when an electric field passes through it [82]. *Table 3.1* shows the typical dielectric constant, electrical conductivity, velocity and attenuation encountered using GPR.

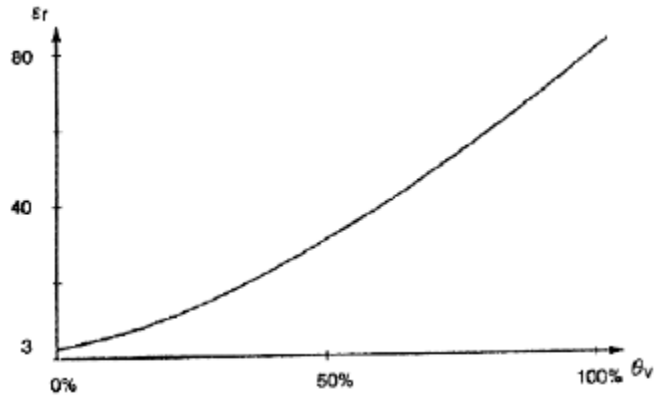

Figure 3. 2: The typical relationship between permittivity and water content of soil

Source: Sato, 2009

Table 3. 1: Typical dielectric constant, electrical conductivity, velocity and attenuation observed in common geologic materials

Material	**Dielectric constant (K)**	**Electrical conductivity, σ (mS/m)**	**Velocity, *v* (m/ns)**	**Attenuation, *a* (dB/m)**
Air	1	0	0.3	0
Distilled water	80	0.01	0.033	$2x10^{-3}$
Fresh water	80	0.5	0.033	0.1
Sea water	80	$3x10^{3}$	0.1	103
Dry sand	3-5	0.01	0.15	0.01
Saturated sand	20-30	0.1-1.0	0.06	0.03-0.3
Limestone	4-8	0.5-2	0.12	0.4-1
Shales	5-15	1-100	0.09	1-100
Silts	5-30	1-100	0.07	1-100
Clays	5-40	2-1000	0.06	1-300
Granite	4-6	0.01-1	0.13	0.01-1
Dry salt	5-6	0.01-1	0.13	0.01-1
Ice	3-4	0.01	0.16	0.01

Source: Annan, 2003

3.4.3. Electromagnetic theory

The operating theory of GPR is founded on the electromagnetic theory. As stated earlier, GPR uses the electromagnetic signals to map the materials property change of the subsurface features. The electromagnetic theory is described by the Maxwell's equations. Maxwell's equations mathematically describe the electromagnetic physics and the their constitutive relationships [83].

3.4.4. Maxwell's equations

Mathematically, electromagnetic fields are expressed in the following terms:

a) $\overline{\nabla} \times \overline{\mathrm{H}} = \overline{J} + \frac{\delta \overline{D}}{\delta t}$ (Ampere's law) 3.3

b) $\overline{\nabla} \times \overline{\mathrm{E}} = -\frac{\delta \overline{\mathrm{B}}}{\delta t}$ (Faraday's law) 3.4

c) $\overline{\nabla} \bullet \overline{D} = q$ (Gauss's law for electric field) 3.5

d) $\overline{\nabla} \bullet \overline{\mathrm{B}} = 0$ (Gauss's law for magnetic field) 3.6

Where:

- $\overline{D}$ is an electric displacement vector (C/m^2)
- $\overline{\mathrm{E}}$ is an electric field strength vector (V/m)
- $\overline{\mathrm{B}}$ is the magnetic flux density vector (T or $V.s/m^2$)
- $\overline{\mathrm{H}}$ is the magnetic field intensity (A/m)
- q is the electric charge density (C/m^3)
- $\overline{J}$ is an electric current density vector (A/m^2)

Equation 3.3 is the Ampere's law, which states that the flow of electric current generates magnetic fields. Faraday's law is illustrated in equation 3.4 describing that a time varying magnetic field generates a closed loop electric field. The Gauss' law of electric field, summarized in equation 3.5 indicates the observation that electric displacement starts and ends on an electric charge. Lastly, the Gauss' observation of magnetic field as summarized in equation 3.6 indicates that when induction occurs, time varying electric fields are in a closed loop form thereby generating a closed loop magnetic flux.

From the Maxwell's equations, it is observed that the charge and current densities q, $\overline{J}$ maybe thought of sources of electromagnetic fields. In EM wave propagation, these are radiated from

space and flow in antenna. They are propagated through large distances to the receiving antenna, forming a closed loop.

3.4.5. Constitutive relations

Annan [83] defines the constitutive relationships as a way of quantifying the physical properties of materials in GPR survey. The equations involved provide a macroscopic description of how electrons, atoms, molecules and ions responds to the application of the magnetic fields. The most important properties in GPR are conductivity, permittivity and permeability.

a) Electrical conductivity $\bar{\sigma}$

This is a measure of charge flow through a medium when an electric field passes through it [80]. It is expressed as:

$$\bar{J} = \sigma \bar{\mathrm{E}} \tag{3.7}$$

Electric conductivity is measured in milliSiemens per meter (mS/m)

b) Dielectric permittivity $\bar{\varepsilon}$

Dielectric permittivity describes the response of constrained charges to an application of electric field. It is measured in farad per meter.

$$\bar{D} = \varepsilon \bar{\mathrm{E}} \tag{3.8}$$

c) Magnetic permeability $\bar{\mu}$

This describes how intrinsic atomic and molecular magnetic moments changes to magnetic fields. It is measured in henry per metre.

$$\bar{\mathrm{B}} = \mu \bar{\mathrm{H}} \tag{3.9}$$

In vacuum, permittivity and permeability takes the form ε_0 and μ_0. They bears the numerical values of $\varepsilon_0 = 8.854x10^{-12}$ farad/m and $\mu_0 = 4\pi x10^{-7}$ henry/m. from these two, the velocity of light, C_0 and characteristic impendence η_0 can be deduced:

$$C_0 = \frac{1}{\sqrt{\mu_0 \varepsilon_0}} = 3x10^8 \text{ m/sec} \quad 3.10$$

$$\eta_0 = \sqrt{\frac{\eta_0}{\varepsilon_0}} = 377\Omega \quad 3.11$$

3.4.6. EM wave equation and its wave nature

As seen from the Maxwell's equations [83], a coupled set of electric and magnetic fields act in a symbiotic manner when the fields vary with time. A change in electric fields creates a magnetic field, which in turn induces electric fields. This symbiotic relationship results in the fields, which move through a medium. The fields may diffuse or propagate as waves. GPR is more interested in the wave propagation not diffusion.

Mathematically, the exploration of the wave nature is seen by rewriting the Maxwell's equations, eliminating either electric or magnetic fields. From equation 3.4, Faraday's law can be written as:

$$\overline{\nabla} x \overline{\nabla} x \overline{\mathrm{E}} = -\frac{\delta}{\delta t}(\overline{\nabla} x \mu \overline{\mathrm{H}}) \quad 3.12$$

Note that $\overline{\mathrm{B}}$ has been substituted using $\overline{\mathrm{B}} = \mu \overline{\mathrm{H}}$ (equation 3.9). Substituting the Ampere's law (equation 3.3) and its constitutive equation 3.7, equation 3.12 becomes:

$$\overline{\nabla} x \overline{\nabla} x \overline{\mathrm{E}} = -\mu \frac{\delta}{\delta t}(\overline{J} + \frac{\delta \overline{D}}{\delta t}) = -\mu\sigma \frac{\delta \overline{\mathrm{E}}}{\delta t} - \mu\varepsilon \frac{\delta^2 \overline{\mathrm{E}}}{\delta t^2} \quad 3.13$$

Rearranging, it becomes:

$$\overline{\nabla} x \overline{\nabla} x \overline{\mathrm{E}} + \mu\sigma \frac{\delta \overline{\mathrm{E}}}{\delta t} + \mu\varepsilon \frac{\delta^2 \overline{\mathrm{E}}}{\delta t^2} = 0 \quad 3.14$$

The equation 3.14 is termed as the transverse vector wave equation [83]. Note that in the formulation of the equation, we eliminated the magnetic fields, if we chose to eliminate the electric fields; the procedure would just be the same and we get the expression with H instead of E.

In order to characterize the transverse wave equation, it is necessary to consider its basic solution form, which considers the vector orientation of the field. The electric or magnetic field vector varies in a spatial direction perpendicular to the field vector. Introducing the vector character and spatial or temporal variation $f(\beta,t)$, the fields will satisfy equation:

$$\frac{\delta^2}{\delta\beta^2} f(\beta,t) - \mu\sigma \frac{\delta}{\delta t} f(\beta,t) - \mu\varepsilon \frac{\delta^2}{\delta t^2} f(\beta,t) \equiv 0 \qquad 3.15$$

Assuming there are no losses ($\sigma \equiv 0$), equation 3.15 reduces to:

$$\frac{\delta^2}{\delta\beta^2} f(\beta,t) = \mu\varepsilon \frac{\delta^2}{\delta t^2} f(\beta,t) \qquad 3.16$$

Which has a solution of the form:

$$f(\beta,t) = f(\beta \pm vt) \qquad 3.17$$

Where v is the wave velocity $\qquad v = \frac{1}{\sqrt{\varepsilon\mu}} \qquad 3.18$

The spatial distribution of the fields translates in the direction β between observation times. *Figure 3.3* illustrates this fact. This fact defines the wave nature of the field.

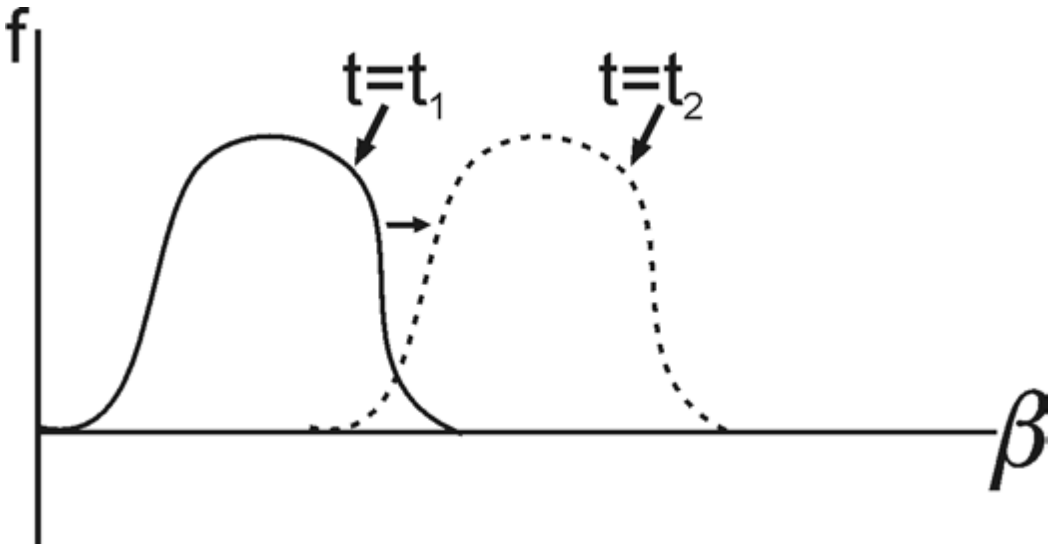

Figure 3. 3: A function of the form $f(\beta \pm vt)$ *representing an event moving at velocity* v *in the direction* β

Source: Annan, 2003

3.5. Survey design

It is very important to make a proper plan and design for the GPR field survey. It is necessary to optimize data acquisition in the field so that the expected results are met after data organization and processing [83]. It is always necessary to define several parameters when designing a field survey. These may include the radar frequency, time window, temporal sampling and sampling interval [82].

3.5.1. Suitability of GPR

Before any survey, it is very important to establish if the method will be effective and feasible[2], otherwise the whole survey work will be a waste of time and money. The environment under investigation needs to be examined for some obstructions, which might affect the results of the survey. For instance, metallic objects and major structural features may seriously affect the results [82]. The following factors were highlighted by Robinson et al [82] as to be considered when examining the suitability of GPR:

- The depth of the target must be within the depth range of the GPR system. If the target depth were higher than the range of the GPR system, then the survey work would not yield anything as to the expectations of the work.
- The target must exhibit electrical properties (dielectric constant and electrical conductivity) which varies with the host subsurface.

It must be noted that with the exhibition of electric properties, the strength of EM reflection is proportional to the magnitude of variation (contrast). The reflected energy is given by reflection coefficient (R).

$$R = \frac{\sqrt{v_2} - \sqrt{v_1}}{\sqrt{v_2} + \sqrt{v_1}} \tag{3.19}$$

Where v_1 and v_2 are the velocities of layer 1 and layer 2, the target and the host subsurface. In all cases, R ranges from +1 and -1 with values further from zero representing greater differences in electrical properties.

3.5.2. Choice of antennae frequency

The choice of antennae frequency determines the resolution and depth of penetration. Low frequency waves penetrate deeper than the high ones because they do not suffer much attenuation as compared to the latter. However, resolution deteriorates with lower frequencies [82]. The selection of an optimum antennae frequency involves a trade-off between the spatial resolution, depth of penetration and system portability. As a rule of thumb, it is better to trade-off resolution for penetration, with high resolution being useless if the target cannot be detected [83].

There are three factors basically considered when selecting the antennae frequency. These are:

1) Spatial resolution
2) Clutter limitation and
3) Penetration depth

Each of the factors yield a constraint on frequency.

Considering the spatial resolution required, and assuming a centre frequency to bandwidth ratio of 1, the constraint of centre frequency, f_c takes the form:

$$f_c^R > \frac{75}{\Delta z\sqrt{K}}\,\text{MHz} \qquad 3.20$$

Where Δz is the spatial separation to be resolved in meters and K is the dielectric constant (relative permittivity).

Clutter refers to the radar signal that is returned from material heterogeneity [83]. The radar response increases with frequency increase, likewise clutter increases with frequency increase. The amount of energy scattered by clutter must be minimized in order to see though the depth. The clutter center frequency constraint takes the form of:

$$f_c^C < \frac{30}{\Delta L\sqrt{K}}\,\text{MHz} \qquad 3.21$$

Where, ΔL is the clutter dimension.

Lastly, the depth of penetration frequency requires that the target cross-section occupy a major part of radar beam. This allows sufficient energy to be reflected for detection. The target dimension should also be close to the size of the Fresnel zone so that the reflected signal should arrive and be detected in the receiver antennae. This frequency constraint takes the form:

$$f_c^D < \frac{v\beta\sqrt{K-1}}{D} \qquad 3.22$$

Where β is the radar beam footprint to target size ratio and D is the depth in meters. In GPR surveys, β can be assumed to be 4, yielding to:

$$f_c^D < \frac{1200\sqrt{K-1}}{D}\,\text{MHz} \qquad 3.23$$

At the end of the computation of the frequency constraints, it should be noted that

$$f_c^R < f_c < \min(f_{cD}, f_c^C) \qquad 3.24$$

If it happens that the resolution frequency is greater than the other two, then the desired spatial resolution is incompatible with the clutter dimension or the depth penetration.

Table 3.2 gives a quick guide to frequency selection. The data is based on the assumption that the spatial resolution required is about 25% of the target depth.

Table 3. 2: Antennae frequency as a function of penetration depth

Depth (m)	Centre Frequency (MHz)
0.5	1000
1.0	500
2.0	200
7.0	100
10.0	50
30.0	25
50.0	10

Source: Annan, 2003

3.5.3. Estimating the time window

The time window is estimated by the following expression:

$$W = 1.3\frac{2xDepth}{Velocity} \qquad 3.25$$

With the maximum depth and minimum velocity likely to be observed in the field work being used. The equation accounts for uncertainty in both depth and velocity variations by increasing the estimated time by 30% [83],[82]. In the absence of information about the electrical properties of the survey area, *Table 3.3* can be used as a guide to this data.

Table 3. 3: Time windows

Depth (m)	Rock	Wet soil	Dry soil
0.5	12	24	10
1	25	50	20
2	50	100	40
5	120	250	100
10	250	500	200
20	500	1000	400
50	1250	2500	1000
100	2500	5000	2000

Source: Annan, 2003

3.5.4. Selecting temporal sampling interval

In radar data acquisition, it is also necessary to design the time interval between points on a recorded waveform [82]. The sampling rate should be approximately six times the centre frequency of the antennae being used and is expressed by equation 3.26.

$$t = \frac{1000}{6f} \tag{3.26}$$

Where t is the maximum sampling interval measured in nanoseconds (ns) and f is the antennae frequency being used. *Table 3.4* shows the suitable sampling intervals against operating frequencies based on the assumption that centre frequency to bandwidth ratio is 2. The sampling frequency is controlled by the Nyquist principle, which recommends sampling at most half the period of the highest frequency signal recorded [82-84]. The problem of using small sample values is that random signals (noise) are given more influence on the trace. Increasing antennae frequency requires increasing sampling rate due to preferential attenuation of high frequencies. Jol et al [84] prefers sampling at quarter the wavelength, where it is anticipated to get the greatest vertical resolution.

Table 3. 4: Sampling intervals corresponding to antennae frequencies

Antenna Centre Frequency (MHz)	Maximum Sampling Interval (ns)
10	16.70
20	8.30
50	3.30
100	1.67
200	0.83
500	0.33
1000	0.17

Source: Annan, 2003

3.5.5. Selecting line spacing (spatial sampling interval)

This is the spacing between the sampling lines. It is usually a compromise between the amount of details required and the extent of the survey area [82]. It is recommended to have the line spacing at quarter the wavelength in the host material. This is governed by Nyquist sampling principle expressed as:

$$\Delta x = \frac{c}{4f\sqrt{K}} = \frac{75}{f\sqrt{K}} \text{(m)} \qquad 3.27$$

Where f is the antennae centre frequency (MHz) and K is the relative permittivity of the host subsurface. The line spacing should be less than the Nyquist sampling spacing to adequately define steeply dipping reflectors or diffraction tails.

3.5.6. Selecting antenna separation

Most GPR systems are bistatic operation; whereby the system has two separate antennae; one for transmitting and another one for receiving the waves. The separation between the antennas can be fixed or varied [82-84]. The ability to vary antenna spacing is a powerful tool to optimize the system for specific target detection. It is recommended to keep this spacing as small as possible depending on the needs of the survey and the antenna wavelength. The depth resolution of the target decreases with the increase in antenna separation; however, this has an

insignificant effect until the space nears half the target depth. An estimate of the optimum antenna separation is given by:

$$S = \frac{2Depth}{\sqrt{K-1}} \qquad 3.28$$

When the separation increases, the reflectivity of flat lying planner targets increases too[83].

3.5.7. Antenna shielding

During GPR data acquisition, not all the EM energy is propagated into the subsurface and reflected to the receiving antennae[80], some energy is diffused and lost through the air[82]. These EM waves as they propagate through the air can encounter an object with a different dielectric constant, and can therefore, be reflected to the receiving antenna. This therefore means that some signals received in the antenna originates from the surface and it is not easy to distinguish this from that originating from the subsurface.

To overcome the effect of these unwanted surface reflections, an antenna can be shielded so that the loss of energy into the air should be minimized. Antenna shield is a 'container' that encloses the antenna to improve the antenna performance by eliminating the airwaves that would give wrong information to the radargram. It should however be noted that antenna shielding can not fully eliminate airwaves, therefore the data from shielded antenna should be treated with caution[83].

3.5.8. Velocity analysis

In GPR it is very necessary to determine the EM wave velocity in order to determine the depth of the target and its subsurface features. This is normally done by converting the TWT into depth.

The value of velocity can be determined by a basic method of probing or excavation to determine depth of a known reflector. Using the measured reflected time and the depth, velocity can be computed. This approach is referred to as ground trothing [84]. However, this is very tedious. During processing, this can be done using some computer applications, such as reflex,

which can estimate the velocity by measuring the angle of hyperbolic reflections. The velocities are determined by fitting the curves to the observed hyperbolas[82].

Velocity analysis in GPR fieldwork can be done in two main ways, (i) using common-offset mode and (ii) common-midpoint mode of data acquisition. Both modes can be used for profiling, but the latter is most suitable in velocity analysis on the data[4].

In the common-offset measurements, as depicted by *Figure 3.4*, the system is configured to detect the object and the lateral and vertical changes are investigated. These are used to compute the velocity of propagation.

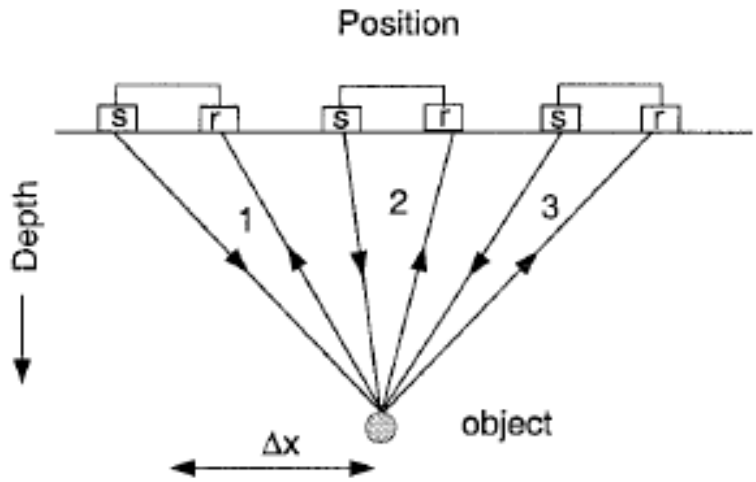

Figure 3. 4: The travel path of the wave from source to receiver

Source: Kruk, 1999

In this method, the antennas are moved by a fixed distance and a measurement is taken. This is repeated along the line. Assuming no change in velocity within the layer, and that the object is small compared to the wavelength used, then the reflection pattern is a perfect hyperbola. Then slopes of the hyperbola tails cab be used to estimate the wave velocity propagated into the layer. This is expressed as:

$$v = \frac{2\Delta x}{\Delta t} \qquad 3.29$$

Where $t = \sqrt{t_1^2 - t_2^2}$ and the factor 2 accounts for TWT.

In common mid-point (CMP) and wide-angle reflection and refraction (WARR) surveys, the signal velocity is estimated by varying the antenna spacing in steps at a fixed location and then measuring the change of TWT to reflections[83, 84]. The schematic configuration of this mode of measurement is presented in *Figure 3.5*. Velocity of propagation is estimated from the difference in arrival time and the offsets. This method is more reliable and most accurate as compared to the common-offset method[4].

In the subsurface, the velocity can be determined by the slope of the event. This is expressed as:

$$v = \frac{\Delta x}{\Delta t} \tag{3.30}$$

From the first reflection wave, it is also possible to determine the velocity as expressed as:

$$v = \sqrt{\frac{b^2 - a^2}{t(b)^2 - t(a)^2}} \tag{3.31}$$

Where a and b are the two different offsets and $t(a)$ and $t(b)$ denotes the corresponding TWT.

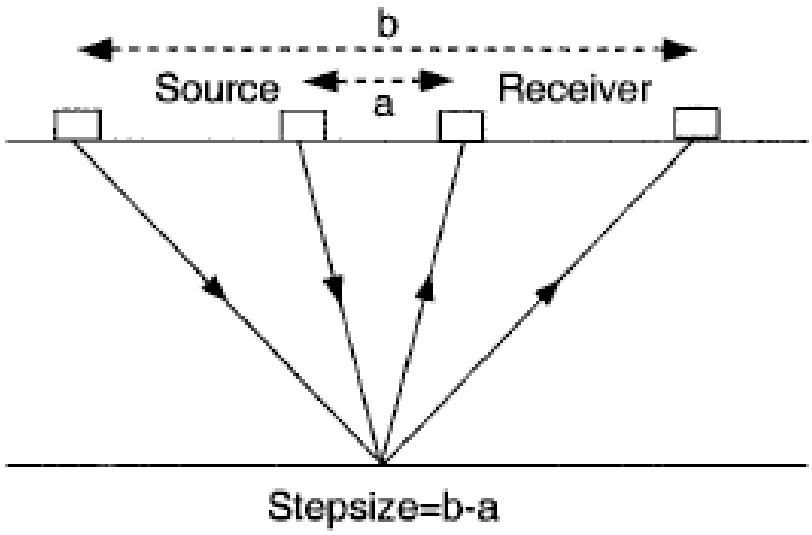

Figure 3. 5: A schematic diagram of CMP configuration for GPR.

The mid-point between the source and receiver is fixed while the source and the receiver are both moved a fixed distance away from the mid-point

Source: Kruk, 1999

3.6. General principle in GPR data processing and interpretation

GPR data are treated as scalar quantities [79] but still the EM fields that forms the basis of the method are vector quantities. Processing of GPR data is very important and f great beneficial before the interpretation of the same, however, it must be cost effective. The objective of this sub-chapter on data processing is simply to give practical guidelines for consistent, efficient and realistic processing. It is always necessary to avoid over processing; it might lead to some biasness and introduction of some potential artefacts into the data[85]. The following paragraphs provide a brief overview of various processing techniques.

3.6.1. Data editing

Data editing is the most time consuming process yet very important. It encompasses data reorganization, data file merging, data header or background information updates, repositioning and inclusion of elevation information with the data[79, 82]. Data acquisition in the field often includes errors, omission or data redundancy and these calls for the reversing, merging or omitting of some traces[85].

3.6.2. Static correction

Static correction involves adjusting the starting time (time zero adjustment) and the topographic correction. Time-zero adjustment involves aligning a common time-zero position[82]. If the positions are correctly aligned, all reflections beneath are correctly aligned[85].

Similarly, topographic correction places the GPR data within its correct spatial context. In horizontal surfaces and subsurface stratigraphy, static correction is employed to correct the GPR data, repositioning the start time in the vertical axis, thereby adjusting all the reflections accordingly[82, 85].

3.6.3. Dewow filtering

This type of temporal filtering gets rid of very low frequency components from the data. Very low frequency components of data are associated with induction or possible limitations of the instrument. Modern GPR instruments apply this process automatically[79, 83].

3.6.4. Time gain

GPR signals rapidly are attenuated as they propagate into the subsurface. This makes it difficult to show deeper information than that from the shallow subsurface. Time gain involves the employing some sort of time dependent gain functions to compensate for the loss of signal energy due to attenuation[83]. Gains improve the visual form of the GPR profile and enhances the appearances of later arrivals due to effects of signal attenuation and geometrical spreading losses. To change the gain functions, one has to alter the time window[85].

3.6.5. Background subtraction/ Removal

Background subtraction often takes a form of a high pass filter or an average trace removal. The average trace removal aims at removing horizontal bandings from the profiles due to system noise, interference and reflections[85]. It allows the subtle weaker signals to become visible after processing[83] by enhancing the dipping events while wiping out horizontal noise [86]. It is necessary to apply background subtraction in areas of suspected horizontal events of interest[42]. However, it is not usually necessary unless the equipment used to acquire the data is flawed[82].

3.6.6. Frequency filtering

Filtering is applied to remove system or human induced noise[85] at frequencies higher or lower than the main GPR signal[84]. This makes filtering work as clean-up devices, resulting in a GPR section looking better. It must be noted that despite the GPR data having collected using a specified source and receiver antennae frequency, the recorded signals include a band of frequencies around this dominant frequency. Filtering attempts to remove these unwanted high or low frequencies in order to produce an interpretable GPR image[81]. High pass filtering removes the low frequencies and maintains the high ones while low pass filters retains the low frequencies. Filters that apply the combination of the two effects are known as the band pass filters; they tend to remove high and low frequencies retaining all frequencies in the pass band.

3.6.7. Deconvolution

Deconvolution is an inverse filtering operation that attempts to remove the effects of source wavelet[81]. It works by compressing the recorded wavelets resulting in the improved data resolution[86]. In deconvolution, the operators are designed on assumption that the propagating source wavelet is minimal and the reflected waveforms have regular signals that do not scatter energy. This is not always true as the ground becomes part of the antennae in the GPR data acquisition, and the source pulse normally varies from trace to trace and is not minimum phase. It is therefore necessary to know the source signatures during data processing; otherwise, it would result in degrading the GPR images[81]. Annan[83] and Conyers[42] criticizes the technique as it is not straight forward and do not often yield a meaningful result.

3.6.8. Migration

This applies a synthetic aperture image reconstruction focusing scattered signals, collapse hyperbolas to their apices repositioning dipping reflections. It aims at eliminating distortions caused by reflections in data collection. When applying migration, the operator must take note of the original velocity, the origins of the distorted reflections and wave travel paths [87, 88].

3.6.9. Volume visualization

Despite that, the GPR profiles can be interpreted after processing, whilst in 2D, the interpretation will be quite interesting if the profiles are integrated into 3D blocks. With the advance in computer technology, affordable and accessible 3D visualization tools have been developed for the analysis of GPR data[83]. Integrating the data profiles into 3D from 2D can be done on already processed files or not[89]. When it is done on unprocessed files, they can be processed in the same way while in 3D. the 3D volume visualization helps to analyze and visualize the blocks in many ways, thereby giving more options for interpretation[1].

3.7. Advantages and limitations

GPR has both advantages and limitations as compared to other geophysical methods employed in site characterization. The following are the extracts from Robinson et al [82], highlighting the advantages and limitations of the method:

- It has a wide range of scale for the resolvable features using the available antennas. The scale can range from several centimeters to hundreds of meters.
- The system has an ability to acquire a large amount of continuous subsurface data, with the ability to allow the acquired data to be reviewed on site for quality control.
- It is non-intrusive and this makes it advantageous over seismic methods. This makes the method more suitable for its application in archaeological investigations.

However, the method has the following limitations:

- The EM energy transmitted and received forms a complex 3D cone. This makes it difficult to identify the reflections on a 2D profile, thereby, might lead to errors in depth estimations and interpretations.
- The survey can be seriously affected by the environment in which it is being conducted. For instance, conductive soils strongly influence the attenuation of EM waves. The rapid attenuation of the waves can produce high frequency ringing subsequently obscuring primary reflections.

- Lastly, the limitations encountered in the fields due to data collection configuration cannot be overcome once the survey has been finished.

3.8. Interpretation concepts and pitfalls

Much attention must be paid when interpreting GPR data as the process is application dependent and subjective to the individual doing it [83]. Not all events on radar cross-section are scattering from a discrete horizon, some arise from other sources such as the periodic events of the antenna used [90]. The antenna and the GPR system can introduce some artefacts. These introduced artefacts can easily be misinterpreted as stratigraphy, multiples, buried objects or other geological features. Below are some of the GPR concepts and how misinterpretation might arise from there, according to Annan [83].

3.8.1. Velocity determination using curve fitting

Hyperbolic fitting is one of the ways to determine velocity of wave propagation in a GPR system. To do this, the GPR measurement must be made along a traverse where the geometry is varying. In places where there are pipes, cables or rebars buried in the ground, the GPR system is moved perpendicular to the strike. The distance varies from the radar system to the pipe or rebar systematically. Traverse parallel to the strike does not yield any change in distance therefore cannot be used in the measurement of velocity as there is no change in the GPR record.

The velocity estimation involves the visual fitting of a hyperbolic model shape to the GPR data file, adjusting the model until it matches. This will give an estimate of the velocity of the wave. *Figure 3.6* illustrates the fitting. The velocity estimation is always erroneous if the traverse was perpendicular to the feature strike. Good field practices entail several perpendicular traverses over an object. It is recommended to use the hyperbolas that are steeper. Traverses not perpendicular result in velocities higher than true velocities thereby making the depth deeper than actual.

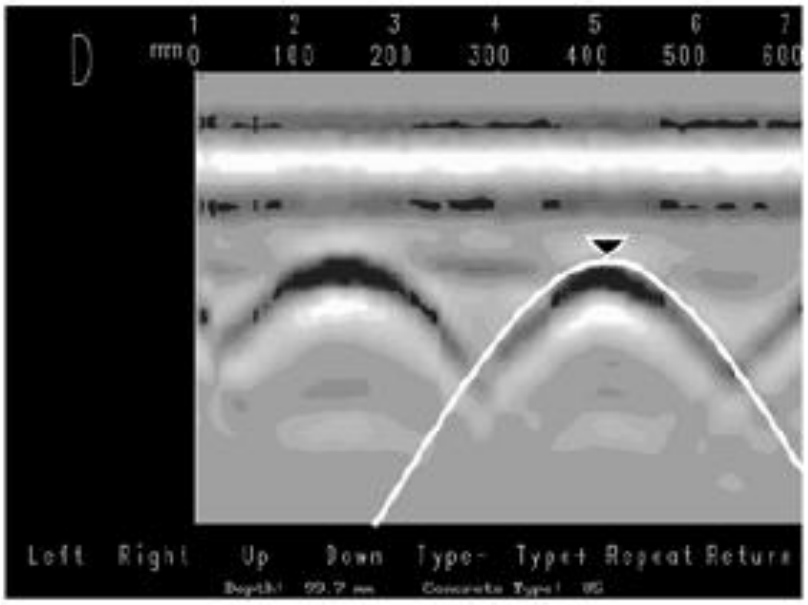

Figure 3. 6: Curve fitting to a target response to estimate wave velocity

Source: Annan, 2003

3.8.2. Airwave events

In GPR system, not all the energy is propagated into the ground, some leaks into the air and get reflected by such objects like telephone and electricity poles, overhead wires, walls, vehicles and so on. The receiving antenna receives both the airwave and the groundwave, making it difficult for the GPR user to differentiate these signals.

Airwave signals are problematic in the sense that they may mask the weaker subsurface signals, making them difficult or impossible to be seen or interpreted. They may end up being interpreted as buried objects while they reflect objects above the ground. It is necessary to question the source of the signal especially when the amplitude-time response is indicating that the signals in the ground are decaying at a rapid rate.

The airwaves can be indicated by:

- Visually potential sources such as trees, walls, overhead cables, poles etc within the survey area
- The tails of hyperbolic events with slopes close to the airwave velocity

- The frequency contents of the events-airwave energy have higher frequencies than groundwave energies.

Remedies applied:

- Optimizing the antenna performance. This can be done by antenna shielding. It should be noted that antenna shielding does not eliminate airwaves; it reduces to a notable factor of 2-10.
- Digital filtering. The airwave event always has a fixed slope (slope indicating the speed of air), this, therefore allows the filtering of these airwave energy, leaving behind the rest in intact.
- Low pass temporal filters can be employed to get rid of high airwave energy and leaving behind the ground response energy.

3.8.3. Antenna shielding

This is applied to achieve the following objectives:

- To maximize the energy propagated though the subsurface and direct to the receiver
- To minimize the energy that leaks into the air, thereby reducing the airwave events
- To minimize noise from external electromagnetic interference

When the shields are used, the propagated signals might be large and reverberate for a long period. This is so because the signals will have to transfer from the transmitting antenna to the shield, then to the shield of the receiving antenna before they reach the receiver. This therefore needs the shields to be interactive with the radio waves; otherwise, they might generate responses detrimental and interfering with the measurements. *Figure 3.7* shows a series of radar traces with and without external noise effects.

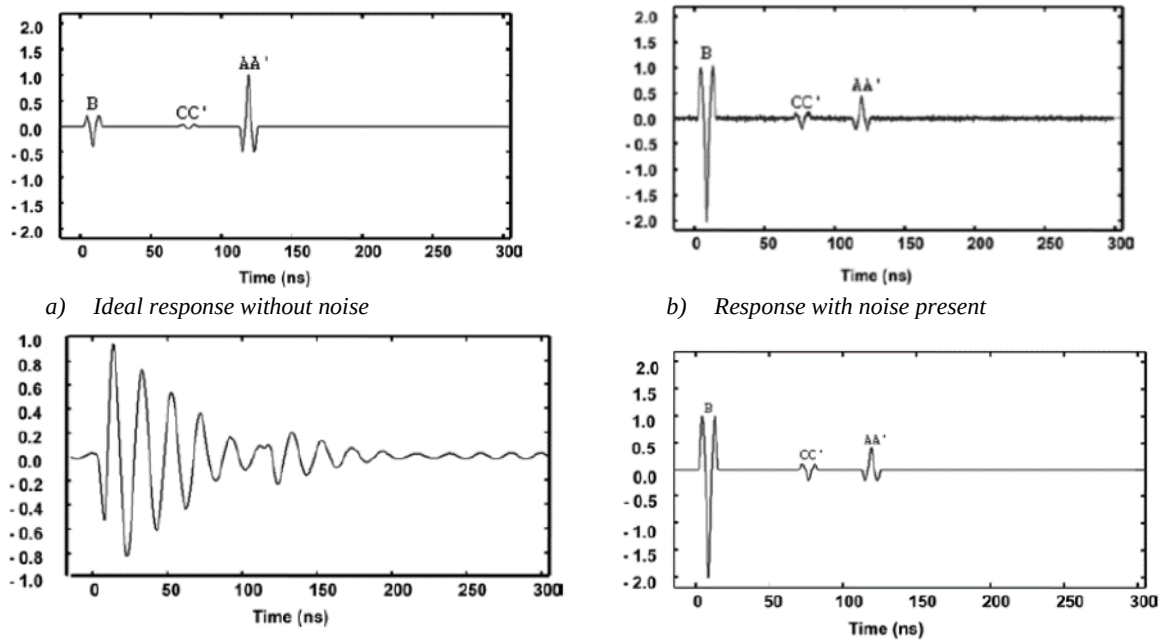

a) Ideal response without noise

b) Response with noise present

c) Response when yielding is not properly used

d) Response when a practical shield is used

Figure 3. 7: Radar responses

Source : Annan, 2003

3.8.4. Ringing on radar records

During GPR survey, a signal can interact with an object and the response becomes a repeated bouncing of the signal around the object. This reverberation of the signal in a regular fashion is termed ringing. Ringing can originate from various sources. Below are some of these sources:

- An undamped dipole antenna: this supports electric current which travels back and forth repeatedly generating signal
- Inappropriate antenna shielding: the current generated bounces back and forth emitting a signal
- A metal object in close proximity of the antennas
- A strong target near the antenna or ground interface.

Generally, the ground dampens the reverberation since it absorbs energy. It is therefore necessary to check what would be the source of any anomaly in GPR data profile to ascertain

if it is not a result of ringing. *Figure 3.8* shows an example of a ringing as originating from a wire scrap.

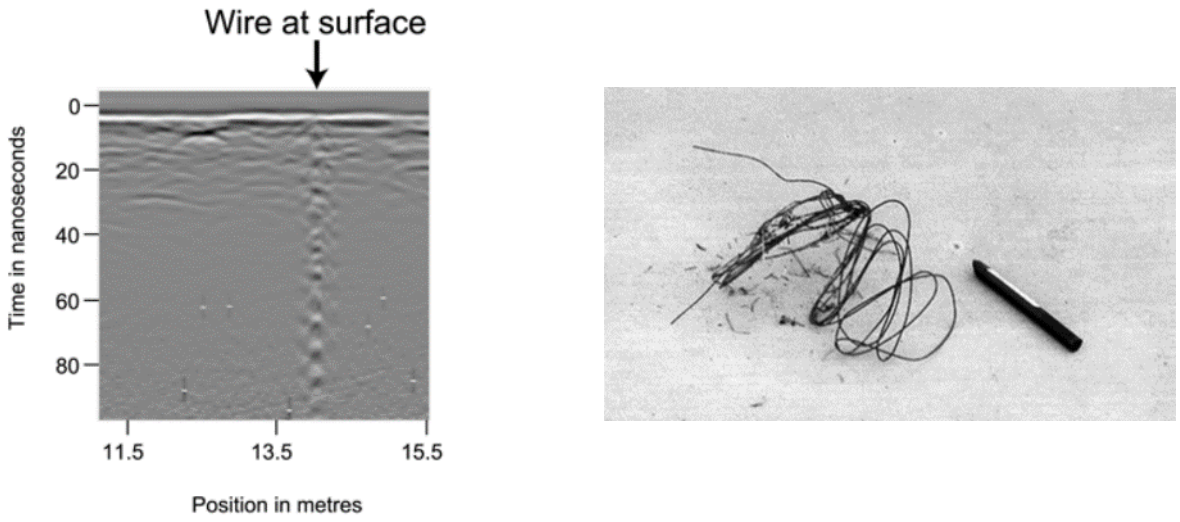

a) A radargram showing a ringing

b) A scrap piece of wire found on the grass and was noted to be the source of ringing

Figure 3. 8: A radargram showing a ringing and its source

Source: Annan, 2003

3.9. Conclusion

Ground penetrating radar finds itself being used in various applications in engineering and other fields. It is more suitable for archaeological studies because of its non-invasive nature, thereby conserving the archaeological evidence. To come up with a good and reliable interpretation of the field data, it must start from a proper survey design, which involves the selection of proper equipment and accessories, strong technical know-how and reliable interpretation tools. It must also be borne in mind that not all the events observed on the radar profiles are from the subsurface events, some might have been originated from the airwaves or from external wave interference.

4

DATA ACQUISITION FROM THE FIELD

"The only thing more expensive than education is ignorance"

Benjamin Franklin

4.1. Introduction

Data acquisition involves the collection of GPR data from the field using the appropriate methods and equipment. For the purpose of this work, a GPR survey was conducted at Castro de Ul archaeological site in the year 2013. The work involved two phases: first phase was the collection of data from the two major paths in the site, and the second phase was the collection of data from the 10 by 10 m squares of the grid that were demarcated in the field. The GPR survey used the TerraSIRch SIR System-3000 by Geophysical Survey System Inc. (GSSI) with 270 MHz and 900 MHz centre frequency antennas.

4.2. Raw data

As stated in the introduction, two phases were involved. In the first phase, seven radargrams were acquired along the two major paths and the perpendicular section joining the first path. Two parallel radargrams were acquired from the first path covering 40 m using a 270 MHz antenna, and another radargram was taken from the perpendicular section from the middle of the first path to 15 m. Another radargram was taken from the second path covering 88 m. The profiles on first path and the perpendicular section were repeated by using a 900 MHz antenna. *Figure 4.1* shows the sketch of map for data acquisition in this phase.

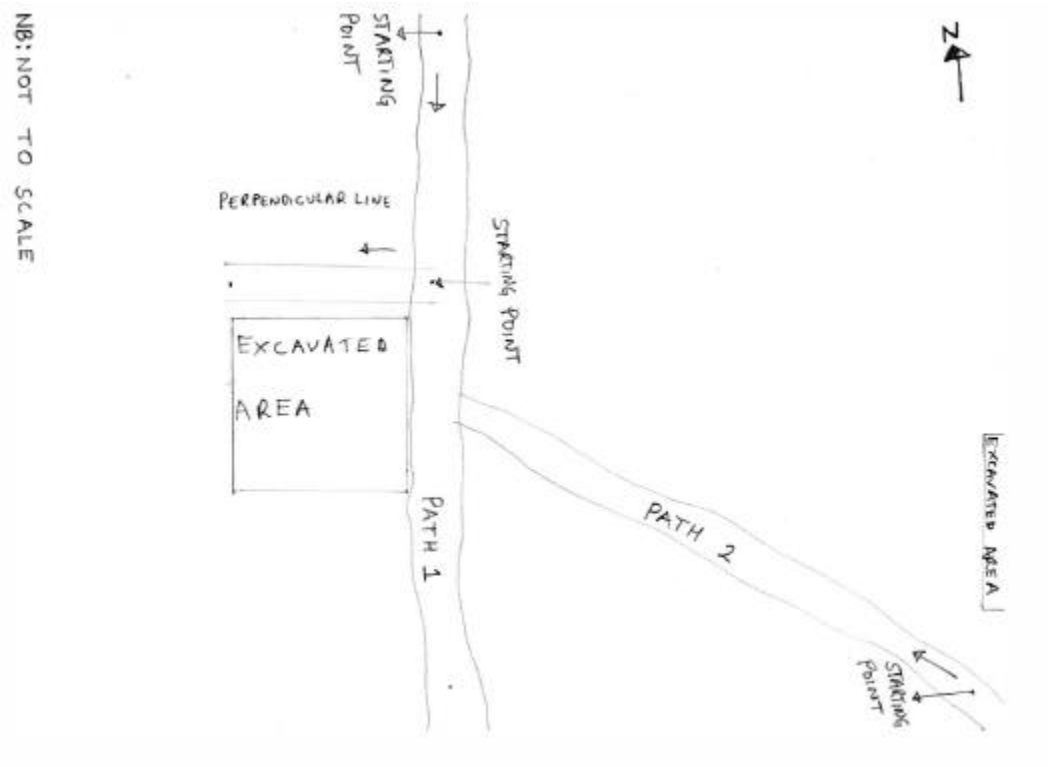

Figure 4. 1: Sketch map for data acquisition in the first phase

The second group of data were acquired from 11 squares with 10 by 10 meters taken by 270 MHz and 900 MHz antennas. The data were acquired along two directions: South-North and West-East, using a 10 by 10 m square grid. The squares where the data was collected depended on the accessibility as most of the parts of the site is covered by trees. *Figure 4.2* illustrates the surface grid of the site and the 11 X's squares where the data was collected. These eleven squares are summarized in *Table 4.1* with the number of profiles and their directions taken in each square. The number of profiles in each square is not equal because it depended on the accessibility of the square to the moving of the GPR equipment.

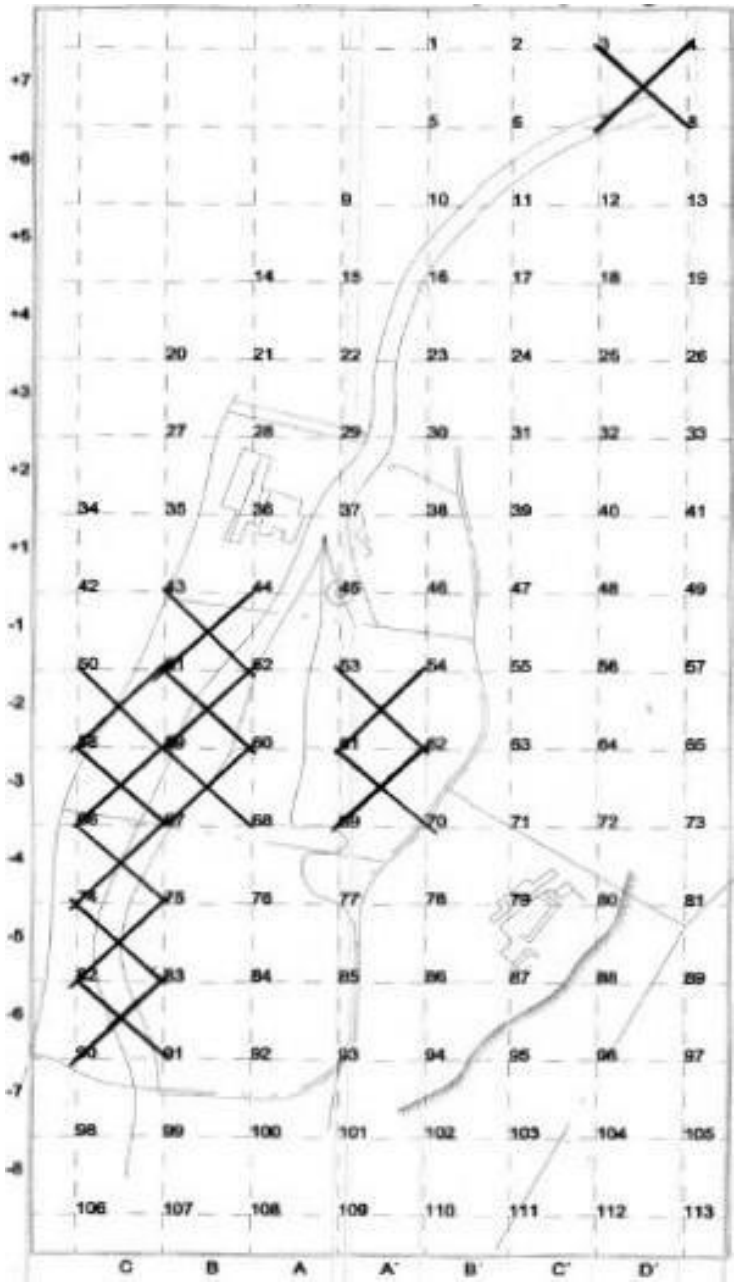

Figure 4. 2: Sketch of grid map used for a 2013 GPR survey

Table 4. 1: Number of profiles in each square and the paths acquired during the GPR survey

SECTION	**NUMBER OF PROFILES**
PATHS	
Path 1 (270 MHz)	2
Perpendicular section (270 MHz)	1
Path 2 (270 MHz)	1
Path 1 (900 MHz)	2
Perpendicular section (900 MHz)	1
SQUARE SECTIONS	
-3C (South-North Direction, 270 MHz)	15
-3C (West-East Direction, 270 MHz)	17
-3C (South-North Direction, 900 MHz)	16
-2C (South-North Direction, 270 MHz)	7
-3B (South-North Direction, 270 MHz)	5
-2B (South-North Direction, 270 MHz)	10
-1B (South-North Direction, 270 MHz)	13
-4C (South-North Direction, 270 MHz)	9
-5C (South-North Direction, 270 MHz)	9
-6C (South-North Direction, 270 MHz)	10
-2A' (South-North Direction, 270 MHz)	16
-2A' (West-East Direction, 270 MHz)	17
-3A' (South-North Direction, 270 MHz)	15
-3A' (West-East Direction, 270 MHz)	17
-3A' (South-North Direction, 900 MHz)	16
7D' (South-North Direction, 270 MHz)	15

4.3. Data acquisition procedure in the squares

In each square, data was acquired using the 270 MHz antennae in one or more directions depending on the accessibility of the squares to the moving cart. The main procedure involved acquiring the data in the South-North direction. This way, the equipment could miss out some important information that would be more helpful in the data interpretation. The repetition of the data collection using different directions or different antennae would help to clear out doubts that might be incurred in the process. In view of this, a 900 MHz antenna was used in some squares and the 270 MHz antenna was also used in some squares but in West-East direction.

The data was collected in radargrams spaced 60 centimeters apart. On 10m by 10 m squares, using 60cm spacing, it was supposed to be acquiring 17 files, but in most squares, it was not practically possible due to obstacles in the field such as trees. The files collected though less, were enough to give a meaningful interpretation.

4.3.1. South-North (S-N) direction

This was the main procedure in the fieldwork. All the squares were surveyed in this way. Files were taken by moving the equipment from south to the north direction with the first point in the southern side taken from zero to 10 meters. The successive files were taken westwards, 60 centimeters apart, except in cases of obstacles. *Figure 4.3 (a)* illustrates how the data were collected in a square.

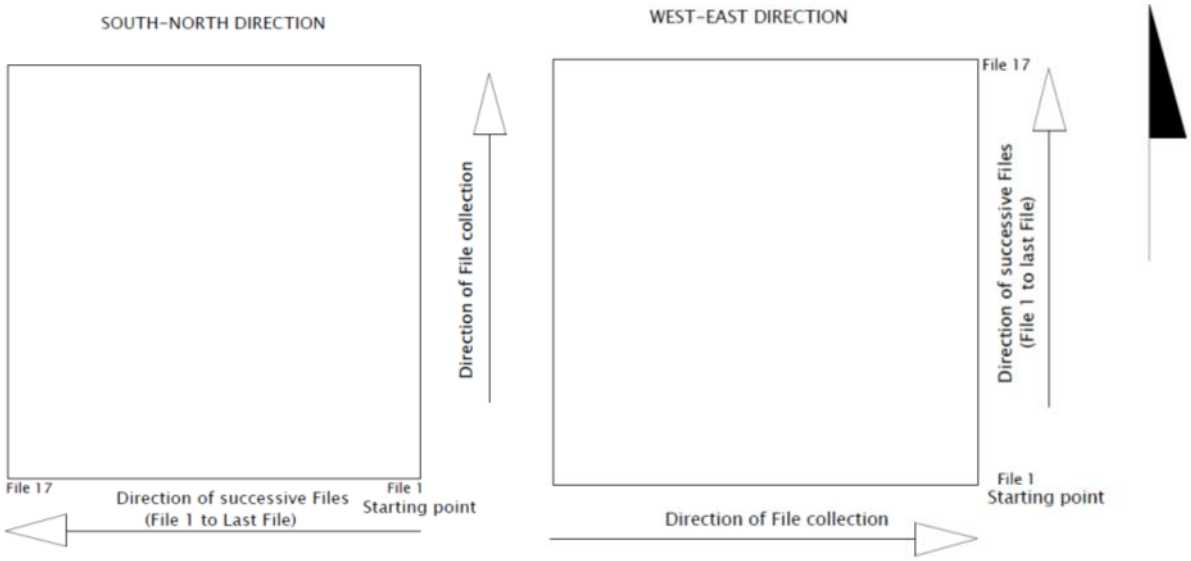

a) South-North direction *b) West-East direction*

Figure 4. 3: Directions of data acquisition profiles

4.3.2. West-East (W-E) direction

This was another important information collected and was so useful in comparison with the main south-north data sets. The cart was moved from west to east during the acquisition using this procedure. This was repeated to collect the successive files going up the north. The processed radargrams were compared to the South-North data sets and to map the possible anomalies within the square. *Figure 4.3 (b)* shows this procedure.

4.4. Conclusion

All the data available were taken using the two antennas: a 270 MHz antenna and the 900 MHz antenna. The use of the two antennas helped to get some details that were missed out by the other antenna. It was also repeated using the 270 MHz antennas in different direction jut to make sure that some details are not missed out. The consideration of the direction of data acquisition was so necessary since the interpretation was based on the integration of the files into 3D blocks, otherwise, the resulting blocks would be oriented in a wrong direction.

5

RESEARCH DATA PROCESSING

"It takes a village to raise a child"

-Malawian proverb-

5.1. Introduction

GPR data processing is extremely important in some cases, yet inappropriate in others. Data processing involves fundamental manipulations applied to data to improve and make it meaningful for interpretation [79]. In data processing, post survey processing are done systematically and employs processing operators to remove or enhance certain features.

The objective of signal processing is primarily to reduce clutter since the signal to clutter ratio of the radar data is the fundamental key to target detection. All this clutter reduction is employed to present an image that can readily be interpreted [33].

A software ReflexW by Sandmeier Geophysical Research was used in data processing. ReflexW is the most popular and useful software applied in GPR, seismic reflection, seismic refraction and ultrasound for near surface processing and interpretation. The software is a powerful tool when using GPR data since it has the ability to analyze data in both 2D and 3D and also has possibilities of generation models and simulations from the data analysis [89].

5.2. Objective of data processing

Data processing in this research was conducted prior to interpretation to improve the signal quality aiming at detecting all anomalies that might be related to possible buried archaeological features.

The second objective of the processing was to integrate the 2D profiles into 3D blocks for a clear visual analysis in each square. This would help detecting anomalies in the block from different orientations (X, Y and Z directions). The aim was to detect possible continuities of anomalies across the blocks (squares).

5.3. Data processing

Data processing was done in such a way as to avoid over processing which would introduce bias and potential artefacts into the raw data [82]. The basic processes included changing the start time, noise removal, deconvolution frequency filtering, and migration.

5.3.1. Start time adjustiment

Data acquired by a survey cart has a time off-set due to the antenna configuration[89]. It is therefore necessary to adjust the zero time to a common position before applying processing [82]. The correct setting of time zero makes all reflections beneath to become correctly aligned [85]. *Figure 5.1* shows a file before and after the time zero was set. *Figure 5.1 (b)* shows that the time zero has been adjusted by -8.901ns, this corresponds to the first strike of the airwave.

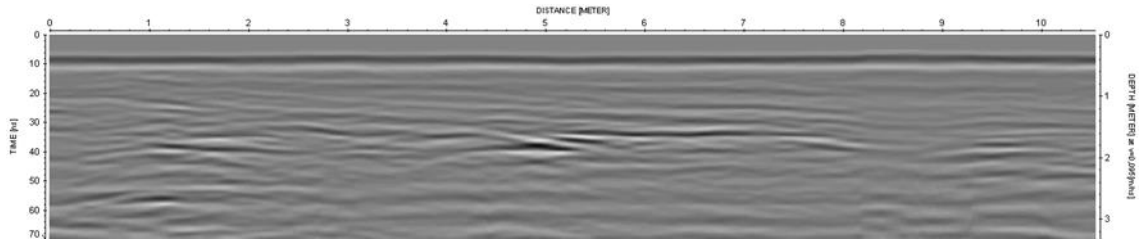

a) A raw radargram before any processing was applied

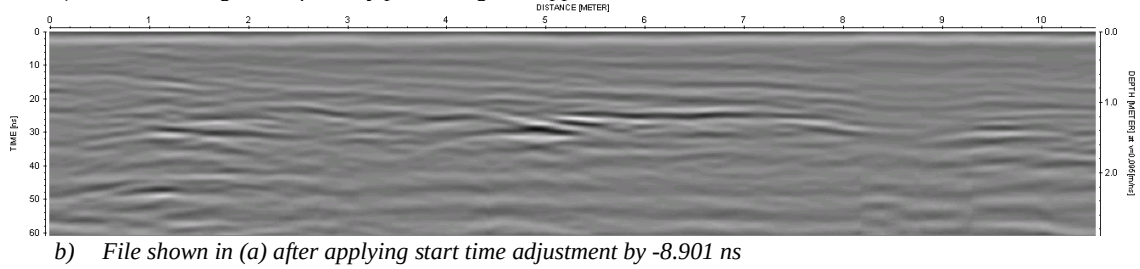

b) File shown in (a) after applying start time adjustment by -8.901 ns

Figure 5. 1: Radargram of the first profile taken from square -3C in the South-North direction

5.3.2. Noise/ Background removal

This was applied to the profiles acquired with an aim of removing the horizontal noise that might have risen from system noise, electromagnetic interference and surface reflections. *Figure 5.2* shows the radargram of profile 1 from square -3C in South-North direction after the background removal was applied. The near surface reflections rising probably during acquisition has been removed as shown in *Figure 5.2 (b).*

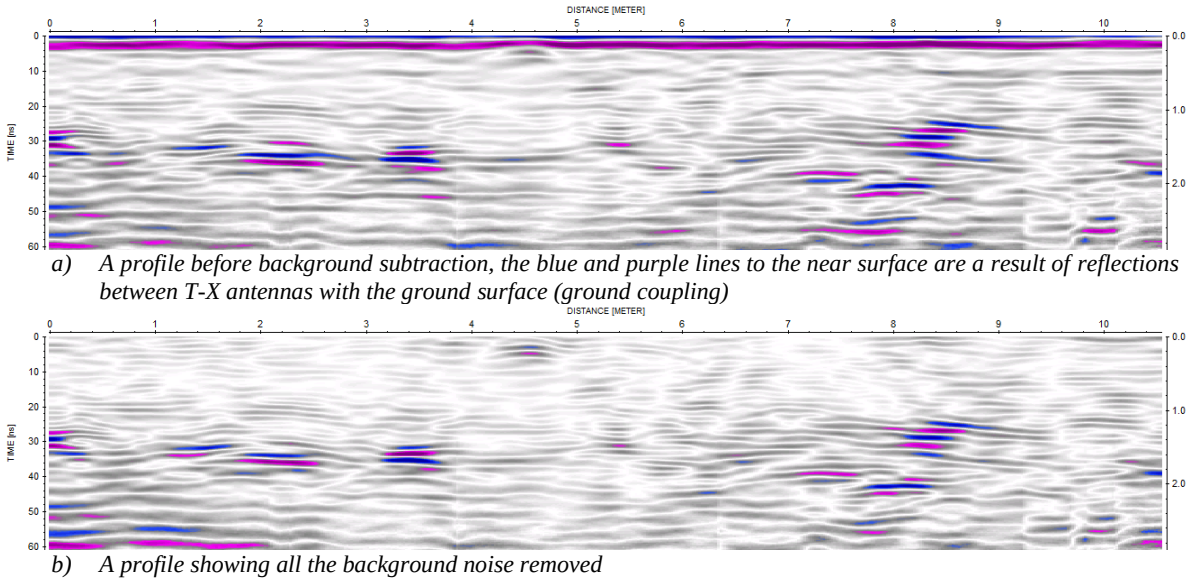

a) A profile before background subtraction, the blue and purple lines to the near surface are a result of reflections between T-X antennas with the ground surface (ground coupling)

b) A profile showing all the background noise removed

Figure 5. 2: Radargram showing the effect of applying background subtraction

5.3.3. Deconvolution

Some profiles were sampled for the application of deconvolution. It was noted that after applying deconvolution, the image contrast increased and was not necessary to employ it as a process. *Figure 5.3* presents two of the sampled profiles where deconvolution was employed. In both cases, the two images before and after deconvolution resemble, the only difference is the contrast. This means that the propagating source wavelet was regular and it did not scattered

energy that could degrade the profile [81], therefore, deconvolution was not necessary to be employed in the processing.

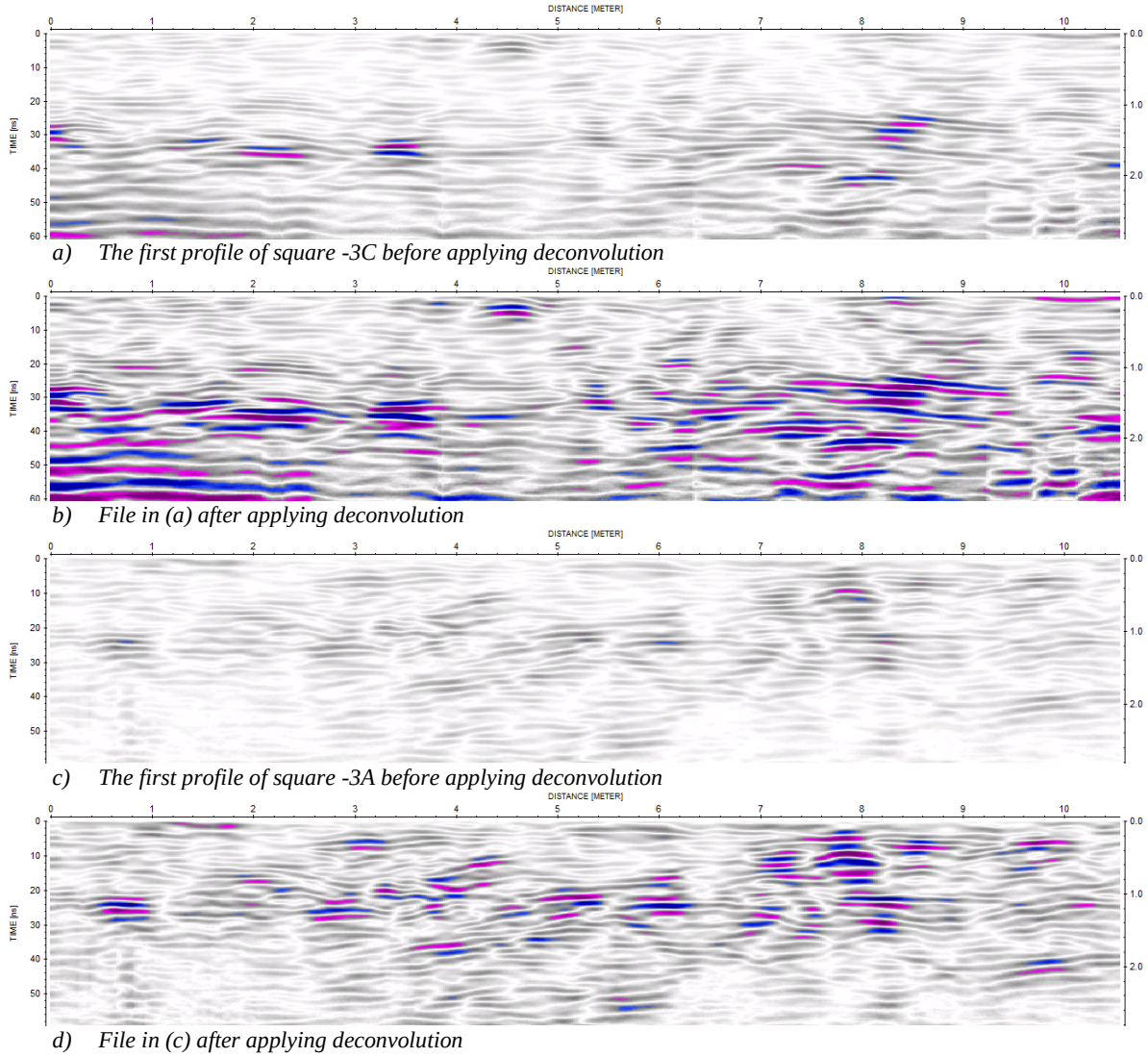

a) The first profile of square -3C before applying deconvolution

b) File in (a) after applying deconvolution

c) The first profile of square -3A before applying deconvolution

d) File in (c) after applying deconvolution

Figure 5. 3: Radargrams from squares -3C and -3A showing the effect of deconvolution after applying background removal

5.3.4. Frequency filtering

The profiles were processed using band pass filter and band pass Butterworth filter to compare which filter best presents a better image of the resulting profile. *Figure 5.4* shows the first profile from square -3C in the S-N direction. It was later decided to use the band pass Butterworth filter for the rest of the profiles since this signal process technique returns a flat frequency response. This results in a uniform sensitivity to the wanted frequency band pass as compared to the normal band pass filters. Band pass frequency filter, filters some necessary

information from the band and hence not good for the purpose. *Figure 5.4(b)* shows the profile with some necessary data filtered.

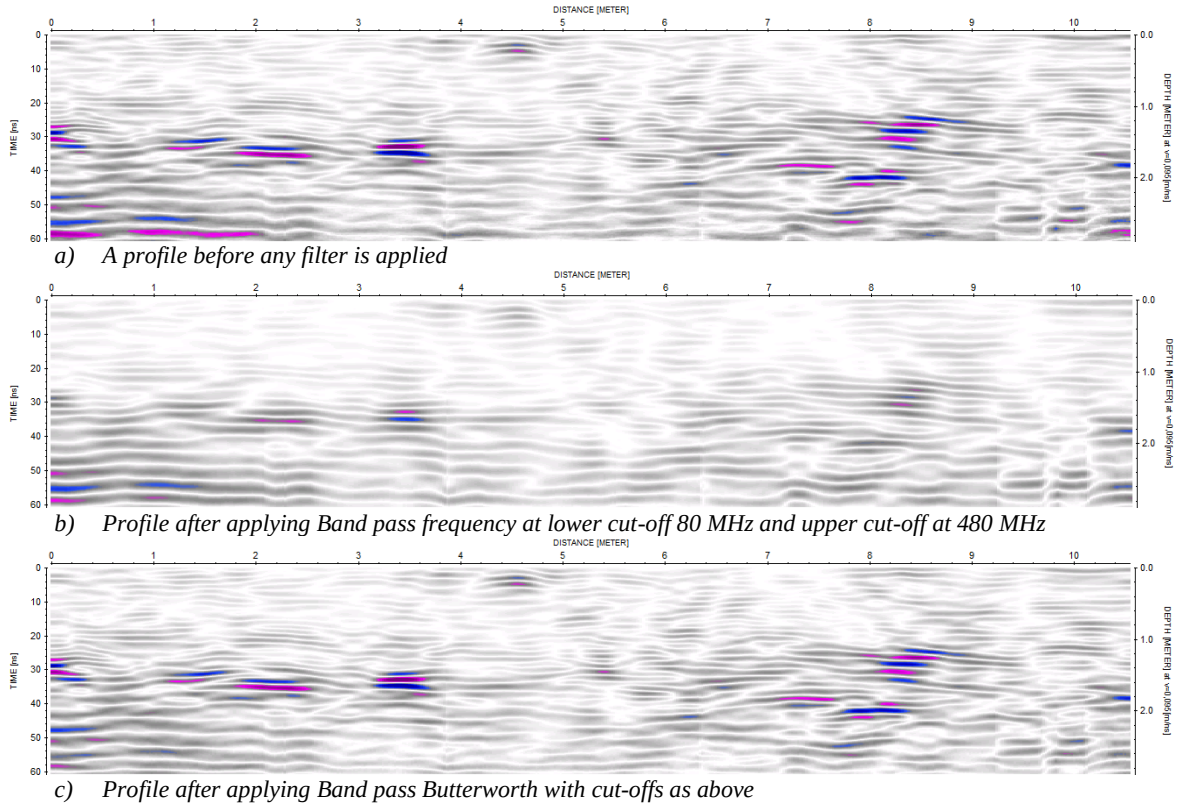

a) A profile before any filter is applied

b) Profile after applying Band pass frequency at lower cut-off 80 MHz and upper cut-off at 480 MHz

c) Profile after applying Band pass Butterworth with cut-offs as above

Figure 5. 4: Radargram from the first profile of the square -3C S-N direction after the effect of applying 1D filter

5.3.5. Migration

The essence of applying migration is to correct distortions that might have been caused by wide transmission beam of radar antennas causing reflections from point sources and look like hyperbolas. Kirchhoff migration technique was used and the results is presented in *Figure 5.5*. Kirchhoff migration is based on the diffraction summation principle [88]. Migration was applied at the velocity between 0.075-0.095m/ns. It was noted that the effect of applying Kirchhoff migration was simply the same as reducing the contrast. This was mainly because the profiles processed did not contain collapsing hyperbolas, and therefore, migration was not necessary to be employed. However, employing migration had no degrading effect on the resultant profile.

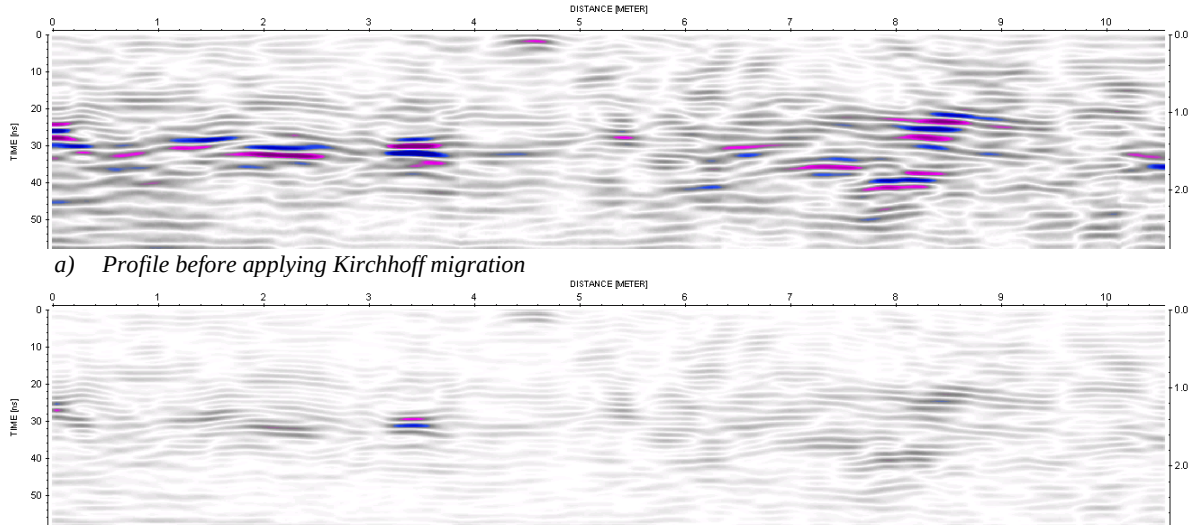

a) Profile before applying Kirchhoff migration

b) Profile in (a) showing the effect of applying migration, just a reduction in contrast

Figure 5. 5: Radargram of file 1 from square -3C S-N direction showing the effect of Kirchhoff migration

5.4. Data processing for the files taken using the 900 MHz antennae

In some squares, square -3C and -3A, a 900 MHz frequency antena was used in the data acquisition. These data were treated in a different way. Static correction was applied in the ranges of -5 to -6 ns, the background noise was removed from the whole profile and then a band pass butterworth filtering with a lower cut of 80/160 MHz and an upper cut of 1000/1200 MHz was applied. In this case there were no collapse hyperbolas and therefore migration was not applied. *Figure 5.6* shows the file taken from square -3A' in the South-North direction using the 900 MHz antena.

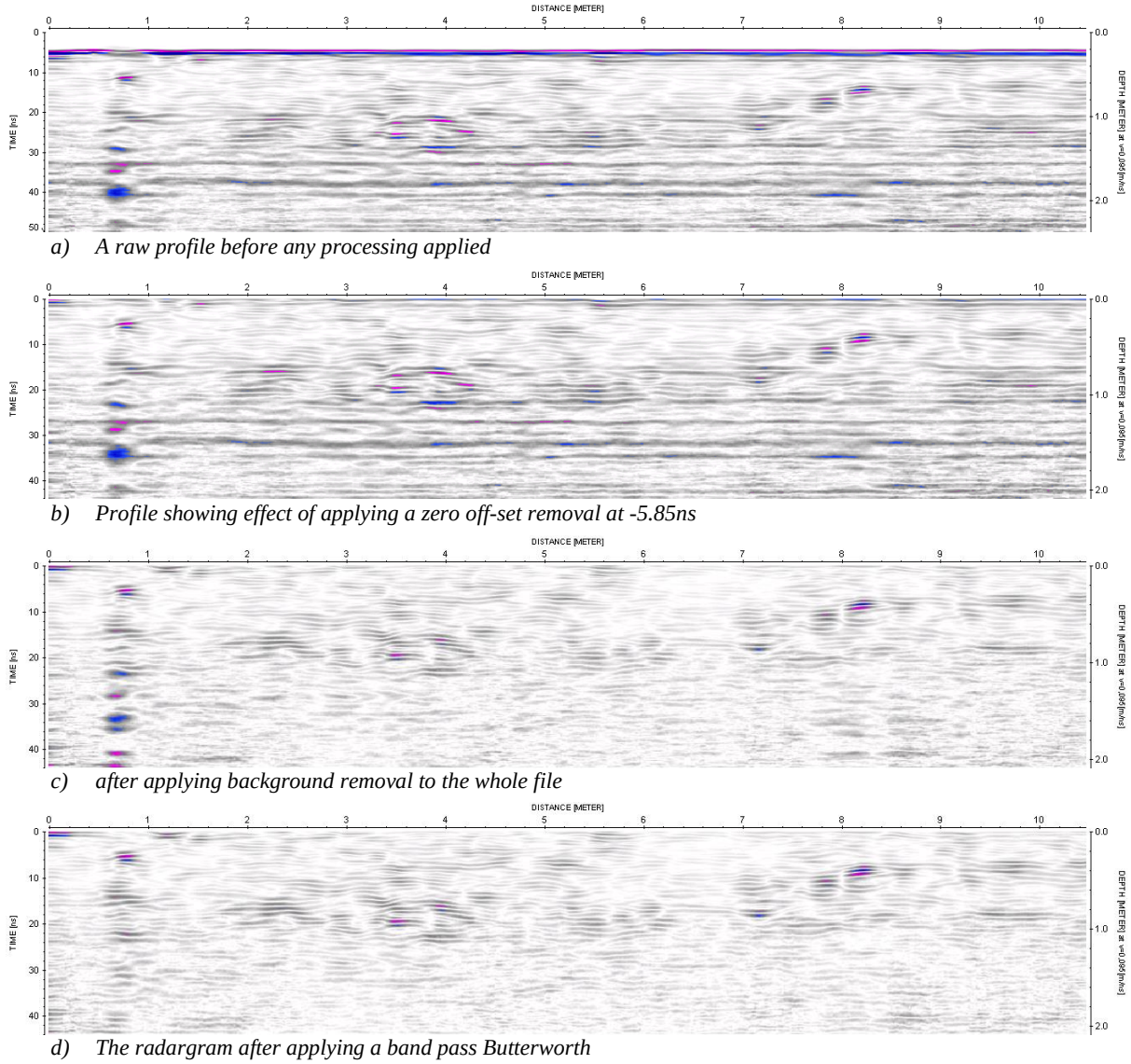

a) A raw profile before any processing applied

b) Profile showing effect of applying a zero off-set removal at -5.85ns

c) after applying background removal to the whole file

d) The radargram after applying a band pass Butterworth

Figure 5. 6: A radargram taken from square -3A' using 900 MHz antennae showing the processing

5.5. Processing flow

All the data acquired from the squares and the paths as indicated on *Figure 4.1* were processed with an aim of improving the image resolution so that they can be used for interpretation. The process flow was the same in all the data taken using different antennas in the field. *Table 5.1* shows the processes applied to the radargrams and Figure 5.7 shows the process flow.

Table 5. 1: Processes applied to the acquired radargrams

PROCESS	**270 MHz**	**900 MHz**
Start-time adjustment	-8.00 to -12.00 ns	-5.00 to -6.00 ns
Noise removal	Whole profile	Whole profile
Filtering	80/160 to 400/480 MHz	80/160 to 1000/1200 MHz

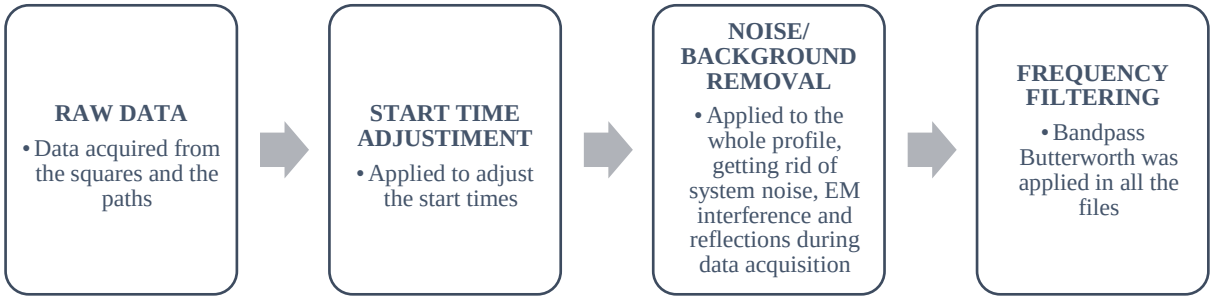

Figure 5. 7: Process flow for the radargrams acquired using the 270MHz antennae

5.6. Processing data acquired in the first phase of the field survey

In the first path, four profiles were acquired in parallel, two using the 270 MHz antenna and the other two using the 900 MHz antenna. The same was done in the 15 meters perpendicular section but not in parallel. The two antennas were used in data acquisition from the paths before the main survey, which involved data acquisition from the squares. In the second path, only the 270 MHz antenna was used. *Figure 5.8* and *Figure 5:9* show the processed radargrams from these paths using 270 MHz and 900 MHz antennas respectively.

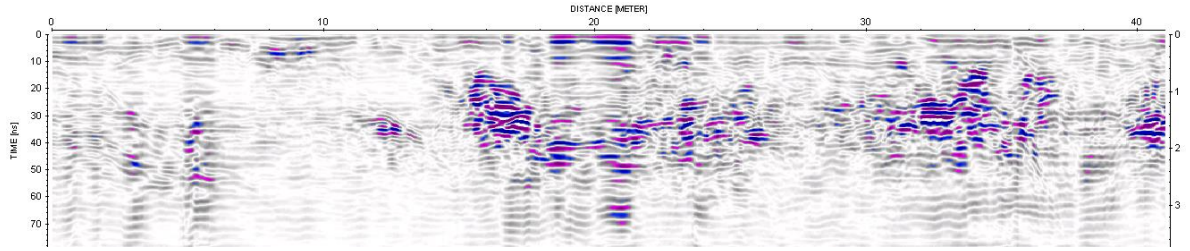

a) Profile of Path 1 after being processed, Parallel profile 1

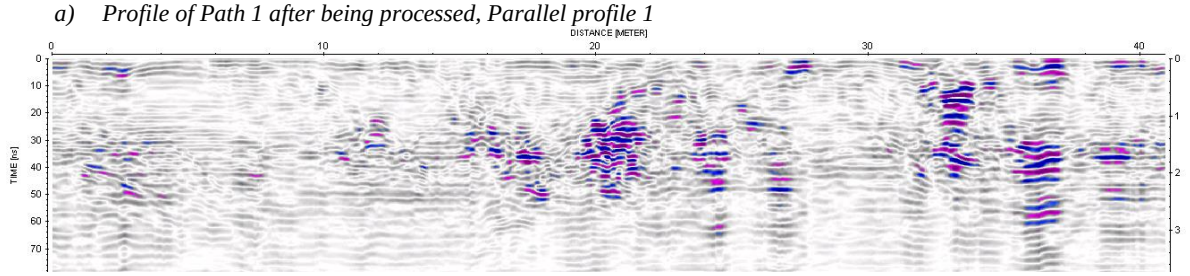

b) Processed profile of Path 1, Parallel profile 2

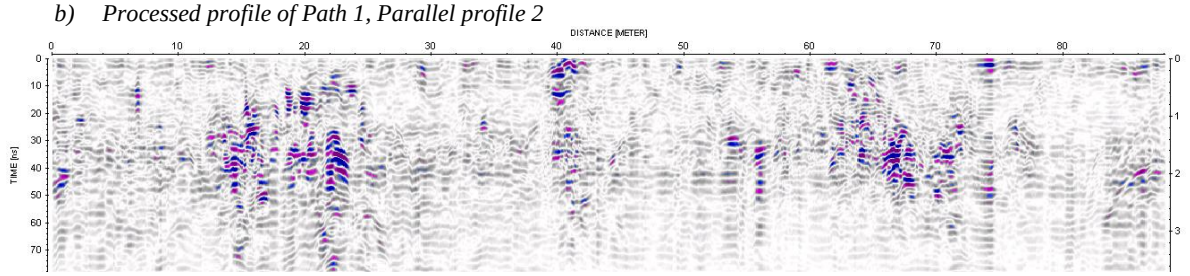

c) Profile of Path 2

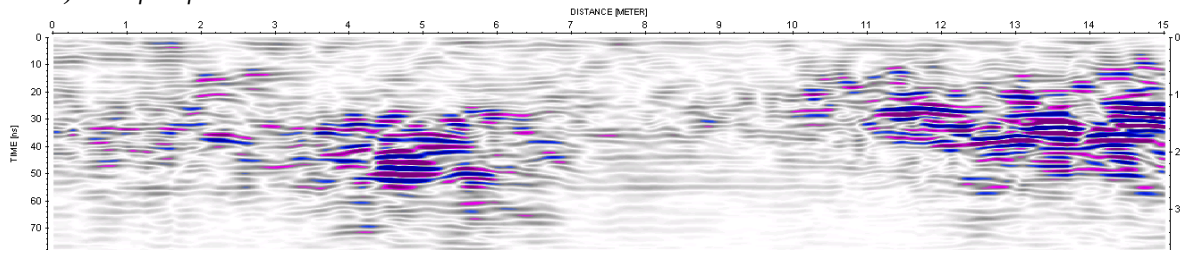

d) Profile of the perpendicular section

Figure 5. 8: Processed radargrams from the main paths taken by a 270 MHz antenna

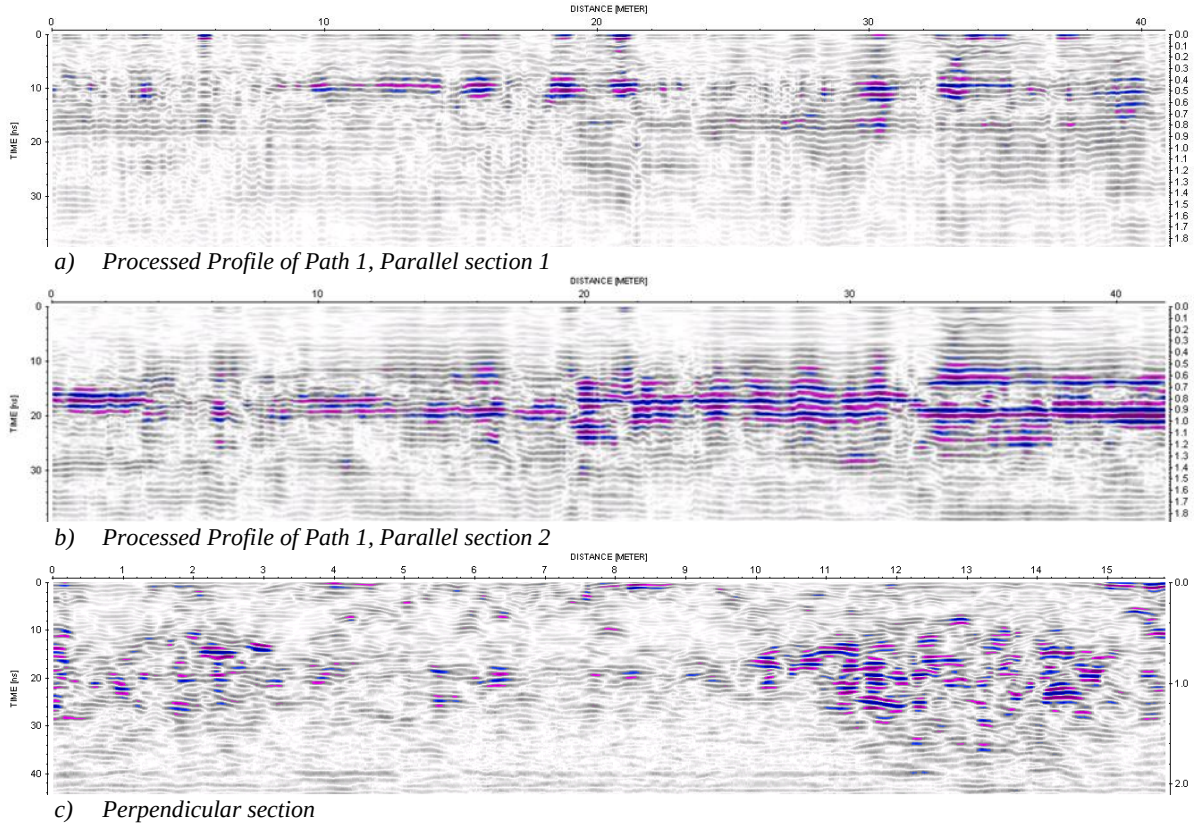

a) Processed Profile of Path 1, Parallel section 1

b) Processed Profile of Path 1, Parallel section 2

c) Perpendicular section

Figure 5. 9: Processed radargrams from the main paths taken by a 900 MHz antenna

5.7. 3D block volume analysis

The radargrams from the squares were processed using ReflexW software and integrated into 3D blocks for each square as acquired from the field survey. The data were acquired in parallel equidistant lines, 60 cm apart as explained in S*ection 4.3.*

The x-axis of the block is the profile direction as taken in the field. These profiles are 10 meters long. The y-axis represents the direction of the consecutive profiles. These were taken in the increments of 60 centimeters and do not necessarily go up to 10 meters as in most of the places were not practically possible to move the cart. The z-axis is the travel time in nanoseconds. In the following sections, blocks and information from respective squares are presented.

5.7.1. Example of generating 3D block: Block -3C

In square -3C, three different data sets were acquired; 15 radargrams were acquired using the 270 MHz antenna in the South-North direction, 17 radargrams acquired using the same 270 MHz antenna in the West-East direction and 16 radargrams acquired using the 900 MHz antenna. *Figure 5.10* shows the blocks generated from files of square -3C. Files from all the other squares have been integrated in the same way, and the resulting blocks are presented in *Appendix B.*

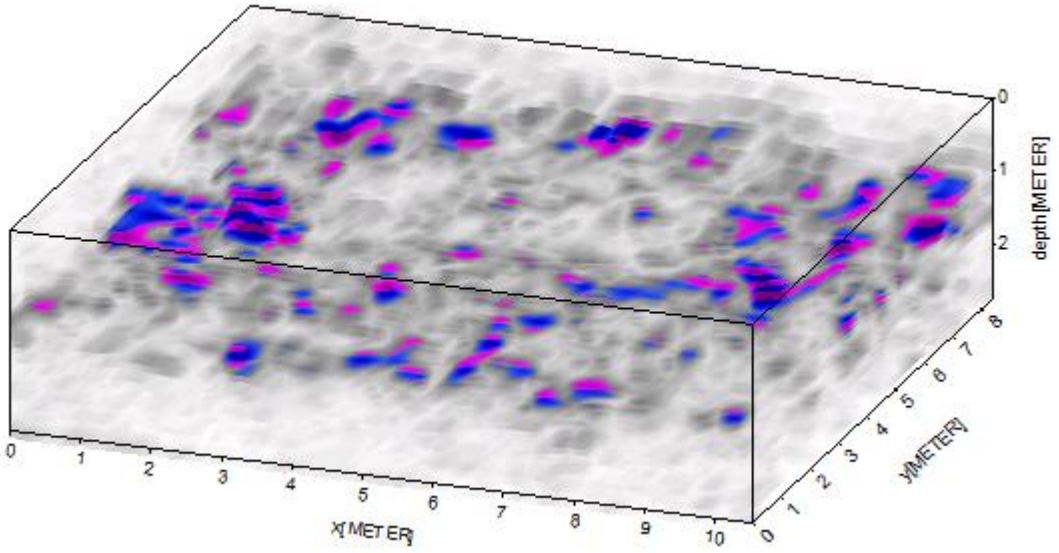

a) Block generated from data taken by a 270 MHz antenna in the South-North direction of data acquisition

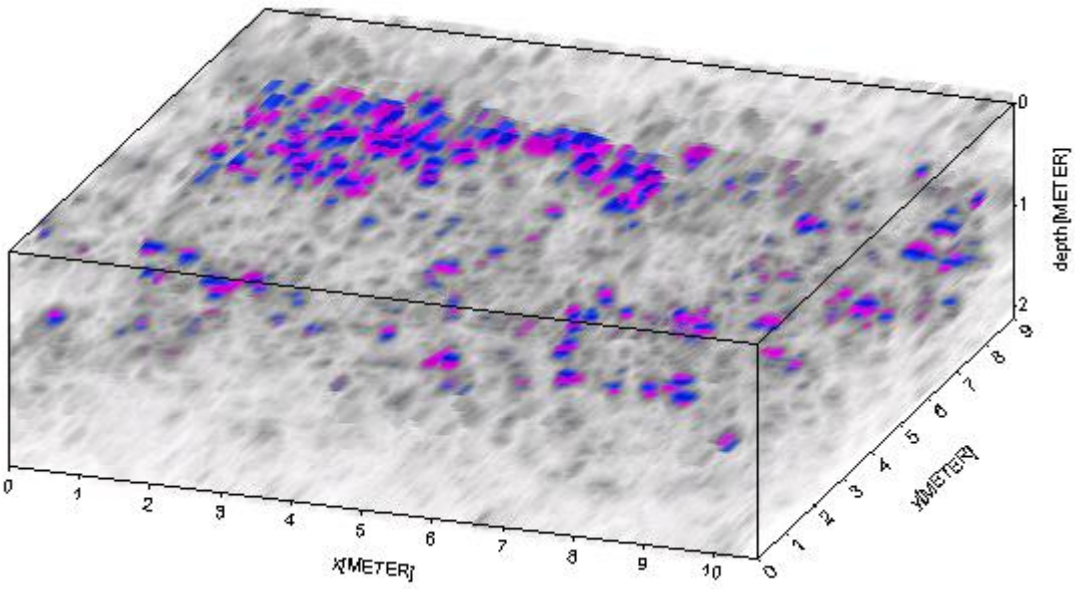

b) Block generated from data taken by a 900 MHz antenna in the South-North direction of data acquisition

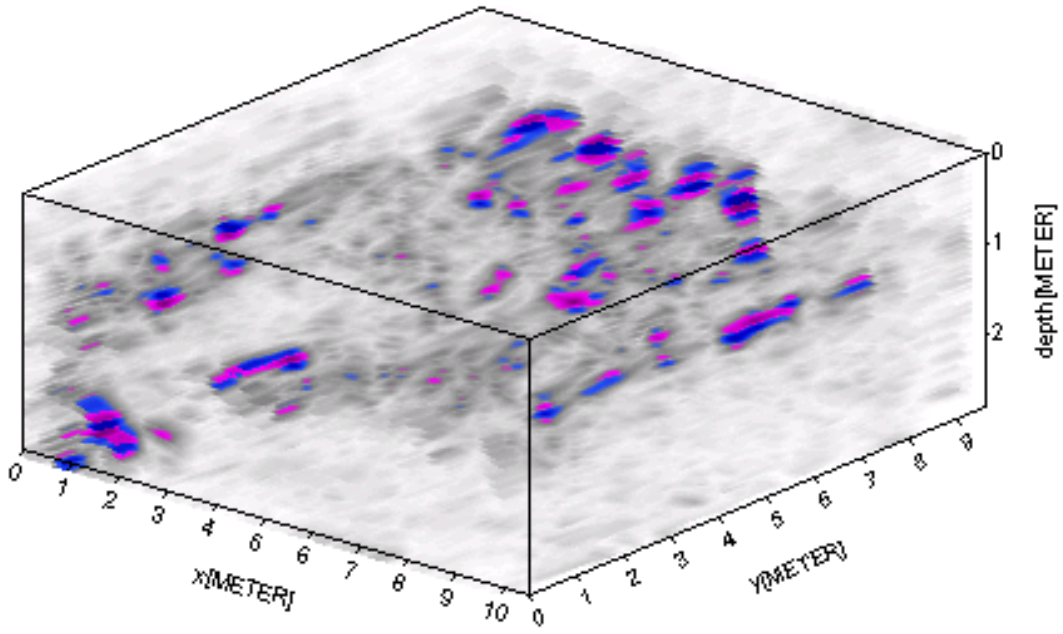

c) Block generated from data taken by a 270 MHz antenna in West-East direction of data acquisition

Figure 5. 10: Blocks generated from data acquired in Square -3C

5.8. Conclusion

The raw data acqured from the field was processed and presented before being integrated into 3D blocks. The processed radagrams showed anomalies that could be probable burried archaeological features. The processing methods employed were enough to improved the resolution and filtered out the noise and make them fit for intepretation. The 3D integration will help to analyse the continuity of the anomalies in the block and the adjacent blocks.

6

DATA INTERPRETATION

'The casino is the only human venture I know where the probabilities are known, Gaussian (i.e., bell-curve), and almost computable.'

Nassim Nicholas Taleb

6.1. Introduction

Interpretation of the acquired data involved generally identification of the shape, position (spatial location and depth) and the orientation of the buried features considered possible archaeological remains. This was done by analysing successive profiles individually, then integrating to visualise the 3D model blocks considering all the three planes: x, y and the z-plane. Much interest was paid on the z-plane, which presents depth from the surface of the block. The data were mainly acquired using the 270 MHz antennae in the South-North direction. In some squares, it was necessary to repeat the same either by a 270 MHz antenna in the west-east direction or by a 900 MHz antenna in the south-north direction. This was necessary to avoid missing out data during data acquisition. It should be noted that the time window was converted to the depth window. This was done by the identification of the velocity of wave propagation by hyperbolic curve fitting. Once the velocity was identified, it was applied in the software and the depth was determined.

The recent research conducted by De Mann et al [7] employed EMI and GPR surveys and linked the findings to the settlement structures of the site by the Romans. There is an existing wall seeming to be separating the area but much about it is not known. The excavation made in 1980 exposes remains from building structures, broken bricks, some concrete works which probably could be walls of ancient buildings. The 2013 GPR survey used this excavation to determine the dielectric constant that was used in depth determination. In 2015, another excavation was made, this time from part of square -3C and ascertain the existence of rubbles of bricks, concrete and stones. These are not in a particular order; probably they are heaps of

demolished structures. These lie from a depth of roughly 30 centimetres from the surface going down to some 1.5 to 2 metres, thereafter is an existing bedrock.

6.2. Data interpretation from the first phase of data acquisition

The first phase of data acquisition involved collecting data from the two major paths and one perpendicular section. *Figure 6.1* below shows the processed radargrams and the anomalies present.

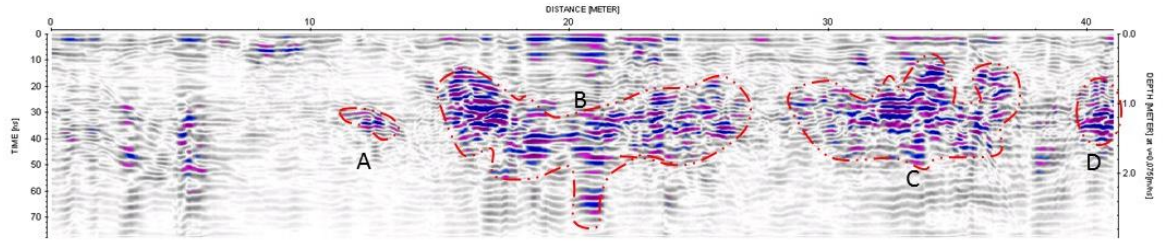

a) Path 1, first parallel line (41 m)

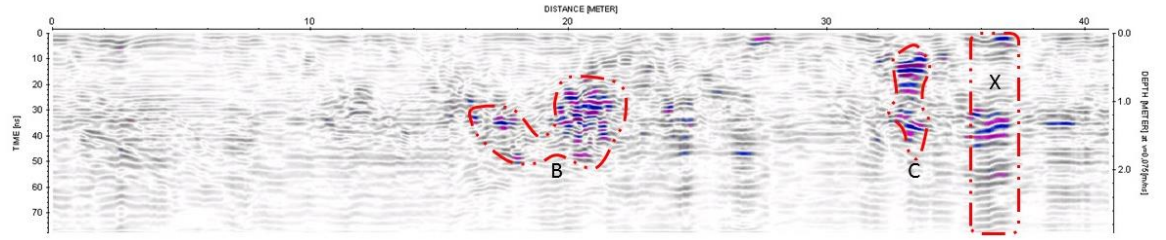

b) Path 1, second parallel line (41 m)

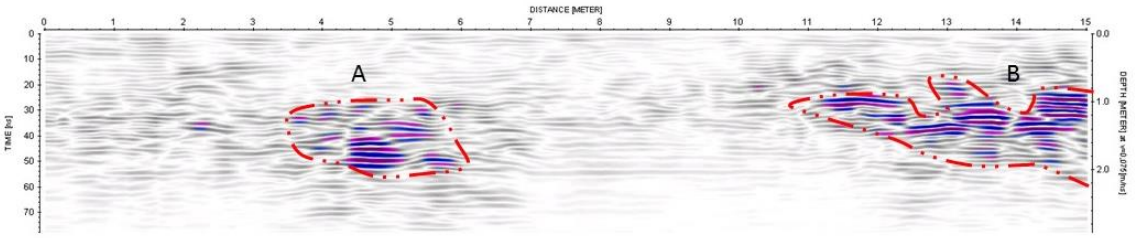

c) Perpendicular section to Path 1, 15 m

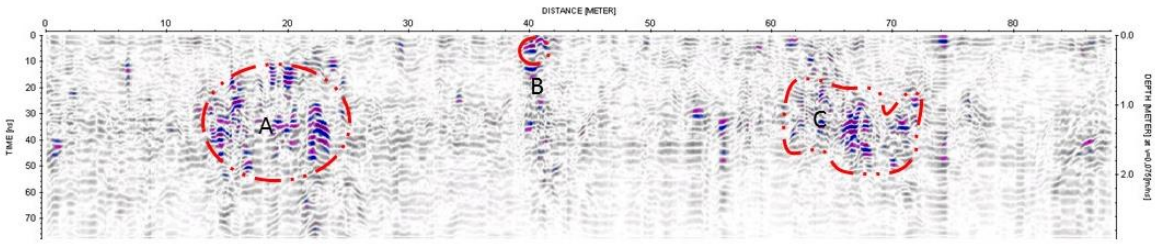

d) Path 2, 88 m

Figure 6. 1: Radargrams from the major paths showing anomalies

Profiles taken by using the 900 MHz antenna are not clear for interpretation. They contained clutter that might mislead the interpretation. In view of this, it was decided to use the data taken by the 270 MHz antenna for the interpretation.

Figure 6.1 (a) shows four main clusters of anomalies labelled A, B, C and D, and *Figure 6.1(b)* is the profile from the corresponding parallel line. Features shown in these radargrams look somehow similar indicating a stretch of dispersed anomalies across the path. *Table 6.1* summarises this.

Table 6. 1: Summary of clusters of anomalies for the first phase

Section		Length	Clusters	Horizontal distance (m)	Vertical distance (m)	Remarks
Path 1	1st Parallel	41	A	11.8-12.6	1.7-2.0	
			B	15.0-26.0	0.8-2.4	
			C	31.0-34.8	0.6-1.8	
			D	40.0-41.0	1.4-1.8	
	2nd Parallel	41	B	15.9.0-22.0	1.0-2.7	
			C	32.2-33.8	0.4-2.0	
			X	35.5-37.5	Whole	Ringing
Perpendicular section		15	A	4.2-5.4	1.8-2.6	
			B	11.0-15.0	1.1-2.3	
Path 2		88	A	13.0-23.0	0.8-2.6	
			B	39.0-42.0	0.0-0.2	
			C	60.0-76.0	0.8-2.5	

The anomaly labelled A in the first parallel line is not seen on the second; it ends and does not continue to the other side of the path. The anomaly labelled B in both profiles (shown in *Figure 6.1(a)* and *&.6.1(b)*) shows the anomaly lies across the path and it is diminishing as going the second parallel profile along the path. Anomaly C crosses from first to second parallel lines. X in *Figure 6.1(b)* represents a ringing; it lies in a range of reverberation from the surface down to the end depth. There are many reasons for a ringing, but in this case, it cannot be established unless it was observed during fieldwork and investigated. From *Figure 6.1(a)* and *(b)* anomaly B can be linked to the findings of the excavated area from 1980. The points lie at 20 m (mid-point) where *Figure 6.1(c)* was taken to the excavated area. This therefore, can lead to the

interpretation of B as being possible remains of walls from the ancient buildings as evidenced by the excavation.

In the perpendicular line that joins the first path to near where it was excavated in 1980, there are two main anomalies labelled A and B (*Figure 6.1(c)*). The estimated depth and location of these points is as shown in *Table 6.1*. These two anomalies can also be linked to the findings of the excavated area. They might be walls remaining from the old buildings.

The second path, as shown in *Figure 6.1(d)* comprises two main anomalies A and C as summarized in *Table 6.1*. B was interpreted as a possible archaeological feature. Walking around the top of the hill, where the path passes, one can notice the existence of rocks and broken concrete works aligned as walls and in some places in heaps. These are observed from the surface. Feature B can therefore be possibly remains of old structures. A and C can be some buried features or rocks in the underground. They might not be linked to any of the remains of old structures but rather, geological. There are some man-made structures at the plateau which shows that there were buildings at the top of the hill. The path starts from the main path going up to the top of the hill.

6.3. Data interpretation from blocks

Data interpretation from the blocks involved the interpretation of the anomalies lying within blocks. It was observed that in most of the area, there were broken bricks and stones possibly from walls or floors of old buildings. Part of square -2C was excavated and exposed these broken materials but does not show any existing remains of walls and floors. These materials could be demolished walls of ancient buildings either from the spot or from somewhere else and were just dumped on this area. At the top of the hill, there were some remains of old building walls, heaped rocks and some lines made of stones aligned as walls. The main purpose of the interpretation was trying to establish the continuity of the anomalies if they can form some shapes or lines, which would form identifiable structures. This is why lines or circles were drawn on scattered clusters of anomalies to visualise if they form a particular continuity within or outside the blocks. Each block was analysed and interpreted before the adjacent blocks were integrated to test for continuity of the anomalies.

To do the interpretation of the blocks, the processed radargrams from the squares were integrated into a 3D block for each square. Then the slices from each plane were extracted, analysed and used for the interpretation. The analysis involved the connection between the observed anomalies in the X, Y and Z planes to establish how the anomalies are distributed in the block. Where two or more surveys were conducted in the same square, the cuts (slices) from the other surveys were compared and noted for some differences and possible omitted information.

6.3.1. Block -3C

Three GPR surveys were conducted in this square: i) using a 270 MHz antenna in the south-north direction, ii) using a 270 MHz antenna in the west-east direction and the last iii) using the 900 MHz antenna in the south-north direction.

Generically, it was observed that the anomalies are scattered throughout the whole block ranging from the depth of 0.8m to 2.0m. *Figure C.1* and *Figure C.2* in *Appendix C*, show that much anomalies lie between 1.046 m and 1.8m. However, at some instances the depth of the anomalies extended down to 2.8 m. This depth of anomalies exists from 6 m to 8.4 m when observed from the east-west direction (along the x-cuts) as shown in *Figure C.1*. Observing from *Figure C.2*, there are less anomalies and lying upper side of the block in the west and to the east, the anomalies lie almost the whole depth.

The time slices, *Figure C.3* shows that the stretch[1] of anomaly started appearing at 0.92 m from the surface, showing anomalies covering the whole part of the block up to 2.0 m and at 7.0 to 8.4 m from the west and 0.0 m to 3.0 m from the south existing a patch[2] of anomaly to a depth of 2.8m.

Results from a 900M Hz antenna shows that anomalies start appearing as early as 0.6m from the surface and ends at 1.9m. The stretches in the *x*-direction and *y*-direction are scattered throughout the block like the way it is observed using the 270 MHz antenna.

[1] A continuous area of anomalies usually covering a wider part of the block
[2] A small area of anomalies within the block

The stretch of anomalies in this square can be interpreted as rubbles comprising the broken bricks and stones from old buildings. These are scattered in the square without any order, as there is no evidence of a line segment that might be interpreted as a wall within the block. However, to the western end there is a stretch of anomalies filling almost the whole depth of the block, forming like a curved line from south east curved towards north-west. This deeper anomaly can be a wall. There is a stone wall forming somehow like a boundary between the lower side and the upper one. This is easily observed when walking on the surface lying on the eastern side of the surveyed site. When observing from the depth slices, from the upper cuts, it is difficult to distinguish the existence of the probable wall lying to the western side of the block, unless one observes deeper than where the scattered rubbles lie, a curved stretch of the anomalies can be seen.

6.3.2. Block -2C

In this square, only seven profiles were taken due to the accessibility of the square to the moving cart. These files were enough to generate a 3D block that was used for the interpretation of the data.

Generally, the stretch of anomaly decreases in depth as going up north, *Figure C.4* in *Appendix C.* The north is the higher side of the slope, so it is expected the overlaying of the broken bricks and stones to spread downwards (to the lower side of the slope). A stretch lying from 0.2 m to the very end of the square in the west to east direction ranging at depths between 1.0 m to 2.6 m. The depth kept increasing a bit to 2.8 m. This goes up to some 6.0 m from the south, and the patches of anomalies reduces as going up the north. The distribution of the anomalies in the west-east direction is almost equal until 3.66 m when the patches split into two spreading in the ends and then diminishes as going up north. *Figure C.5* illustrates this.

Looking from the y-cut, a stretch starting from 1.0 m stretching northward to the very end of the square at a depth range of 1.0 m to 2.2 m. 60 centimetres away, the stretch only exists in the south side, up to 4.0 m. The longest it goes to the north is 7.5 m but not much patches of anomalies are registered there. The depth range as shown in *Figure C.6* is 0.578 m but with very few anomalies, more exist from a depth of 0.9287 m and ends at 2.331 m. There is a gap of the anomaly from 7.0 m. This gap lies at 10 m along the south-north direction from depths 1.8 m to 2.3 m throughout the block.

Interpretation of these anomalies are simply the rubbles from old buildings as evidenced by the excavation made in the quarter part of this square in the year 2015. Walking on the site, one easily observes an existing wall passing diagonally in the block. However, this wall cannot be seen from the images since the rubbles are lying all over the block and the waves do not differentiate these two. The wall is between the thicker parts of the anomalies. The existence of the wall might have lied in the deeper part of the anomalies: passing diagonally in the north western side of the block.

6.3.3. Block -3B

The spreading of the anomalies is relatively uniform with two main stretches of anomalies lying along the *x*-axis (from south to north), *Figure C.7* in *Appendix C*. The first stretch appearing from the beginning measuring roughly 3.5m in length from the south at 0.2 to 2.3m depth and ranges from 0.0m to 0.5m eastwards. The second stretch from 3.06m to 3.94m then reduces in size gradually. It then starts increasing in size from 5.26m stretching to end of the block at a depth range of 0.8m to 2.6m.

In the west-east cut, two long stretches from 0.0m to 4.4m and another one starts from 5.0m going slender all the way to the end of the square. The first main stretch lies at depth range of 0.4-2.0m and reducing to 1.1-1.6m. The second one is long and slender, stretching at a depth of 1.1-1.6m. Other smaller ones lie below these two main ones: the first lies from 1.0m to 2.8m at 1.6-2.0m while the other is at 5.4-6.0m at 1.8-2.1m deep. There are two patches at 6.4-7.0m at the depth of 1.0-1.2m and 2.2m deep at 6.0-6.3m. Another anomaly starts from 1.2m to the end of the square, stretching from 8.0m to the end and increases westwards to 5.0m from the west. Another stretch appears from 1.8m from west to the end and lies at the middle of the survey line, 3.0-5.8m at depth range 0.6-2.2m.

Figure C.9 shows the time slices with two lines lying side by side in the south-north direction. The anomalies start ranges at the depth of 0.11m to 2.6m.

The anomalies from this square can be linked to the findings in square -2C and is presumed to be the scattered broken bricks and stones. There is some resemblance of some lines as viewed from the time slices. There might be remains of walls from old buildings. This can only be confirmed by excavation or after integrating with neighbouring squares.

6.3.4. Block -2B

Block -2B shows that the anomalies are spread almost throughout the whole block at depths from 0.578-2.098m from the surface, with some little patches existing in some parts down to 2.68m especially to the north-eastern part from 4.0-9.5m and 0.0-2.0m, *Figure C.12. Figure C.10* shows the anomalies cover almost the whole block when going along the survey line, but with a void at 1.5-3.0m.

The Y-cuts shows that the existence of the anomalies start appearing from 0.6m from the start of the survey, with more concentrations at 3.0-10.0m at depths between 0.5-2.68m (*Figure C.11.* The anomalies exist in the whole block. From 3.6m along y-plane, they tend to reduce from 7.0-10.0m along the x-plane, at the depths between 0.5-1.2m.

The anomalies lying in this block can be rubbles of bricks and stones from old buildings either on the same site or on somewhere else and they were dumped on the site. There are still some possibilities of having some wall remains especially in the north-eastern part where anomalies are seen up to 2.68m deep.

6.3.5. Block -1B

In this square, one main anomaly stretches from the south to north covering the whole block. There are some parts with more concentrations of the anomalies than the others, but generically, it is the whole block covered by these anomalies. They lie in depths from 0.461-1.396m. Some dispersed patches exist up to 2.448m deep and some even closer to the surface from 0.11m. *Figure C.13 to Figures C.15* in *Appendix C* and *Table 6.2* show all these. *Table 6.2* shows the existence of a reverberation at 8.34-9.66 m in the south-north direction. The cause of this cannot be established unless the surface was inspected is there was an object on the surface causing this.

As viewing from *Figure C.15* two linear stretches can be observed from 0.811m to 1.2709m from the surface diagonal to the square from southeast to the north western side. This can be interpreted as an existing wall of the ancient buildings on the site. The block is near the excavated area, the 1980 excavation that exposes the existing walls of old buildings.

Table 6. 2: Table showing the lengths and depths ranges of anomalies in block -1B

Block -1B											
S-N	**0.42**	**0.86**	**1.3**	**1.74**	**2.18**	**2.62**	**3.06**	**3.5**	**3.94**	**4.38**	**4.82**
Length	0-7.2	0-7.2	0-7.2	0-7.2	0-6.0	0-7.2	1-5.5	2-6.3	0-7.2	0-7.2	0-7.2
Depth	0.11-2.4	0.11-1.7	0.1-2.0	0.11-2.4	0.11-2.4	0.1-2.0	0.11-1.6	0.11-1.8	0.1-2.4	0.1-2.2	0.1-2.2
S-N	**5.26**	**5.7**	**6.14**	**6.58**	**7.02**	**7.46**	**7.9**	**8.34**	**8.78**	**9.22**	**9.66**
Length	0-7.2	0-7.2	0-7.2	0-7.2	0-7.2	0-7.2	0.2-7.2	6-7.2	6-7.2	6-7.2	6-7.2
Depth	0.1-2.2	0.1-2.0	0.1-2.0	0.1-2.4	0.1-2.0	0.1-2.4	0.1-2.4	0-2.6	0-2.6	0-2.6	0-2.6
Comments								Reverberation			

a) Lengths and depts. Ranges of anomalies when going south-north direction in the block

E-W	0	0.6	1.2	1.8	2.4	3	3.6
Length	0-10.0	0-10	0-10.0	0-10	0-10.0	0-10	0-10
Depth	0.1-1.6	0.1-2.2	0.1-1.2	0.1-2.6	0.1-2.6	0.1-1.2	0.1-2.2
E-W	4.2	4.8	5.4	6	6.6	7.2	7.8
Length	0-10	0-8.6	0-8.6	0-8.0	0-10	3.0-10	
Depth	0.1-2.0	0.1-2.1	0.1-2.4	0.1-2.6	0.1-2.0	0.1-2.2	

b) Lengths and depths ranges of anomalies when going east-west direction in the block

6.3.6. Block -4C

Figure C.16 to Figure C.18 show the main stretch of anomaly in both directions ranging at depths from 0.4611m to 2.682m, with much heavily packed at 0.6949 to 2.0m. The most noticeable arrangement of the materials in the block is that, the thickness of the anomalies decreases as going up the north. No any defined order of the placed materials within the block. There is much doubt that there can be an existing wall within the block. There might be a wall and it was demolished, leaving behind the rubbles of concrete, stones and bricks, or either nothing like that ever existed but rather the rubbles were just dumped from somewhere upper.

6.3.7. Block -5C

In this block, there is also a stretch of anomalies lying to both directions. The anomaly starts at a depth from the very near to the surface, but much of them are found at 0.6949m to 2.331m. This can be viewed from any side as shown in *Figure C.19 to Figure C.21*. There is no noticeable order of the anomalies in the block. This is simply the same as the block -4C that is linked to the spreading of the rubble materials from old buildings.

6.3.8. Block -6C

In this block, as shown by *Figures C.22* to *Figure C.24* in *Appendix C*, the anomalies are found in the whole block spreading in both directions. In the south-north direction, there is a void from 1.3-2.18m from the south. The void is having a maximum width of 0.6m, located between 3.0-3.611m along the eat-western direction, *Figure C.22*. *Figure C.24* shows that the anomalies a found at a depth range between 0.461m and 2.331m. It also shows a thin line in the middle of the square especially at depth between 1.396-2.098 separating the stretch of anomalies.

All this does not show anything of interest rather than the scattered rubbles of building materials from the ancient structures.

6.3.9. Block -2A´

A comparison between the slices from the W-E and S-N directions using the same antenna frequency shows some common and similar features but the ones from a S-N direction shows a lot of doubts. The survey might be affected by some noise maybe due to improper configuration or improper shielding of the antenna. The discussions and interpretations are based on the W-E direction.

Figure C.25 shows three main anomalies, A, B and C that joint at 3.5m from the west and form one stretch of anomaly to the rest of the block. A starts from beginning of the block at a width from 0-1m in the south-north direction. The anomaly increases in its width to up to 0-4.0m. B runs in parallel with A, from 0.42m to 1.7m where it joins A and form one stretch. This stretch

extends to 3.5m and joins C forming one stretch covering the whole block. C is the longest strip of anomaly in the block running from 0.42-2.18m.

In the south-north direction, *Figure C.26* the first noticeable is marked X, this is avoid located at 5.4m. the block is filled with anomalies in both directions until 7.8m where two main anomalies can be noticed. These are marked 1 and 2, *Table 6.3* describes these anomalies. From 8.4m, anomaly marked 3 emerges from 1 and then, therefore three anomalies are noticed to the end of the block. *Figure C.27* shows that the anomalies were noticed from very near the surface at the depth of 0.1104m to 1.513m. Some little patches of anomalies were noticed up to 2.8m deep. It can be noticed that in the south part, the anomalies fill the whole block with no any voids, but this breaks into some stretches as going up north.

Generally, in the W-E direction three anomalies are noticeable from 0-3.50m, thereafter, the whole block is filled with a big stretch across the whole block. The block is at the top most of the hill (castro). Where there are anomalies is the higher part and to the lower side (east side) lies a stretch filling the whole block. The individual anomalies to the higher side might be remains of walls of old buildings while the lower side might be filled with broken bricks and stones. Likewise, in the S-N direction, the separate anomalies lie in the northern part which happens to be the higher side. The patches of remains can be noticed while in the lower side of the block (south) has a lot of scattered broken bricks and stones. Walking on the surface, one can notice the existence of some wall remains and some heaped rocks on the surface. It is not easy to establish the shape of the lines or walls within this site.

Table 6. 3: Summary of anomalies in block -2A´

W-E				
Anomaly	**Length**	**Width**	**Depth**	**Comments**
A	0.42-1.3	0 to 3.0-4.0	0-2.1	A, B and C join at 3.5m from the west and fill the whole block to the end
B	0.42-1.3	2.0-6.0/4.6-7.5	0-1.2	
C	0.42-2.18	8-9.6	0.5-2.0	
S-N				
X	5.4	2.1-4.5	0.2-1.0	Void
1	7.2-9.6	2.8-7.0	0-2.6	
2	7.8-9.6	9-10.1	0-2.6	
3	8.4-9.6	0-2.1	0-1.8	

6.3.10. Block -3A´

Figures C.28 to *Figure C.30* show the block filled with the anomalies from top to bottom of the survey. No specific points can be viewed from either side: south-north and west-east directions. Viewing from the top going down the block, *Figure C.30*, the anomaly starts right from the surface, at 0.0835m going down to 1.582m. This can be a bedrock from the very near to the surface going down the block.

6.3.11. Square +7D'

Figures C.31 to *Figure C.33* do not show any interesting features from either side. The anomalies are just spread all over the square in all directions spreading at depths from 0.69 to 2.3m. No specific order can be observed in the square. A small anomaly noticed in the south-north direction from 0.42m, it keeps increasing its size until 2.18m where the increment filled the whole block. These can also be interpreted as possibly broken bricks and stones scattered in the block. No traces of remaining walls could be established unless it could be excavated and confirmed.

6.4. Integration of adjacent squares

One of the specific objectives of this research project was to test for the continuity of anomalies within the adjacent squares. It can be noted from the previous discussion of individual blocks that interesting features are found at an area covered by blocks -1B, -2B, -3B, -2C and -3C and at the top of the hill where there are blocks -2A and -3A. It was therefore necessary to pay much attention in these adjacent blocks.

6.4.1. Parallel lines in between squares -2C, -2B, -3C and -3B

Three survey lines each 20.0m were taken between the squares -2C, -2B, -3C and -3B passing from point 67 through 59 to 51. These three lines show a continuous anomaly from south to

north in the four squares. The radargrams show that in all the three lines, there is a stretch of anomalies from the beginning of the two squares, squares -3C and -3B from the south to north crossing the squares to the adjacent squares, -2C and -2B and ends at 15.0m. The three profiles have been integrated into a 3D block of 20.0 in length by 1.2m in width by 2.8m depth. *Figure 6.2* shows this 3D block. It therefore indicates that the four adjacent blocks have features in common, all connected to the possible remains of archaeological in nature.

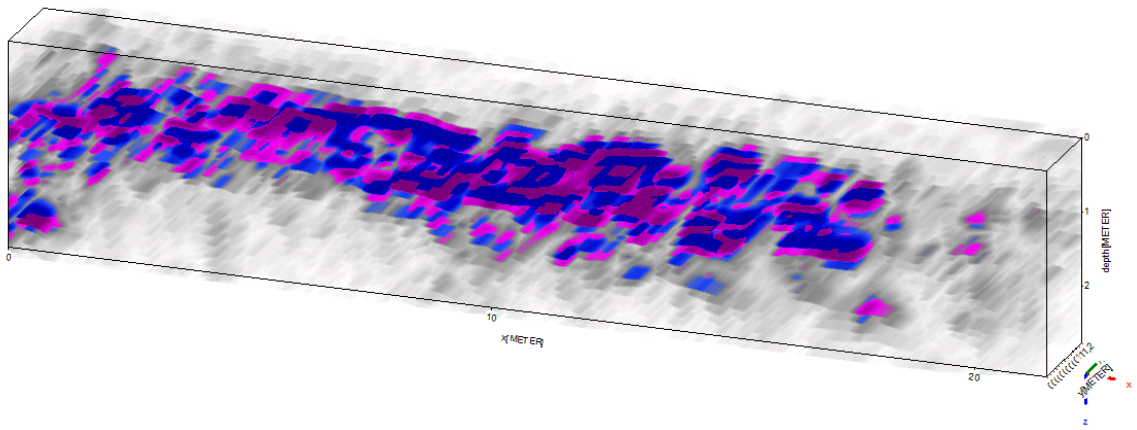

Figure 6. 2: A 3D block showing features to be related to the archaeological remains in between the four blocks

6.4.2. Levels of the blocks

The blocks in the investigation were explored by integrating the depth slices in three layers and observe the possibilities for continuities of anomalies existing from one block to the other. Generically, most anomalies were observed from 50 cm to 80 cm, with more concentrations up to around 1.5 m. in some areas, it was going down to 2 m or even more. Interpretation in individual blocks shows specifically how deep the anomalies were observed. In view of this, three levels were determined to be 50 cm, 1.0 m and 1.5 m. The images from the blocks could not fully fit the squares because, not all the parts of the square were accessible during data acquisition. This therefore, made it not practically possible to acquire data from the whole square. In most cases, the data collected resulted in a rectangular shape of an image.

In general, more anomalies are noticed at 1.0 m from the surface (*Figure 6.18*), near the surface, at 50 cm, less anomalies are noticed. When going up north, which is the higher side, the number

of anomalies noticed reduce, and the bedrock can be seen very near to the surface. As has been interpreted that these are likely to be the broken bricks and stones from the old buildings, and are scattered in the area. It is likely that most of these will be found in the lower part than the upper. The distribution of the anomalies is thicker down south than the north.

Figure 6.17, shows the anomalies at level 0.5 m. There are three main continuities in the level; A, B and C. A is a continuity to the west of the squares. It lies in square -3C and -2C along the stone wall observed. This can be scattered broken materials from old buildings lying along the stone wall. B lies in square -2B and -1B in the south-north direction. It cannot be ascertained if it is a wall, unless it is excavated to confirm. It is still possible to think that B can be a remain of a wall as that there are wall remains observed in the excavation made in 1980 near the squares up north. C is just showing a continuity in the two squares -2A´ and -3A´, no specific order is observed rather scatters in the squares. On the surface, walls and heaps of rocks are observed.

Figure 6.18 shows almost the same observed anomalies in level 0.5 m. the difference is that there are a lot of scattered anomalies in squares -3C, -4C, -5C and -6C. There are no features observed in these squares. It is thought that these might be scattered materials from destroyed old structures. The bedrock is found a bit deeper as compared to the northern part where there is square -1B

Figure 6.19 shows less anomalies as compared to those observed in level 1.0 m. anomaly B is not seen here. It is because the bedrock is near to the surface. There are even less observed scattered materials in squares -3C south to -6C and the bedrock can be observed. The anomalies A and C observed at this depth might prove that these are wall remains passing in these places to some depths.

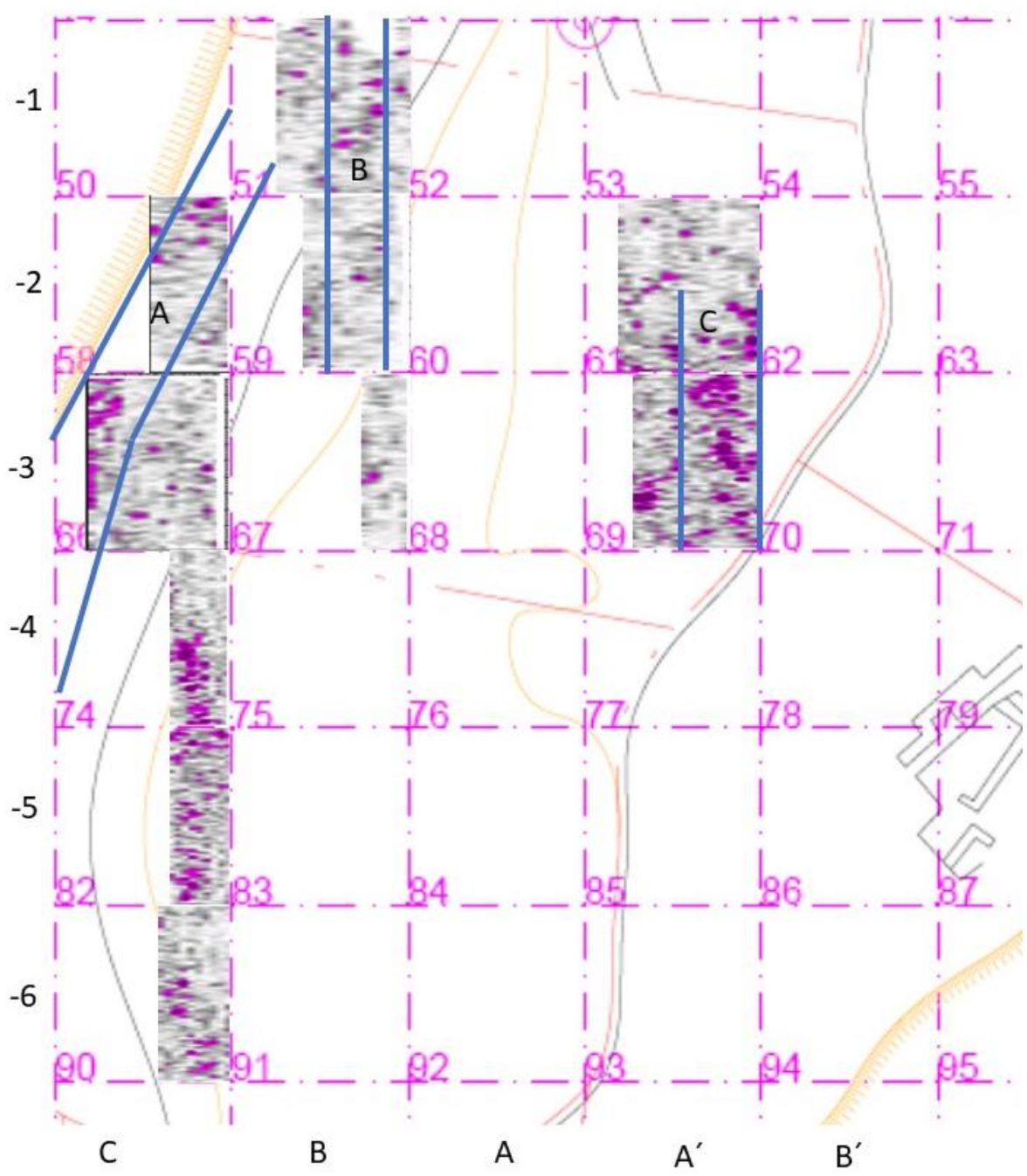

Figure 6. 3: A sketch map showing anomalies in the squares at 0.5 m from the surface

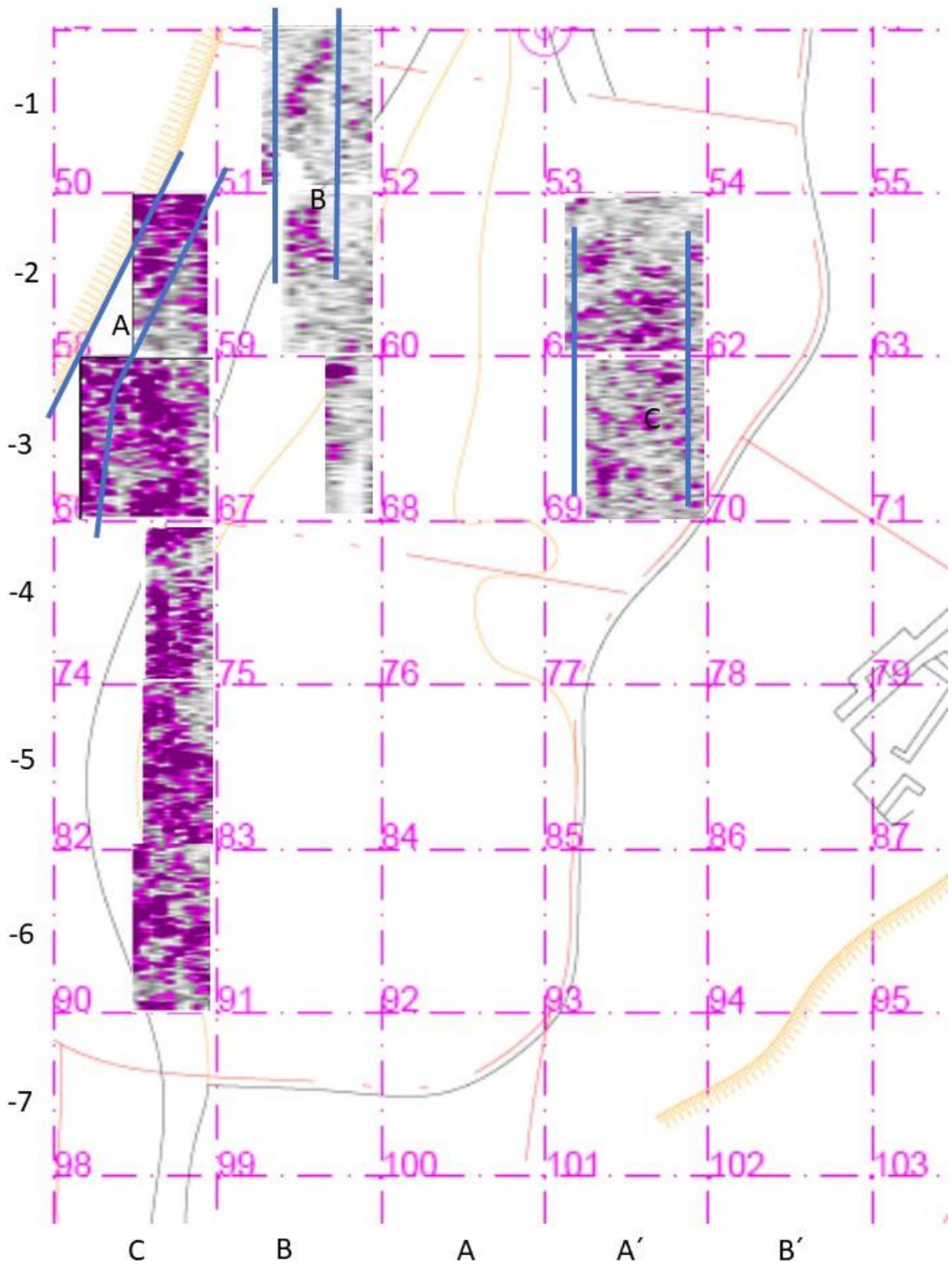

Figure 6. 4: A sketch map showing anomalies in the squares at 1.0 m from the surface

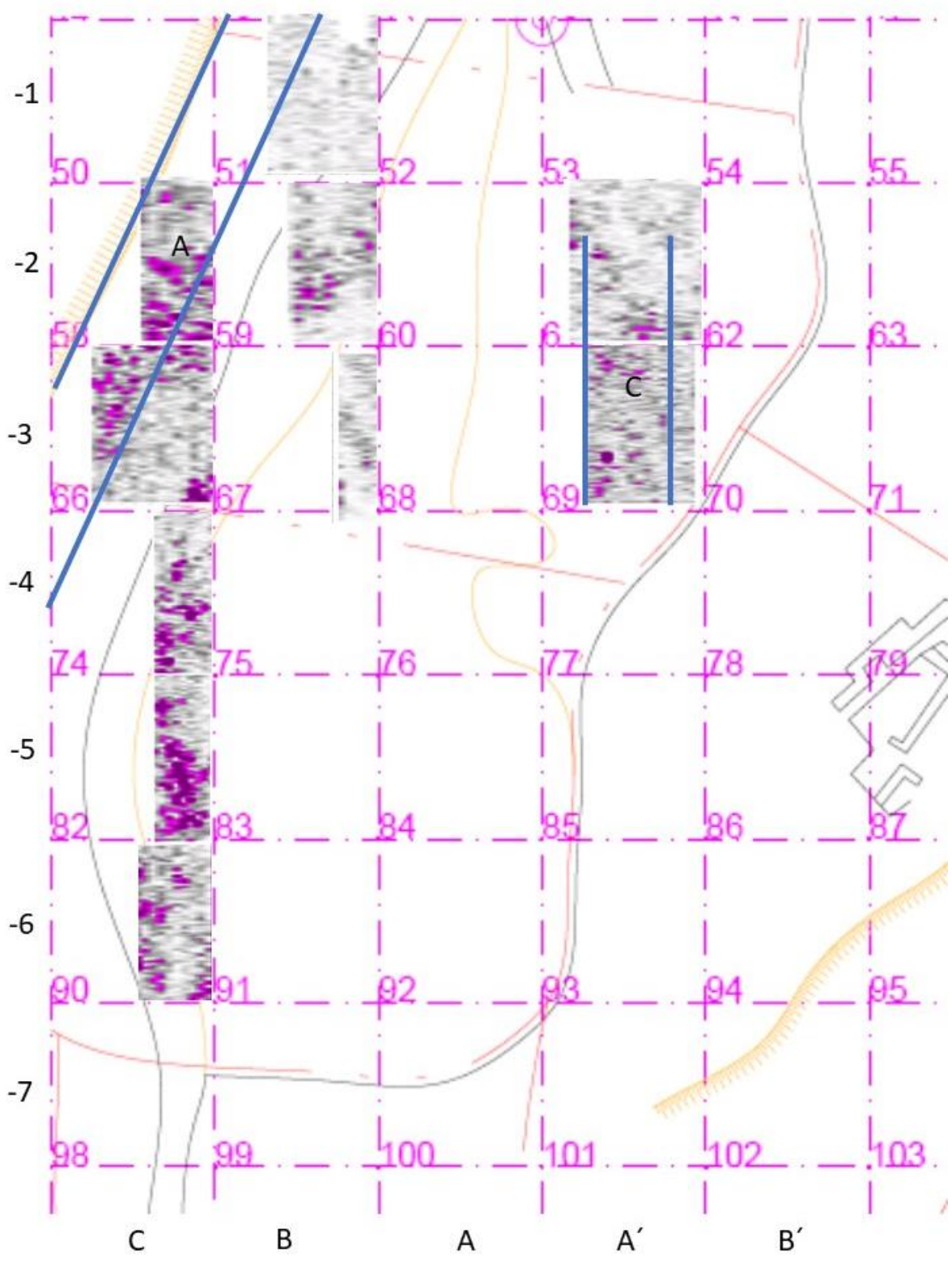

Figure 6. 5: A sketch map showing anomalies in the squares at 1.5 m from the surface

6.5. Conclusion

The interpretation of the data from Castro de Ul involved mainly the detection of the stretches of anomalies within and across the blocks. This was to test for the continuity of the anomalies from block to block. The use of different antennas and in different directions helped not to miss out some important features that would be linked to the possible archaeological remains.

The general trend of the anomalies at the site is that, there are a lot of anomalies scattered and distributed without any defined order in the southern part of the area. These were interpreted as possibly destroyed materials from old buildings. There were no traces of walls or floors, rather the existing of these materials. The materials could be from the demolished old buildings either right on the place or from somewhere else and was dumped on this site. When going up north, the anomalies are arranged in a certain defined orders and continuity. These could be possible walls of old buildings. Two excavations on the site confirmed the possible interpretation of the squares. This therefore, would mean that the structures were located up north and down there were no buildings. There is a stone wall to the western side of the surveyed area marking a boundary between the area.

7

DISCUSSION AND CONCLUSION

"*The future depends on what you do today*"

-Mahatma Gandhi-

Ground penetrating radar is a very useful too in archaeological studies. It has been used for decades of years and has been recommended by several researchers because of its non-destructive and high resolution nature. However, a good work must be coupled with a good workmanship in both the field and during data processing. Mistakes in the field cannot be corrected even if one is using very sophisticated software to process and interpret the data. It therefore leads to wrong interpretation of the data.

The work of data processing and interpretation of archaeological data from Castro de Ul involved the processing of the GPR data that were acquired from the field in 2013 using the Terra SIRch SIR System-3000 by Geophysical Survey System Inc. (GSSI). The data was processed using software ReflexW by Sandmeier Geophysical Research. The acquired processed data, that was in a 2D radargrams was integrated into 3D blocks and interpreted for the possible features to be considered of archaeological in nature.

The interpretation shows the possible existence of archaeological features that would be the remains of old structures on the site. The first phase of data interpretation, which involved the interpretation of the data acquired from the main two paths revealed the existence of some possible features of archaeological in nature in places near the excavation that was made in 1980 on the site. These features may be linked to the findings on the excavation, more possibly can be wall remains as the excavation shows the existence of the wall remains.

The main work was the interpretation of the data acquired from the eleven squares on the site. This work showed the existence of buried features almost in all the squares investigated with a few observed structures that might be linked to the remains of old structures. There are some continuities of anomalies in the squares especially near the excavation made in 1980. This

might mean that the findings here might be wall remains as observed in the excavation. Another excavation was made in 2015 and shows scattered destroyed materials from old structures. This links the findings from the lower squares (squares to the southern part of the site) as being the scattered destroyed materials.

It was observed that to the northern part, and the top of the hill, there existed some structures of anomalies. In these parts, the bedrock was observed very close to the surface.

The research observes that scattered anomalies were mostly observed from 50 cm from the surface, and much of them were concentrated at depths 1.0 m to 1.5 m, but still in other parts, the anomalies could be observed as 2.0 m from the surface. Findings from the 2015 survey that was conducted by De Mann et al [7] which employed GPR and Electromagnetic Induction found out that most data were found at depths ranging from 25 cm to 2.0 m, with more consistency at 75 cm and 1.0 m.

7.1. Limitations

The interested area for the archaeological studies is big, with demarcated squares. It was only a few squares that were accessible by the equipment. This was either due to obstacles such as trees that cover the area or the steepness of the slopes that could not accommodate the moving of the cart for data acquisition.

The data were not acquired with the GPS mounted and therefore do not have the coordinates. This limited the integration of the squares using the software. It would be easier if the data were acquired with a GPS, the software would integrate the squares and produce models that would be used in the interpretation. Again, the use of GPS allows the software to interpolate the data entered from the different directions of the survey.

7.2. Recommendations for future GPR work

It is recommended for future similar work to get as much data as possible using different directions in each square. Since there are some obstacles on the site, other methods such as

magnetic and electrical can be employed to have access in data collection in places impassable by the moving cart.

The data acquisition should be accompanied by a GPS which gets the coordinates of the data acquired. This shall make it better and easier in the processing and modelling of the integrated data using the software. Data collected without the GPS needed to be organized and ordered before integrated into 3D files, for managing many data; this would be tedious and erroneous.

The interpretation would be more interesting if other approaches were applied on top of using ReflexW. It is suggested to apply geostatistical analysis in the data acquired in order to interpolate and interpret the data. The use of geostatistcs in the interpretation would help compare the results and possibly clear out some doubts encountered in the interpretation.

Data acquisition was done in profiles at 60 cm apart, this distance may be too large considering that some anomalies might be small and possibly be missed out. It would be recommended to reduce the spacing in the future work. Data collected close to each other would give more information for interpretation.

REFERENCES

1. Wenke Zhao, E.F., Michele Pipan, Gang Tian, *Gorund Penetrating Radar (GPR) attribute analysis for archeological prospection.* Journal of Applied Geophysics, 2013. **97**: p. 11.
2. Yelf, R.J., *Application of Ground Penetrating Radar in Civil and Geotechnical Engineering.* Electromagnetic Phenomena, 2007. **7**(18): p. 16.
3. Porsani, J.L., G. de Matos Jangelme, and R. Kipnis, *GPR survey at Lapa do Santo archaeological site, Lagoa Santa karstic region, Minas Gerais state, Brazil.* Journal of Archaeological Science, 2010. **37**(6): p. 1141-1148.
4. van der Kruk, J., E.C. Slob, and J.T. Fokkema, *Background of ground penetrating radar measurements.* Geologie en Mijnbouw, 1998. **77**(2): p. 177-188.
5. Qin, H., et al., *Underground structure defect detection and reconstruction using crosshole GPR and Bayesian waveform inversion.* Automation in Construction, 2016. **68**: p. 156-169.
6. Conyers, L.B. and D. Goodman, *Ground-penetrating Radar: An Introduction for Archaeologists*. 1997: AltaMira Press.
7. De Man, A., J.T. Tavares, and J. Carvalho, *GPR AND ELECTROMAGNETIC INDUCTION SURVEYS AT THE HILLTOP SITE OF UL (OLIVEIRA DE AZEMEIS, PORTUGAL).* Mediterranean Archaeology & Archaeometry, 2017. **17**(1): p. 179-188.
8. Unknown. *Município de Oliveira de Azeméis*. 2017 [cited 2017 21 February]; Available from: https://www.cm-oaz.pt/oliveira_de_azemeis.1/localizacao.39/localizacao.a53.html.
9. Santos J.M. and Pereira E, *Geochemical and Metalogenic Specialisation of some Hercynian Granitoids from Northern Portugal.* p. 115-119.
10. Unknown. *Castro de Ul*. 2012 January 30 2012 [cited 2017 21 February 2017]; Available from: http://azemeis-no-passado.blogspot.pt/2012/01/castro-de-ul.html.
11. Sala R, Garcia E, and Tamba R, *Archeological Geophysics-From Basics to New Perspectives.* Archeology, 2012: p. 133-166.
12. Anghel, S. and T. Bruster, *Geophysical Methods used in the Archaeological studies of the Ancient town of "Argamum"*. Geo-Eco-Marna, 2007. **13**: p. 23-25.
13. Tsokas, G.N., et al., *Non-destructive electrical resistivity tomography for indoor investigation: the case of Kapnikarea Church in Athens.* Archaeological Prospection, 2008. **15**(1): p. 47-61.
14. Di Fiore, V., et al., *Multichannel Analysis of Surface Waves and Down-Hole Tests in the Archeological "Palatine Hill" Area (Rome, Italy): Evaluation and Influence of 2D Effects on the Shear Wave Velocity.* Surveys in Geophysics, 2016. **37**(3): p. 625-642.
15. Francese, R.G., E. Finzi, and G. Morelli, *3-D high-resolution multi-channel radar investigation of a Roman village in Northern Italy.* Journal of Applied Geophysics, 2009. **67**(1): p. 44-51.

16. Pipan, M., et al., *2-D and 3-D processing and interpretation of multi-fold ground penetrating radar data: a case history from an archaeological site.* Journal of Applied Geophysics, 1999. **41**(2–3): p. 271-292.
17. Shaaban, F.A., et al., *Ground-penetrating radar exploration for ancient monuments at the Valley of Mummies -Kilo 6, Bahariya Oasis, Egypt.* Journal of Applied Geophysics, 2009. **68**(2): p. 194-202.
18. Economou, N., et al., *Advanced Ground Penetrating Radar Signal Processing Techniques.* Signal Processing, 2017. **132**: p. 197-200.
19. Batayneh, A.T., *Archaeogeophysics–archaeological prospection – A mini review.* Journal of King Saud University - Science, 2011. **23**(1): p. 83-89.
20. Wynn, J.C., *A review of geophysical methods used in archaeology.* Geoarchaeology, 1986. **1**(3): p. 245-257.
21. Aziz, A.S., et al., *Locating and characterizing burials using 3D ground-penetrating radar (GPR) and terrestrial laser scanning (TLS) at the historic Mueschke Cemetery, Houston, Texas.* Journal of Archaeological Science: Reports, 2016. **8**: p. 392-405.
22. Fassbinder, J.W.E. *Geophysical Prospection: a Powerful Non-destructive Research Method for the Detection, Mapping and Presevation of Monuments and Sites*. in *The New Technologies for Aquileia 2011*. 2011. Aquileia, Italy: CEUR-WS.
23. Epov, M.I., et al., *Integrated archeological and geophysical studies in West Siberia.* Russian Geology and Geophysics, 2016. **57**(3): p. 473-482.
24. Vaz, F.C., et al., *Iron Age ovens and hearths from the hilltop of Quinta de Crestelos, Sabor Valley (NE Portugal): An archaeobotanical approach on typology, functionality and firewood use.* Quaternary International, 2017.
25. Figueiredo, E., et al., *Smelting and recycling evidences from the Late Bronze Age habitat site of Baiões (Viseu, Portugal).* Journal of Archaeological Science, 2010. **37**(7): p. 1623-1634.
26. Tereso, J.P., et al., *Massive storage in As Laias/O Castelo (Ourense, NW Spain) from the Late Bronze Age/Iron Age transition to the Roman period: a palaeoethnobotanical approach.* Journal of Archaeological Science, 2013. **40**(11): p. 3865-3877.
27. Chester, D.K., *Pleistocene and Holocene geomorphological development in the Algarve, southern Portugal.* Geomorphology, 2012. **153–154**: p. 17-28.
28. Waterman, A.J., et al., *Environmental change and economic practices between the third and second millennia BC using isotope analyses of ovicaprid remains from the archeological site of Zambujal (Torres Vedras), Portugal.* Journal of Archaeological Science: Reports, 2016. **5**: p. 181-189.
29. Burbidge, C.I., et al., *Luminescence dating and associated analyses in transition landscapes of the Alto Ribatejo, central Portugal.* Quaternary Geochronology, 2014. **20**: p. 65-77.
30. Arias, P., et al., *Looking for the traces of the last hunter–gatherers: Geophysical survey in the Mesolithic shell middens of the Sado valley (southern Portugal).* Quaternary International, 2016.
31. Ranieri, G., et al., *Geophysical prospection of the Roman city of Pollentia, Alcúdia (Mallorca, Balearic Islands, Spain).* Journal of Applied Geophysics, 2016. **134**: p. 125-135.
32. Fernández-Álvarez, J.-P., et al., *Discovery of a mass grave from the Spanish Civil War using Ground Penetrating Radar and forensic archaeology.* Forensic Science International, 2016. **267**: p. e10-e17.
33. David J. Daniels, *Ground Penetrating Radar*. 2nd ed. 2004: Institution of Engineering and Technology.

34. Martinho, E. and A. Dionísio, *Main geophysical techniques used for non-destructive evaluation in cultural built heritage: a review.* Journal of Geophysics and Engineering, 2014. **11**(5): p. 053001.
35. Evangelista, L., et al., *Application of ERT and GPR geophysical testing to the subsoil characterization of cultural heritage sites in Napoli (Italy).* Measurement, 2016.
36. Vinod Chandra Tewari, B.V., *Geotechnical Applications of Ground Penetrating Radar (GPR).* Journal, Indian Geological Congress, 2014. **6**: p. 13.
37. Teixidó, T., *The Surface Geophysical Methods: A useful Tool for the Engineer.* Procedia Engineering, 2012. **46**: p. 89-96.
38. Quinta-Ferreira, M., et al., *Contribution of engineering geology for the construction of a new museum gallery over an archaeological site at Lorvão Monastery, Portugal.* Journal of Cultural Heritage, 2015. **16**(6): p. 922-927.
39. Butzer, K.W., *Challenges for a cross-disciplinary geoarchaeology: The intersection between environmental history and geomorphology.* Geomorphology, 2008. **101**(1–2): p. 402-411.
40. Metwaly, M., *Application of GPR technique for subsurface utility mapping: A case study from urban area of Holy Mecca, Saudi Arabia.* Measurement, 2015. **60**: p. 139-145.
41. Basile, V., et al., *A ground-penetrating radar survey for archaeological investigations in an urban area (Lecce, Italy).* Journal of Applied Geophysics, 2000. **44**(1): p. 15-32.
42. Conyers, L.B., *The use of ground-penetrating radar in archaeology A2 - Creagh, D.C*, in *Radiation in Art and Archeometry*, D.A. Bradley, Editor. 2000, Elsevier Science B.V.: Amsterdam. p. 1-14.
43. Eppelbaum, L.V., B.E. Khesin, and S.E. Itkis, *Archaeological geophysics in arid environments: Examples from Israel.* Journal of Arid Environments, 2010. **74**(7): p. 849-860.
44. Leucci, G. and S. Negri, *Use of ground penetrating radar to map subsurface archaeological features in an urban area.* Journal of Archaeological Science, 2006. **33**(4): p. 502-512.
45. Baker, J.A., N.L. Anderson, and P.J. Pilles, *Ground-penetrating radar surveying in support of archeological site investigations.* Computers & Geosciences, 1997. **23**(10): p. 1093-1099.
46. Bellón Ruiz, J.P., et al., *Archaeological methodology applied to the analysis of battlefields and military camps of the Second Punic War: Baecula.* Quaternary International, 2016.
47. Cardarelli, E. and G. Di Filippo, *Integrated geophysical methods for the characterisation of an archaeological site (Massenzio Basilica — Roman forum, Rome, Italy).* Journal of Applied Geophysics, 2009. **68**(4): p. 508-521.
48. Daniels, J.J. and R.L. Roberts, *Ground Penetrating Radar for Geotechnical Applications*, in *Geophysical Characterization of Sites*, R.D. Woods, Editor. 1994, International Science Publisher: New Delhi, India. p. 1-13.
49. Orlando, L., *GPR to constrain ERT data inversion in cavity searching: Theoretical and practical applications in archeology.* Journal of Applied Geophysics, 2013. **89**: p. 35-47.
50. Wiwatrojanagul, P., et al., *A new method to determine locations of rebars and estimate cover thickness of RC structures using GPR data.* Construction and Building Materials, 2017. **140**: p. 257-273.
51. Orlando, L., *Detecting steel rods and micro-piles: A case history in a civil engineering application.* Journal of Applied Geophysics, 2012. **81**: p. 130-138.

52. Negri, S., G. Leucci, and F. Mazzone, *High resolution 3D ERT to help GPR data interpretation for researching archaeological items in a geologically complex subsurface.* Journal of Applied Geophysics, 2008. **65**(3–4): p. 111-120.
53. Leucci, G., et al., *3D GPR survey for the archaeological characterization of the ancient Messapian necropolis in Lecce, South Italy.* Journal of Archaeological Science: Reports, 2016. **7**: p. 290-302.
54. Grandjean, G., J.C. Gourry, and A. Bitri, *Evaluation of GPR techniques for civil-engineering applications: study on a test site.* Journal of Applied Geophysics, 2000. **45**(3): p. 141-156.
55. Dinh, K., et al., *Understanding depth-amplitude effects in assessment of GPR data from concrete bridge decks.* NDT & E International, 2016. **83**: p. 48-58.
56. Xiao, X., et al., *Use of electromagnetic two-layer wave-guided propagation in the GPR frequency range to characterize water transfer in concrete.* NDT & E International, 2017. **86**: p. 164-174.
57. Benedetto, A., et al., *Railway ballast condition assessment using ground-penetrating radar – An experimental, numerical simulation and modelling development.* Construction and Building Materials, 2017. **140**: p. 508-520.
58. Khamzin, A.K., et al., *Utilization of air-launched ground penetrating radar (GPR) for pavement condition assessment.* Construction and Building Materials, 2017. **141**: p. 130-139.
59. Afshar, A., et al., *Geophysical investigation of underground water content zones using electrical resistivity tomography and ground penetrating radar: A case study in Hesarak-Karaj, Iran.* Engineering Geology, 2015. **196**: p. 183-193.
60. Baek, S.-H., et al., *Ground penetrating radar for fracture mapping in underground hazardous waste disposal sites: A case study from an underground research tunnel, South Korea.* Journal of Applied Geophysics.
61. Benedetto, A., et al., *An overview of ground-penetrating radar signal processing techniques for road inspections.* Signal Processing, 2017. **132**: p. 201-209.
62. López-Rodríguez, F., et al., *Analysis of ground penetrating radar data from the tunnel beneath the Temple of the Feathered Serpent in Teotihuacan, Mexico, using new multi-cross algorithms.* Advances in Space Research, 2016. **58**(10): p. 2164-2179.
63. Cui, F., et al., *Application of the Ground Penetrating Radar ARMA power spectrum estimation method to detect moisture content and compactness values in sandy loam.* Journal of Applied Geophysics, 2015. **120**: p. 26-35.
64. Sukhobok, Y.A., et al., *Soil Formation Lithological Profiling Using Ground Penetrating Radar.* Procedia Engineering, 2016. **143**: p. 1236-1243.
65. Fabregat, I., et al., *Reconstructing the internal structure and long-term evolution of hazardous sinkholes combining trenching, electrical resistivity imaging (ERI) and ground penetrating radar (GPR).* Geomorphology, 2017. **285**: p. 287-304.
66. Porsani, J.L., et al., *GPR applied to mapping utilities along the route of the Line 4 (yellow) subway tunnel construction in São Paulo City, Brazil.* Journal of Applied Geophysics, 2012. **80**: p. 25-31.
67. Atef, A., et al., *Multi-tier method using infrared photography and GPR to detect and locate water leaks.* Automation in Construction, 2016. **61**: p. 162-170.
68. Doolittle, J.A. and N.F. Bellantoni, *The search for graves with ground-penetrating radar in Connecticut.* Journal of Archaeological Science, 2010. **37**(5): p. 941-949.
69. Schultz, J.J. and M.M. Martin, *Monitoring controlled graves representing common burial scenarios with ground penetrating radar.* Journal of Applied Geophysics, 2012. **83**: p. 74-89.

70. Schultz, J.J., B.S. Walter, and C. Healy, *Long-term sequential monitoring of controlled graves representing common burial scenarios with ground penetrating radar: Years 2 and 3.* Journal of Applied Geophysics, 2016. **132**: p. 60-74.
71. Fiedler, S., et al., *The effectiveness of ground-penetrating radar surveys in the location of unmarked burial sites in modern cemeteries.* Journal of Applied Geophysics, 2009. **68**(3): p. 380-385.
72. Damiata, B.N., et al., *Imaging skeletal remains with ground-penetrating radar: comparative results over two graves from Viking Age and Medieval churchyards on the Stóra-Seyla farm, northern Iceland.* Journal of Archaeological Science, 2013. **40**(1): p. 268-278.
73. Salsarola, D., et al., *The utility of ground-penetrating radar and its time-dependence in the discovery of clandestine burials.* Forensic Science International, 2015. **253**: p. 119-124.
74. Mohana, M.A., et al., *Discrimination between landmine and mine-like targets using wavelets and spectral analysis.* NRIAG Journal of Astronomy and Geophysics, 2013. **2**(1): p. 54-66.
75. Khan, U.S., W. Al-Nuaimy, and F.E. Abd El-Samie, *Detection of landmines and underground utilities from acoustic and GPR images with a cepstral approach.* Journal of Visual Communication and Image Representation, 2010. **21**(7): p. 731-740.
76. Ferrara, V., et al., *GPR/GPS/IMU system as buried objects locator.* Measurement, 2017.
77. Gonzalez-Huici, M.A. and F. Giovanneschi, *A combined strategy for landmine detection and identification using synthetic GPR responses.* Journal of Applied Geophysics, 2013. **99**: p. 154-165.
78. Gurbuz, A.C., J.H. McClellan, and W.R. Scott, *Compressive sensing of underground structures using GPR.* Digital Signal Processing, 2012. **22**(1): p. 66-73.
79. Annan, A.P. *Practical processing of GPR Data*. in *Second Government Workshop on GPR*.
80. Sato, M., *Principles of Mine Detection by Ground-penetrating Radar*, in *Anti-personnel Landmine Detection for Humanitarian Demining*, K. Furuta and J. Ishikawa, Editors. 2009, Springer: Japan. p. 19-26.
81. Cardimona, S., *Subsurface Investigation Using Ground Penetrating Radar*. 2002, Department of Geology and Geophysics.
82. Robinson, M., et al., *Ground Penetrating Radar*. 2013, British Society for Geomorphology.
83. Annan, A.P., *Ground Penetrating Radar: Principles, Procedures & Applications*. 2003: Sensors & Software Incorporated.
84. Jol, H.M. and C.S. Bristow, *GPR in sediments: advice on data collection, basic processing and interpretation, a good practice guide.* Geological Society, London, Special Publications, 2003. **211**(1): p. 9-27.
85. Cassidy, N.J., *Chapter 5 - Ground Penetrating Radar Data Processing, Modelling and Analysis A2 - Jol, Harry M*, in *Ground Penetrating Radar Theory and Applications*. 2009, Elsevier: Amsterdam. p. 141-176.
86. Dojack, L., *Ground Penetrating Radar Theory, Data Collection, Processing, and Interpretation: A Guide for Archaeologists.* 2012.
87. Beres, M., et al., *Using two- and three-dimensional georadar methods to characterize glaciofluvial architecture.* Sedimentary Geology, 1999. **129**(1–2): p. 1-24.
88. Kempen, L.V. and H. Sahli, *Ground Penetrating Radar: A selective survey of the state of the art literature*. 1999, IRIS.

89. Sandmeier. *Reflexw - GPR and seismic processing software*. 2017 [cited 2017 1 May]; Available from: http://www.sandmeier-geo.de/reflexw.html.
90. Radzevicius, S.J., E.D. Guy, and J.J. Daniels, *Pitfalls in GPR data interpretation: Differentiating stratigraphy and buried objects from periodic antenna and target effects.* Geophysical Research Letters, 2000. **27**(20): p. 3393-3396.

APPENDICES A, B and C

Appendix A: Map of Oliveira de Azeméis showing the location of Castro de Ul

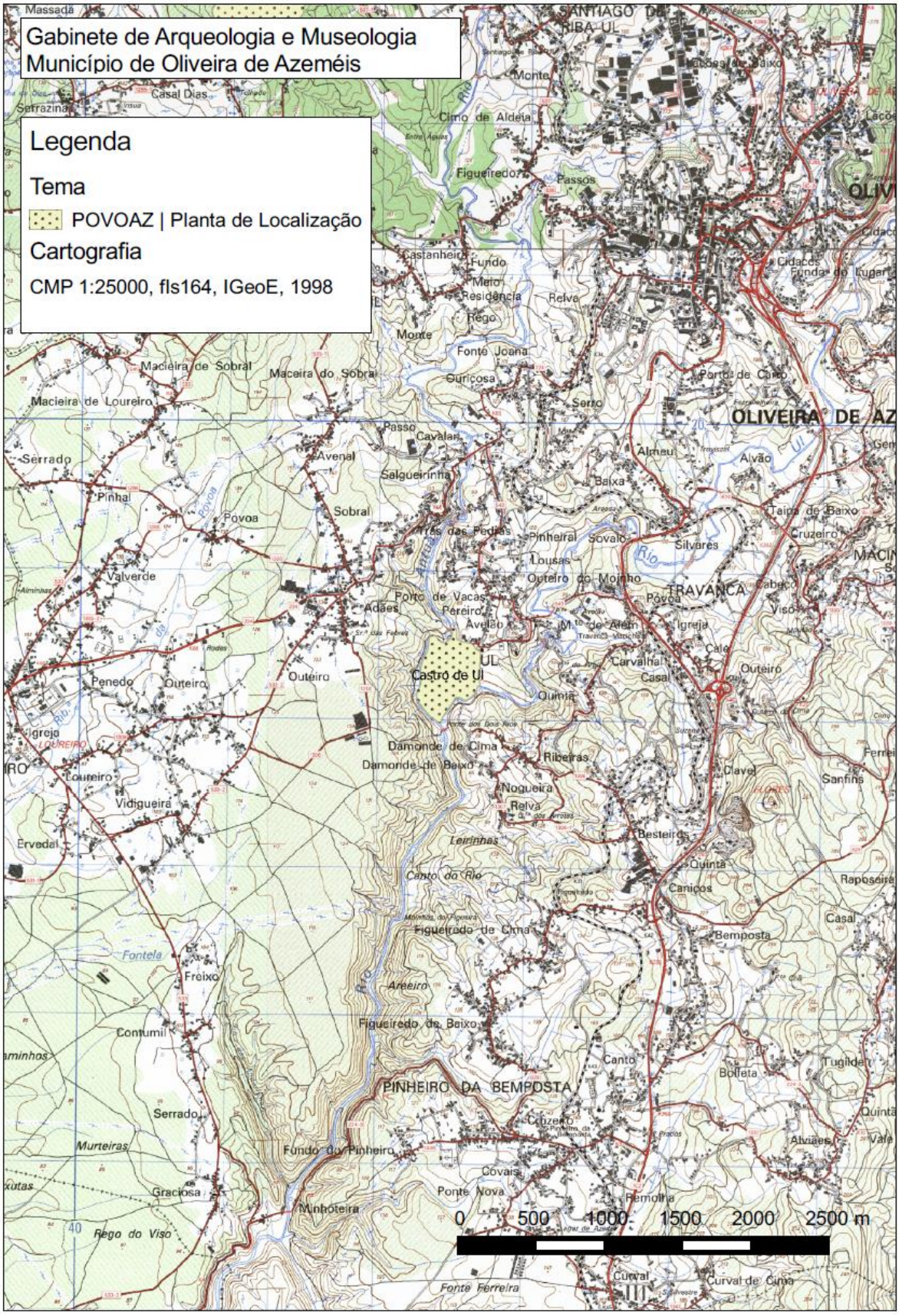

Figure A. 1: Topographical map of Oliveira de Azeméis showing Castrro de Ul

Source: Municipality of Oliveira de Azeméis

Appendix B: 3D bocks generated from the 2D profiles of each square

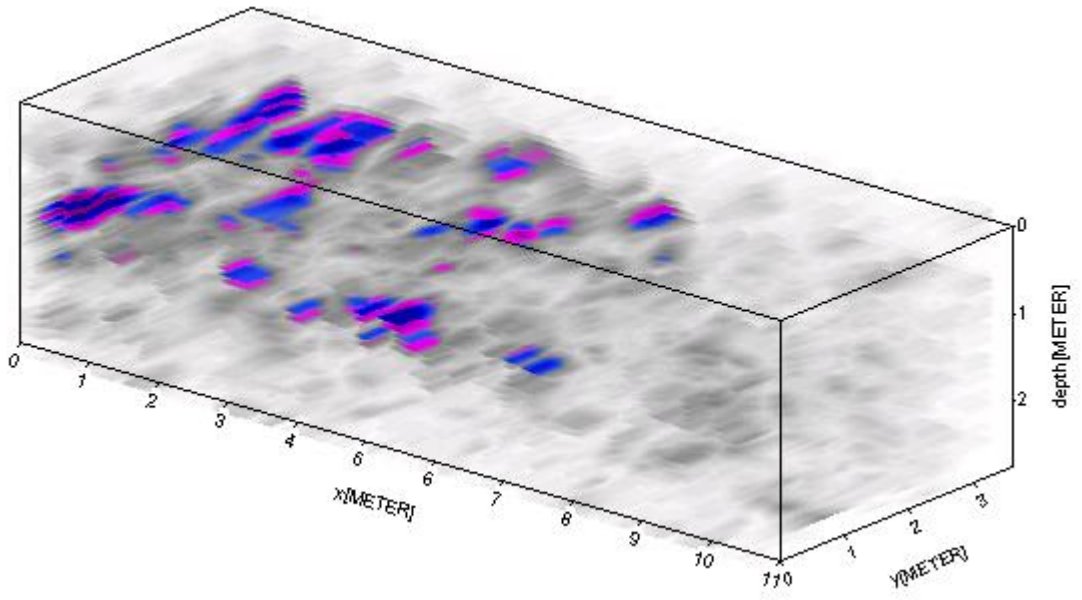

Figure B. 1: 3D block for square -2C taken in S-N direction using 270 MHz antenna

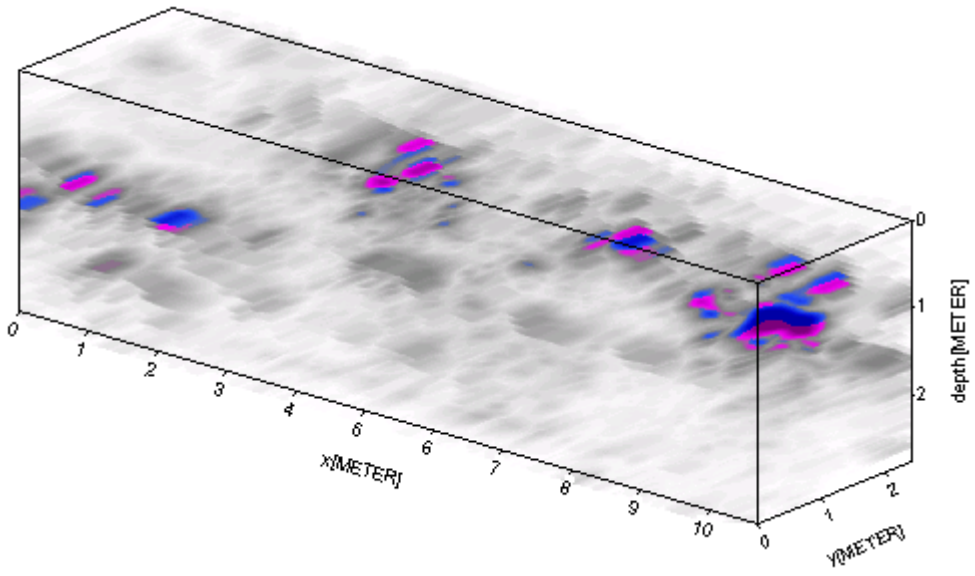

Figure B. 2: 3D block for square -3B taken in the S-N direction using 270 MHz antenna

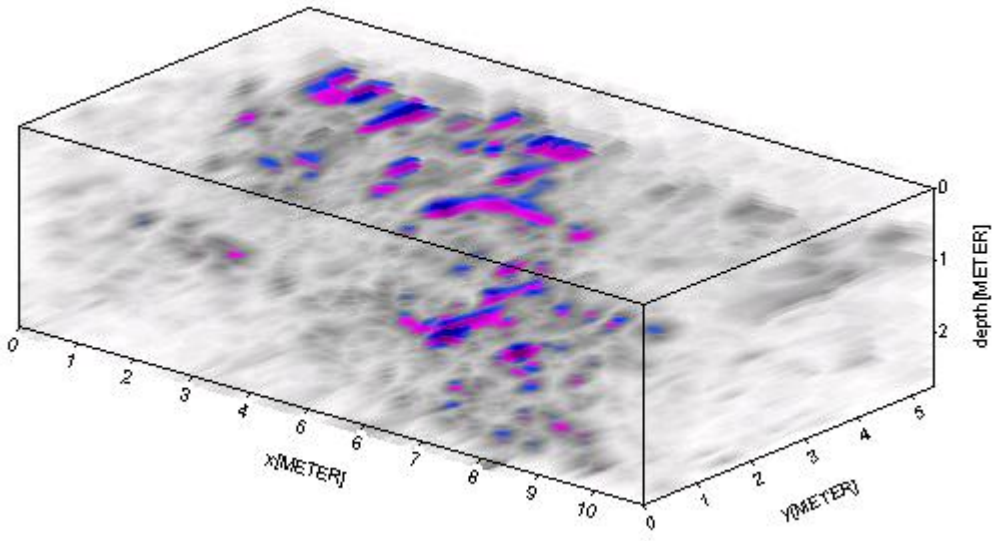

Figure B. 3: 3D block for square -2B taken in the S-N direction using 270 MHz antenna

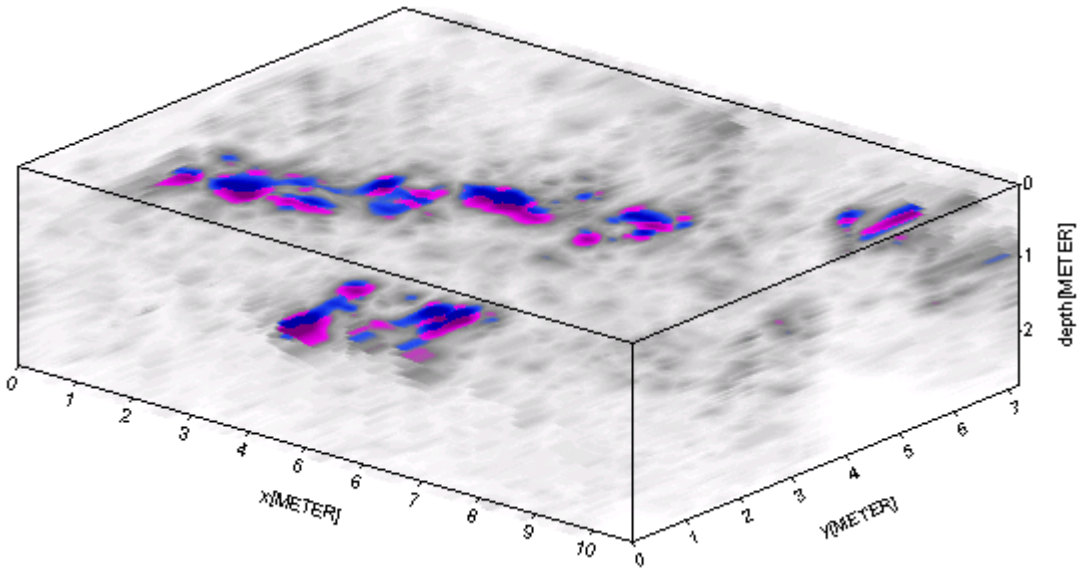

Figure B. 4: 3D block for square -1B taken in the S-N direction using 270 MHz antenna

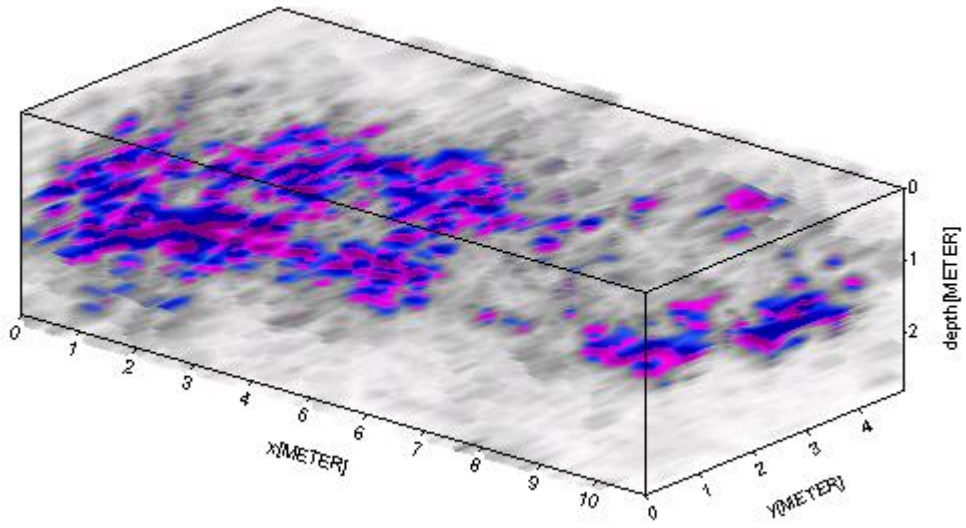

Figure B. 5: 3D block for square -4C taken in the S-N direction using 270 MHz antenna

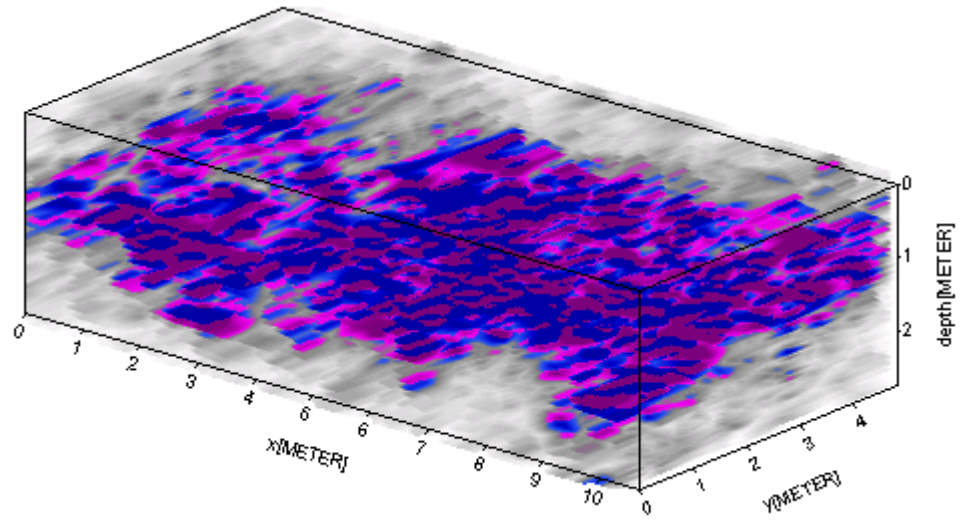

Figure B. 6: 3D block for square -5C taken in the S-N direction using 270 MHz antenna

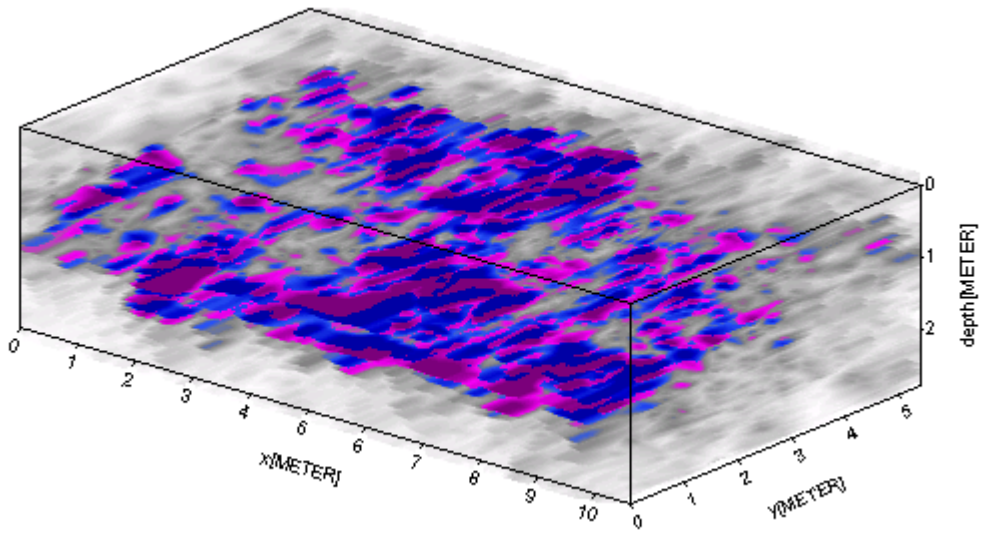

Figure B. 7: 3D block for square -6C taken in the S-N direction using 270 MHz antenna

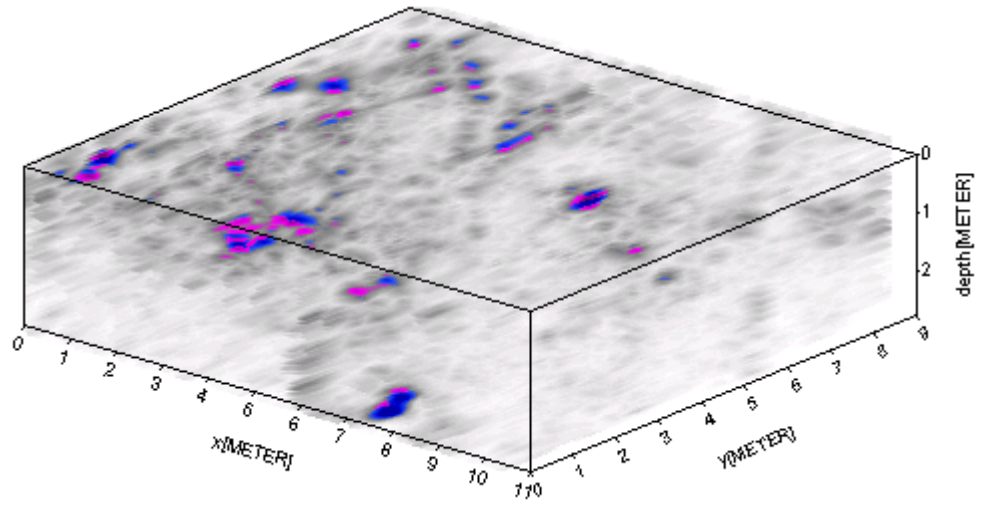

Figure B. 8: 3D block for square -2A' taken in the S-N direction using 270 MHz antenna

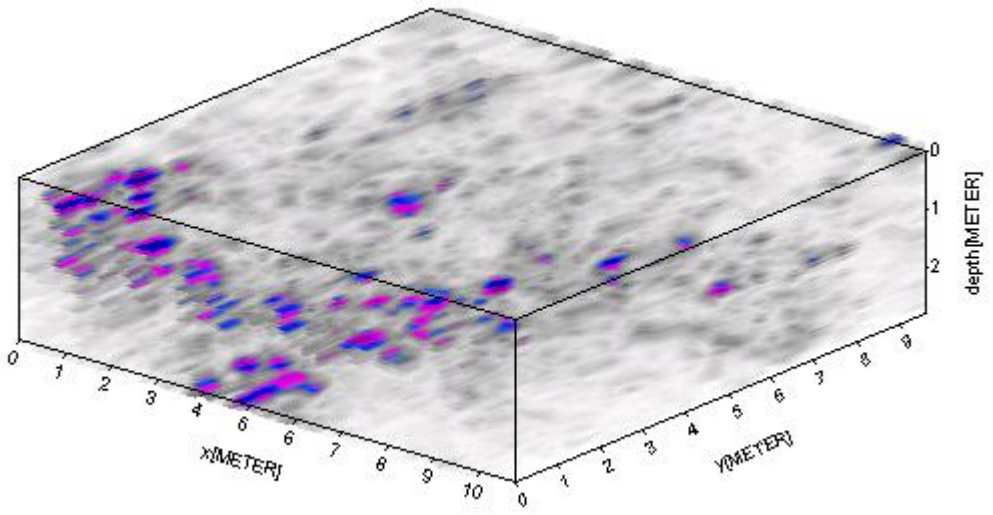

Figure B. 9: 3D block for square -2A' taken in the W-E direction using 270 MHz antenna

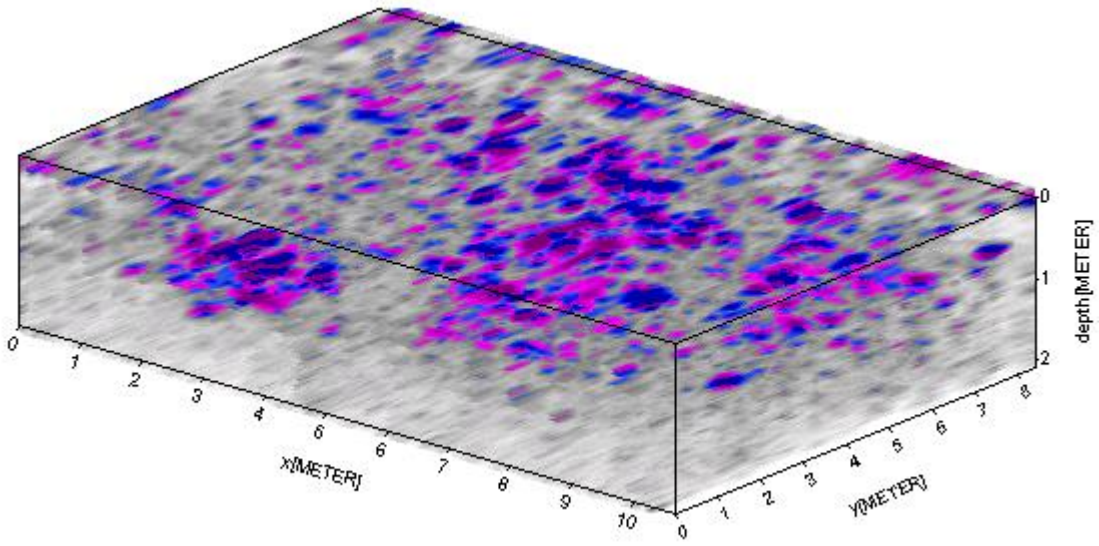

Figure B. 10: 3D block generated from data acquired by 270 MHz antenna from square -3A'in the S-N direction

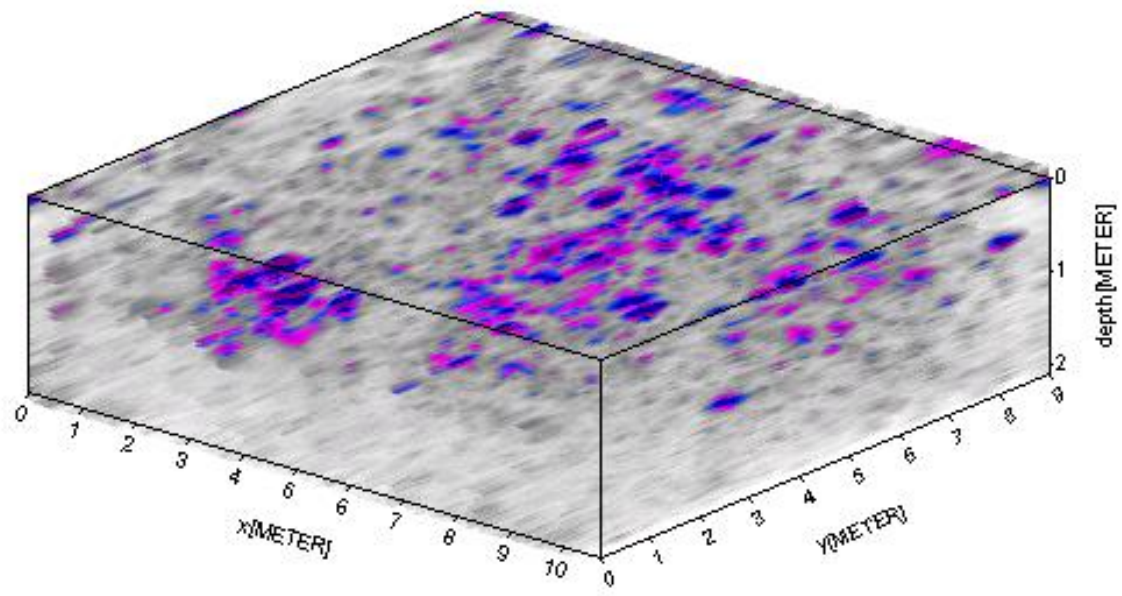

Figure B. 11: 3D block generated from data acquired by 900 MHz antenna from square -3A'in the S-N direction

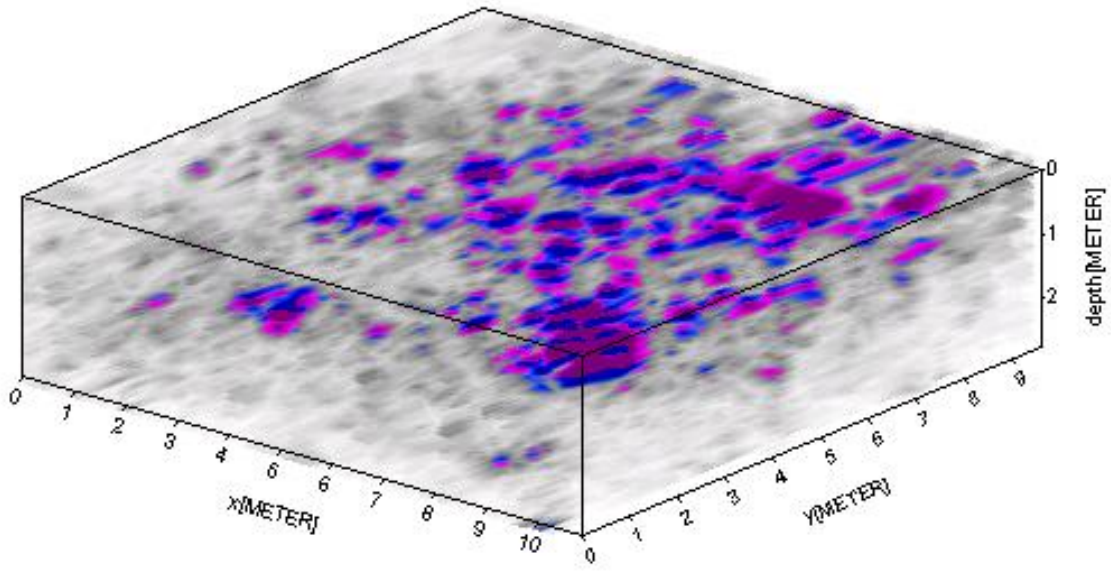

Figure B. 12: 3D block generated from data acquired by 270 MHz antenna from square -3A'in the W-E direction

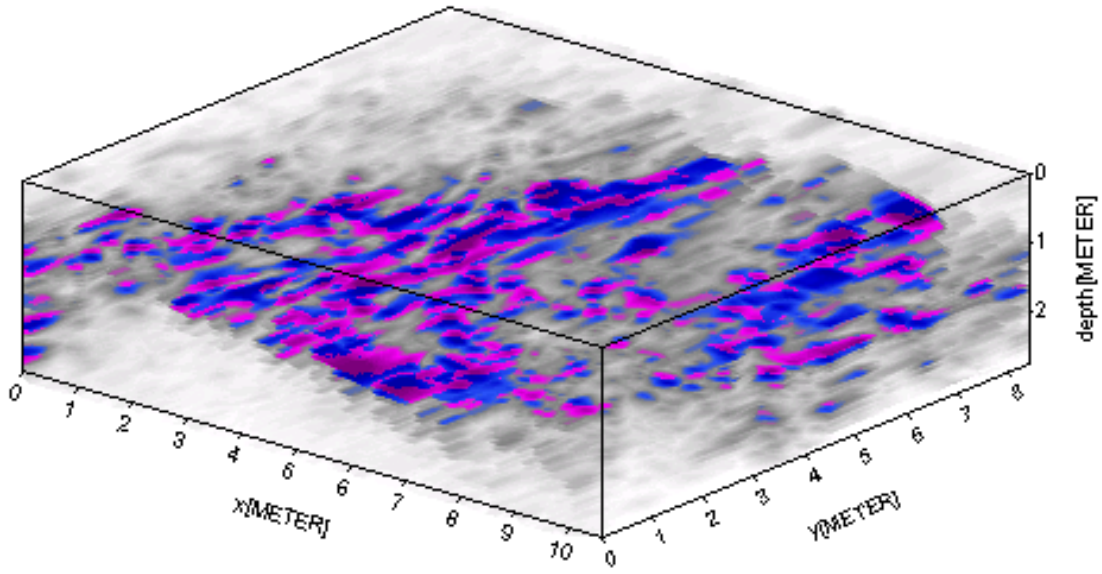

Figure B. 13: 3D block for square +7D' taken using 270 MHz antenna in the S-N direction

Appendix C: Slices from 3D blocks generated from 2D profiles

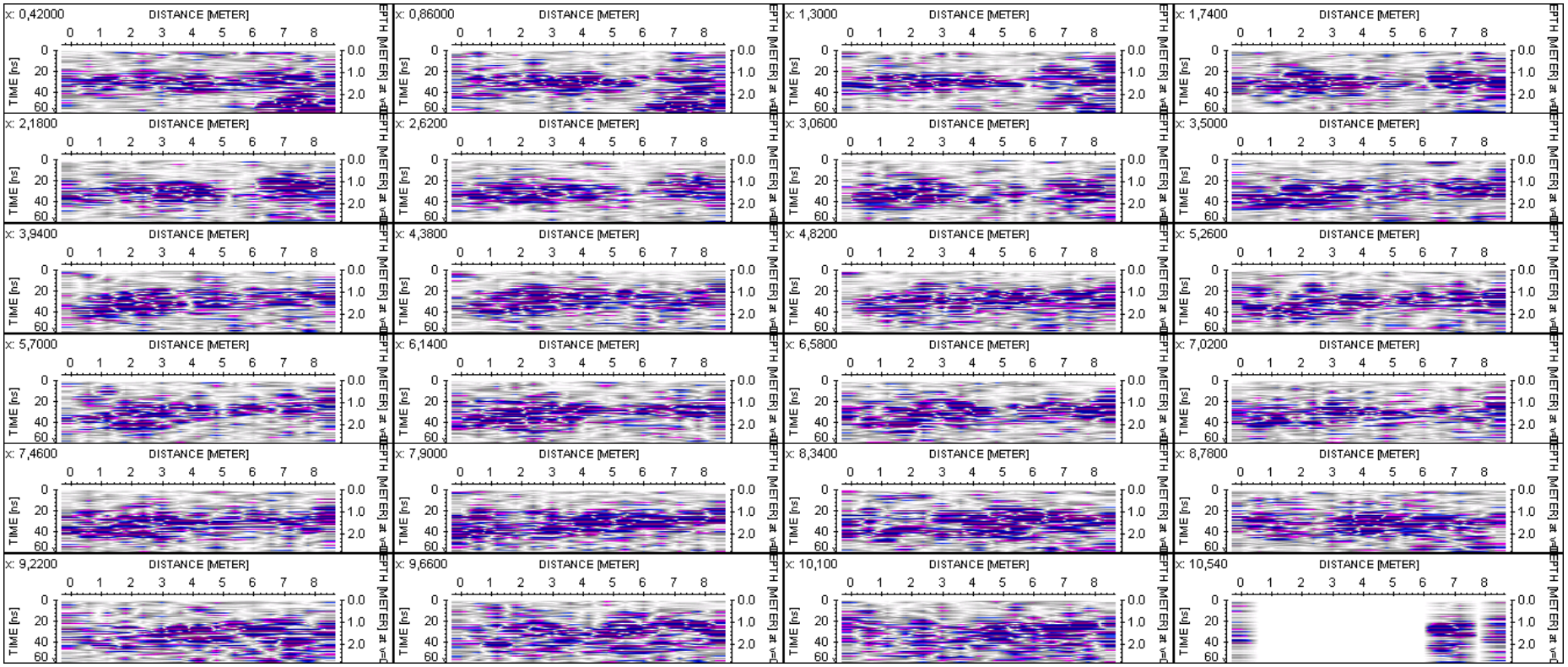

Figure C. 1: X-cuts of block -3C, S-N direction using a 270 MHz antenna

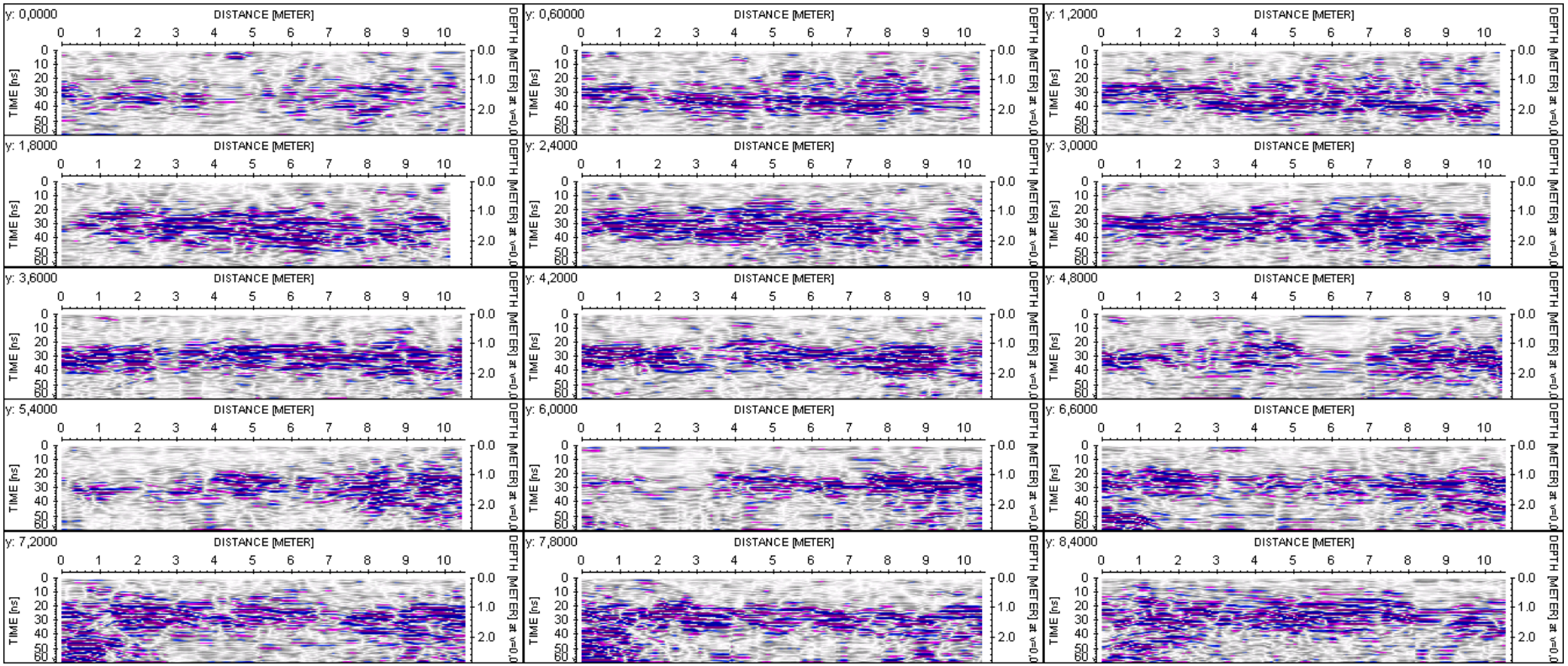

Figure C. 2: Y-cuts of block -3C, S-N direction using a 270 MHz antenna

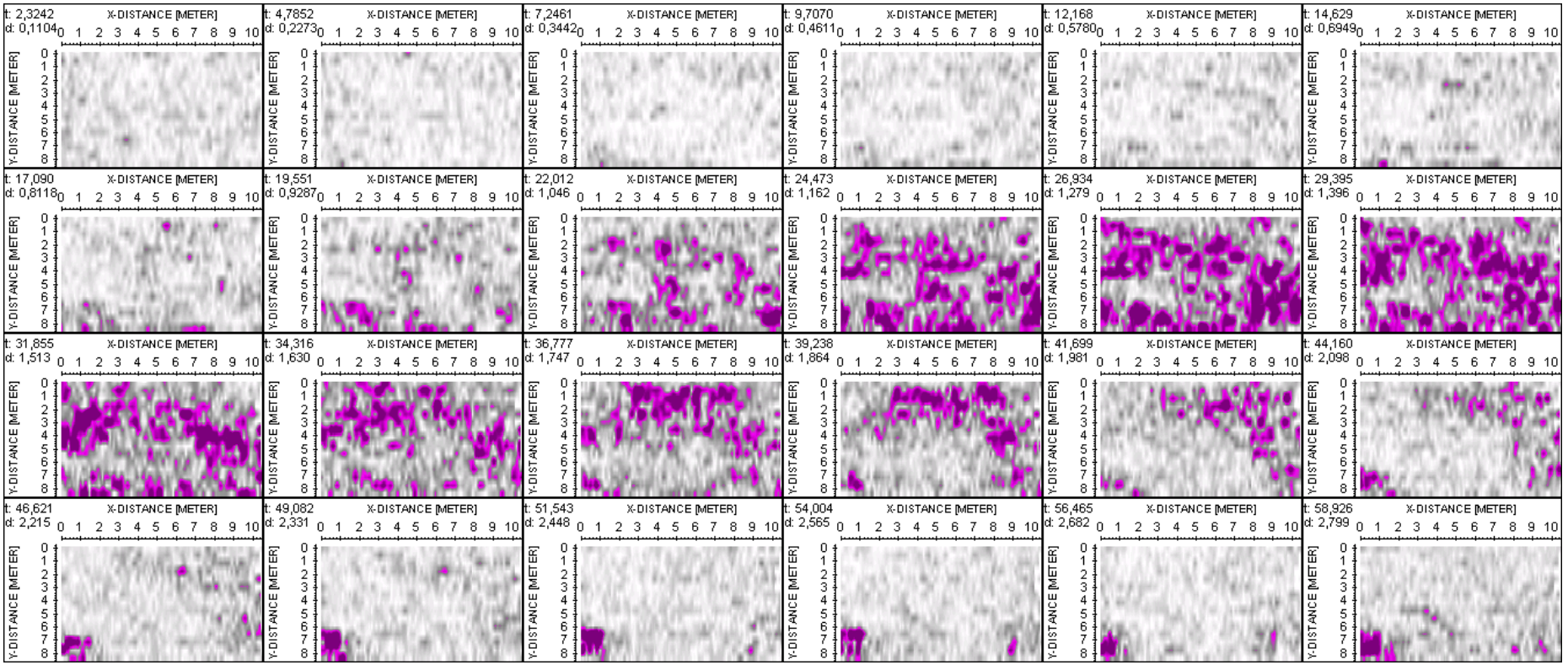

Figure C. 3: Time slices of block -3C, S-N direction using a 270 MHz antenna

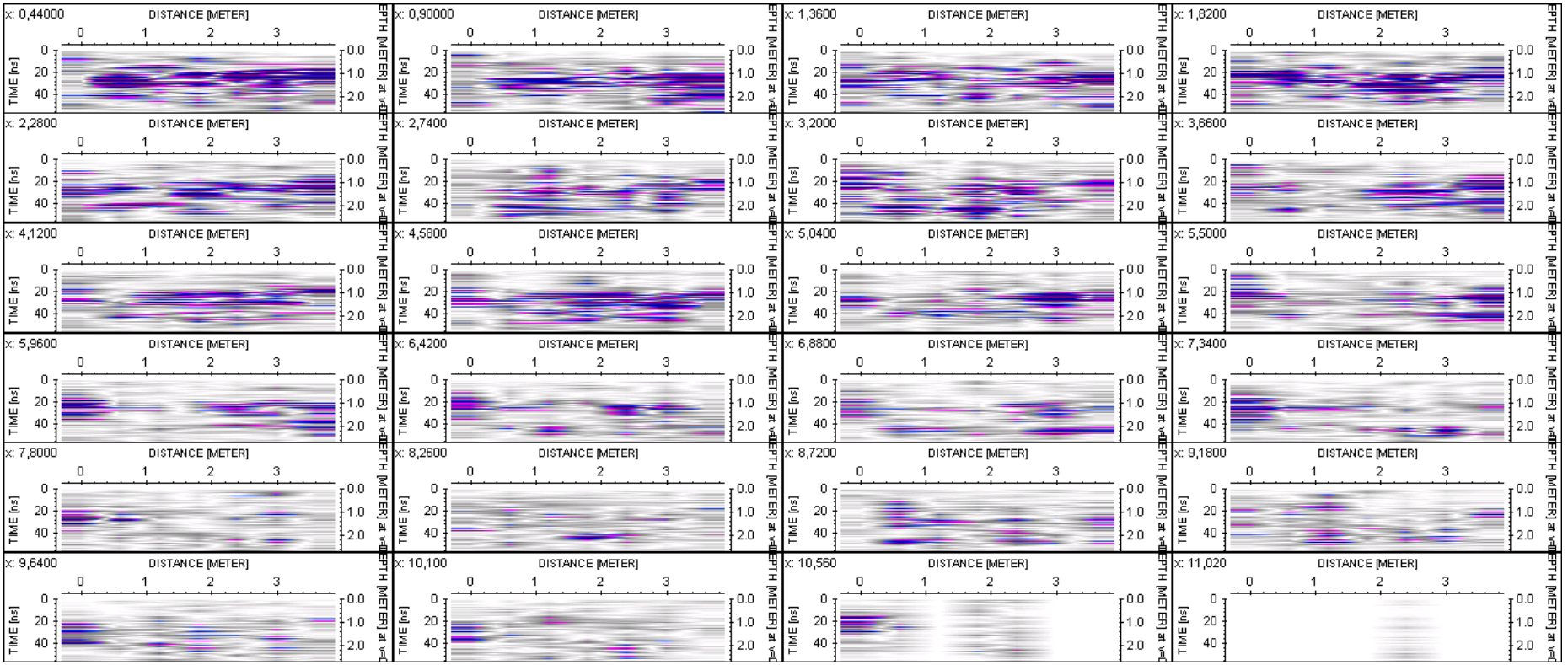

Figure C. 4: X-cuts of block -2C, S-N direction using a 270 MHz antenna

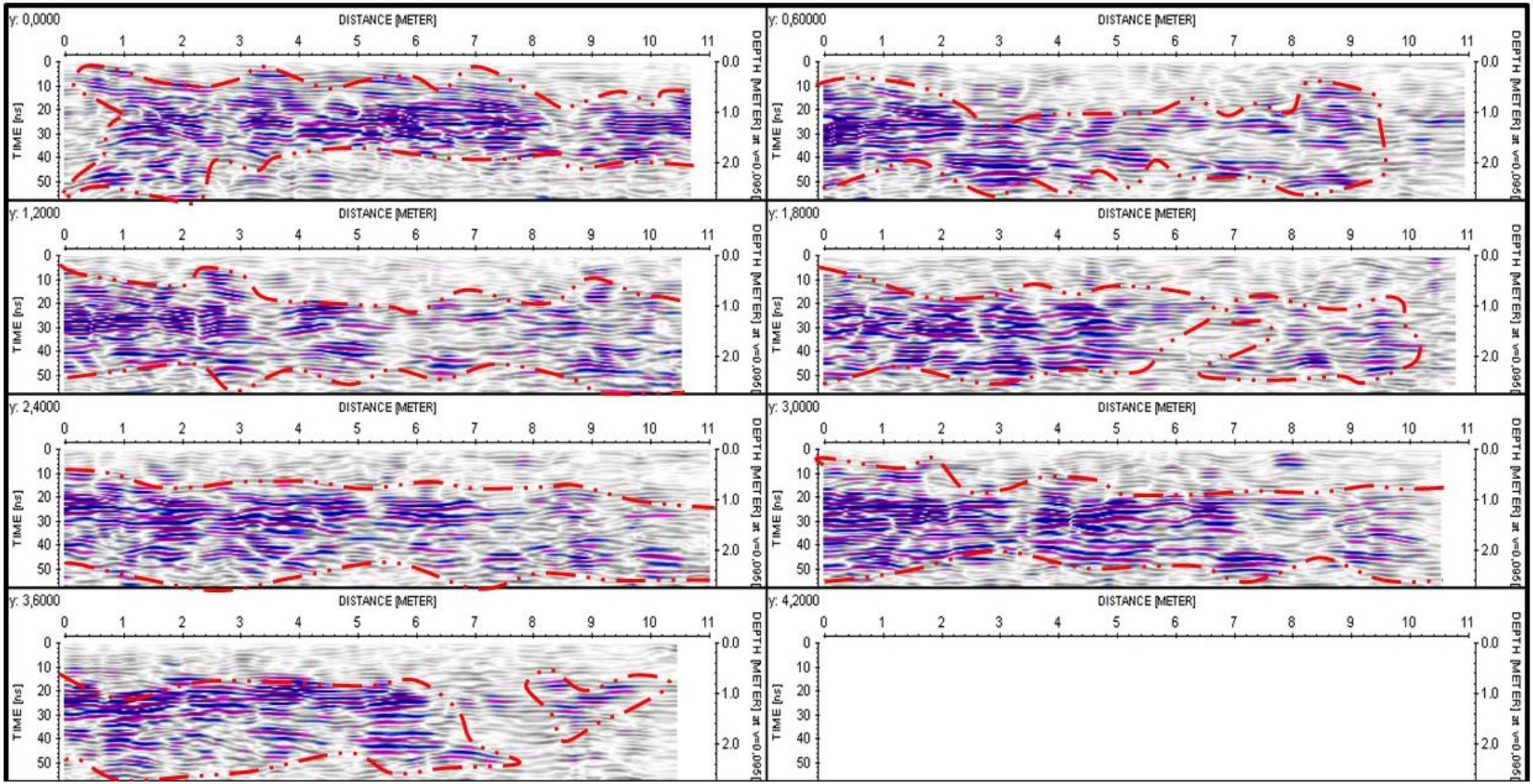

Figure C. 5: Y-cuts of block -2C, S-N direction using a 270 MHz antenna

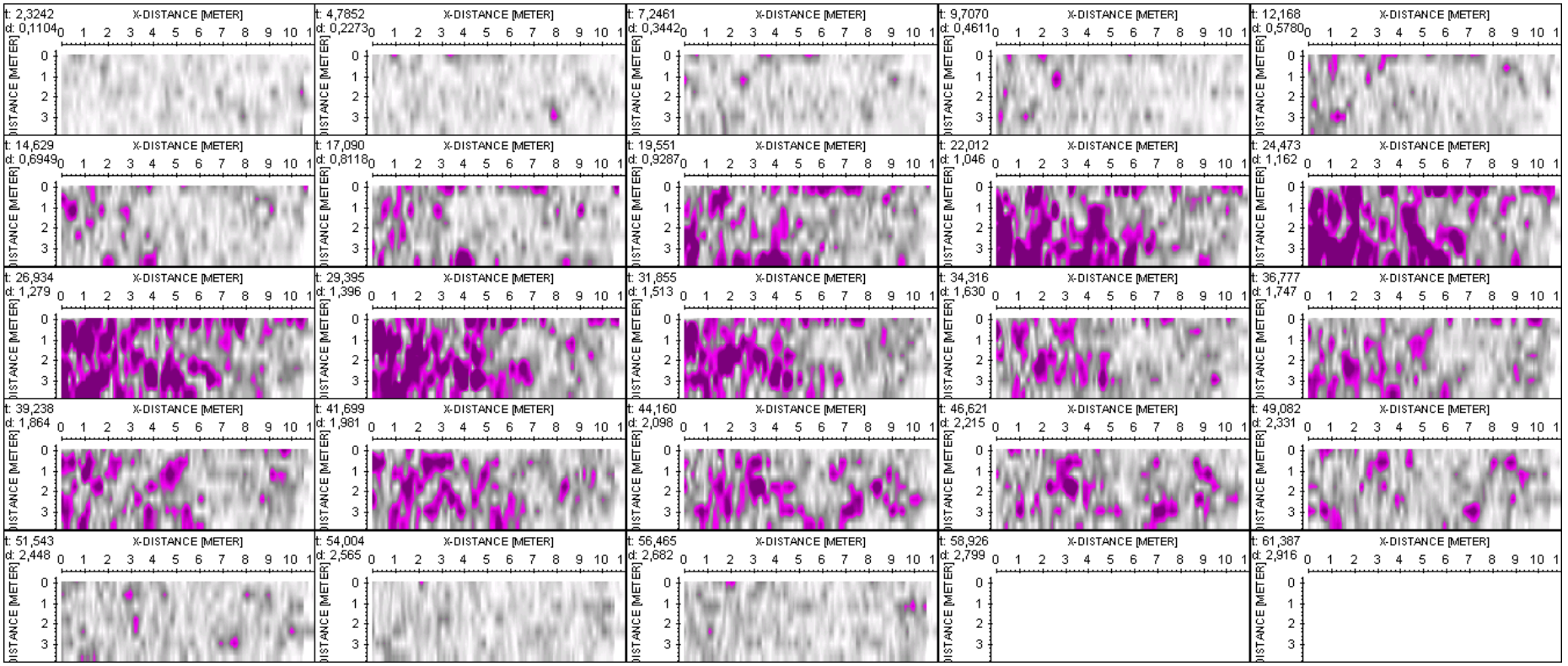

Figure C. 6: Time cuts of block -2C, S-N direction using a 270 MHz antenna

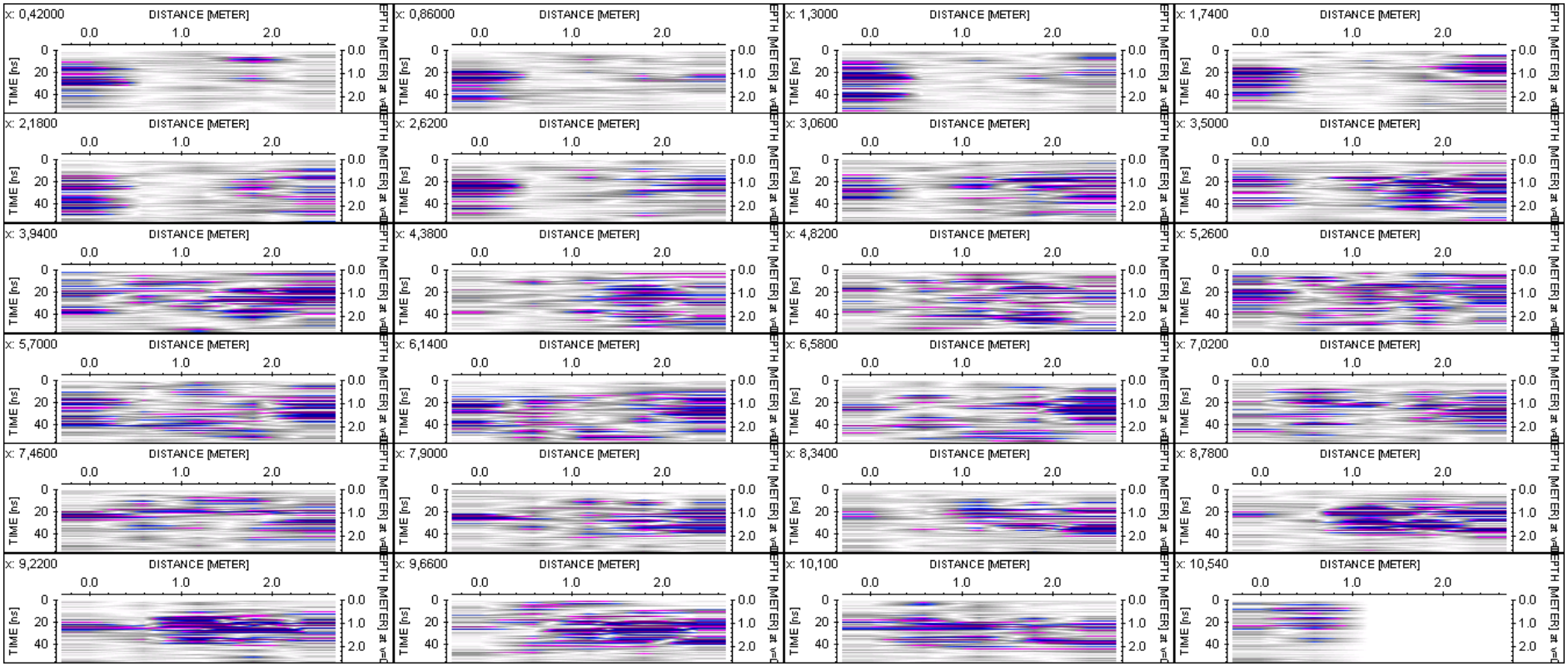

Figure C. 7: X-cuts of block -3B, S-N direction using a 270 MHz antenna

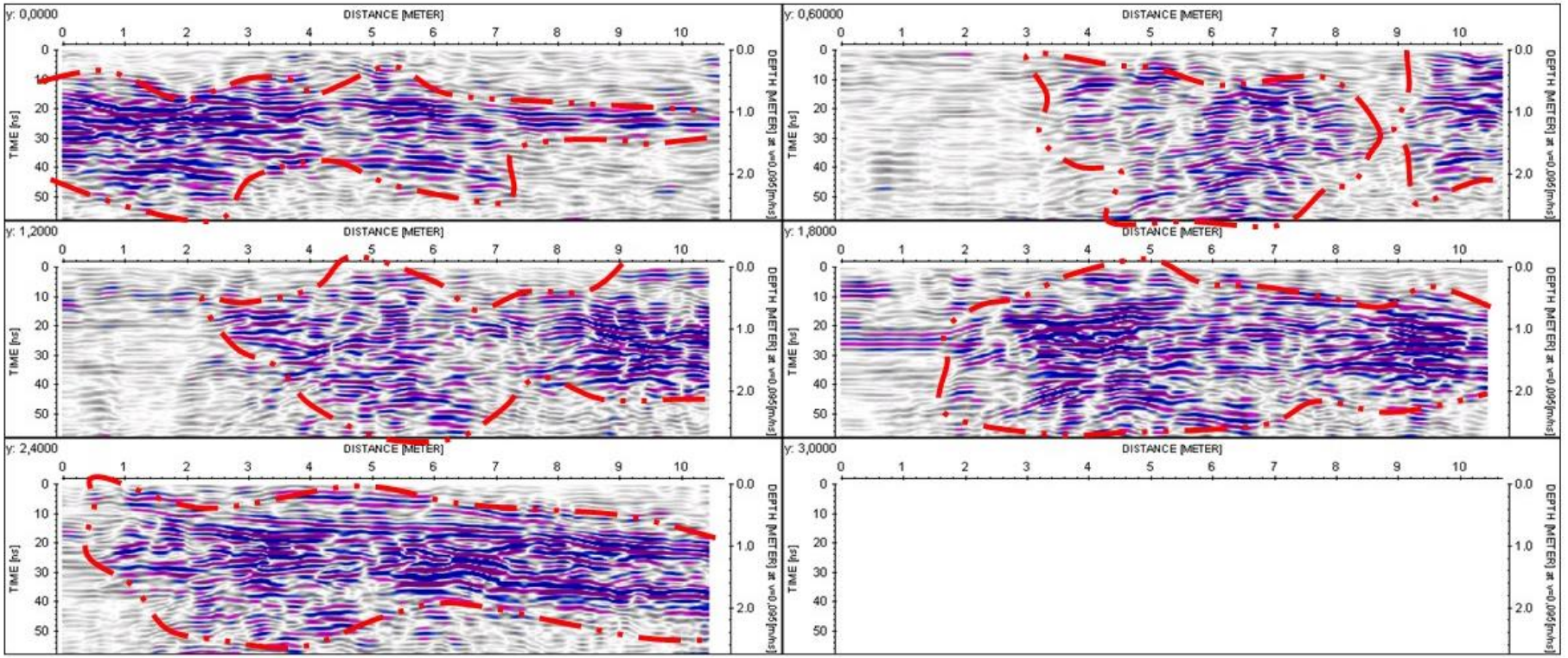

Figure C. 8: Y-cuts of block -3B, S-N direction using a 270 MHz antenna

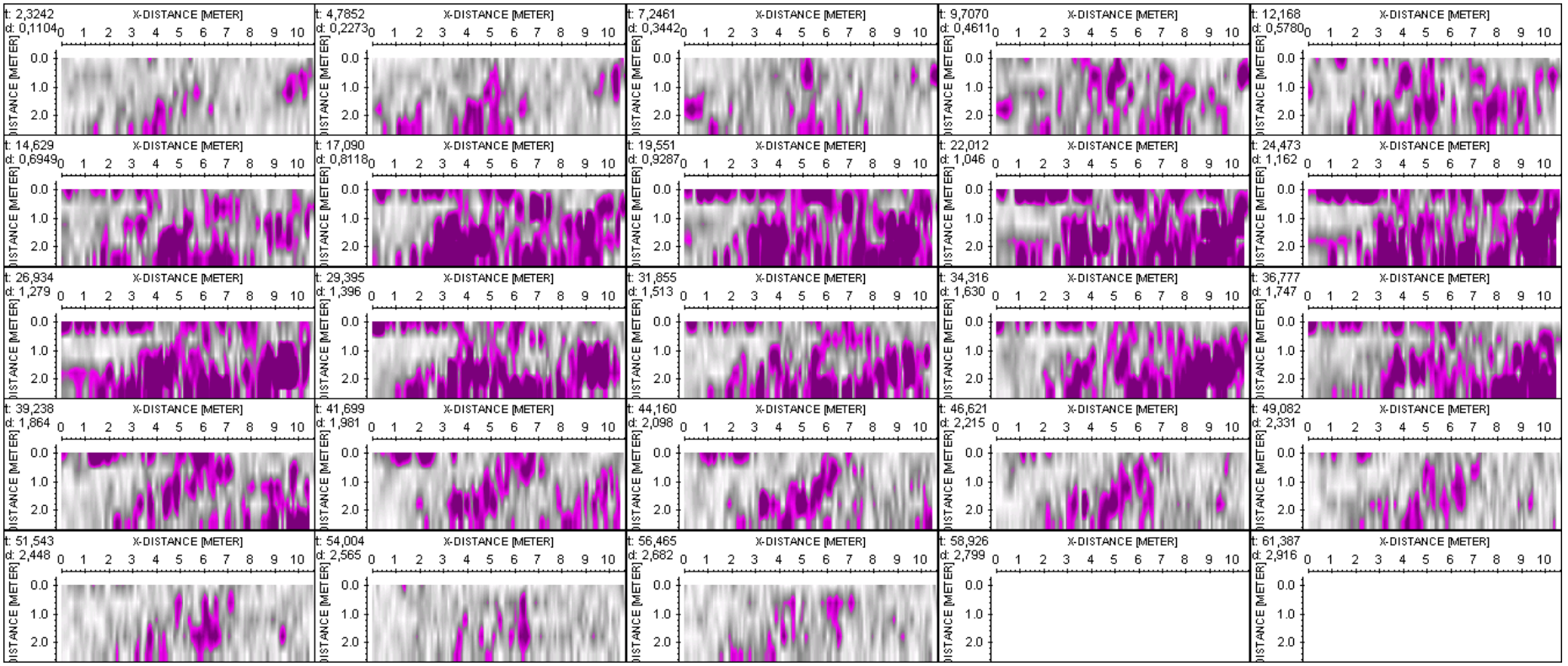

Figure C. 9: Time cuts of block -3B, S-N direction using a 270 MHz antenna

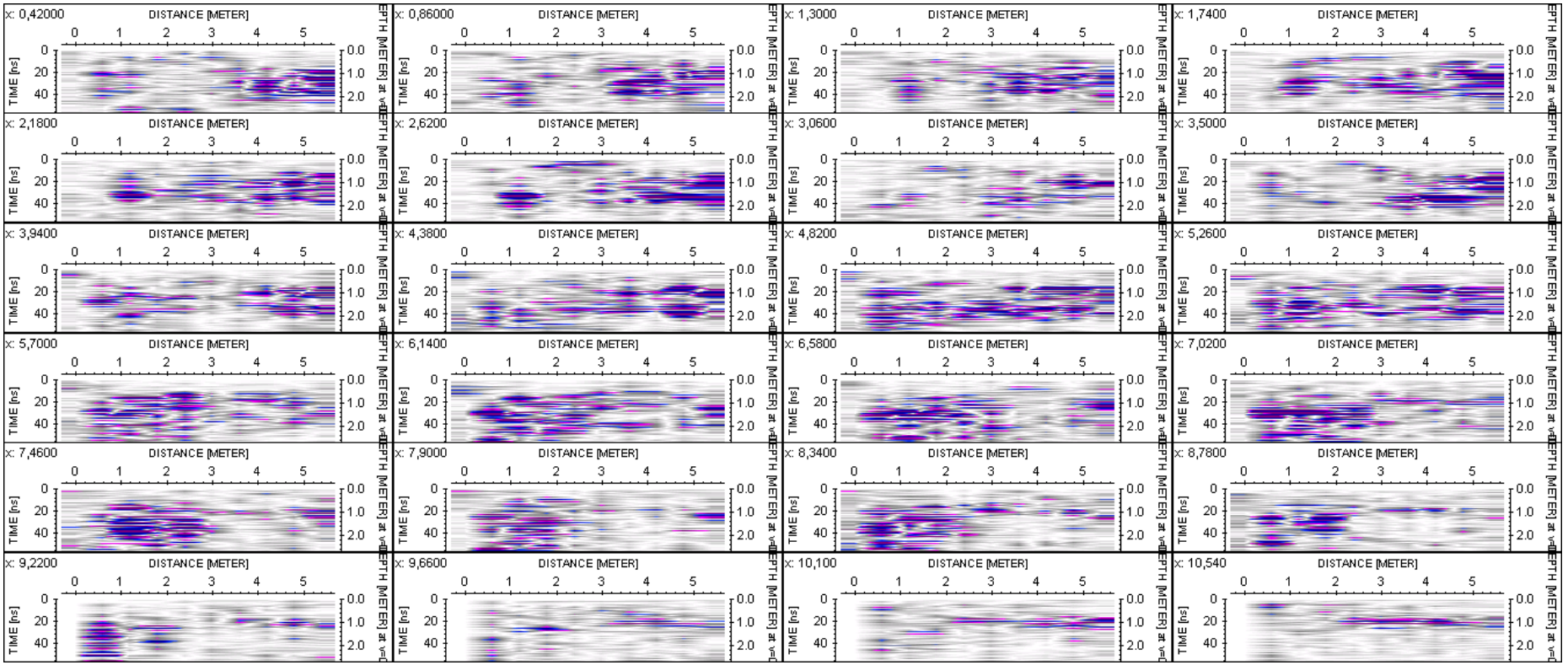

Figure C. 10: X-cuts of block -2B, S-N direction using a 270 MHz antenna

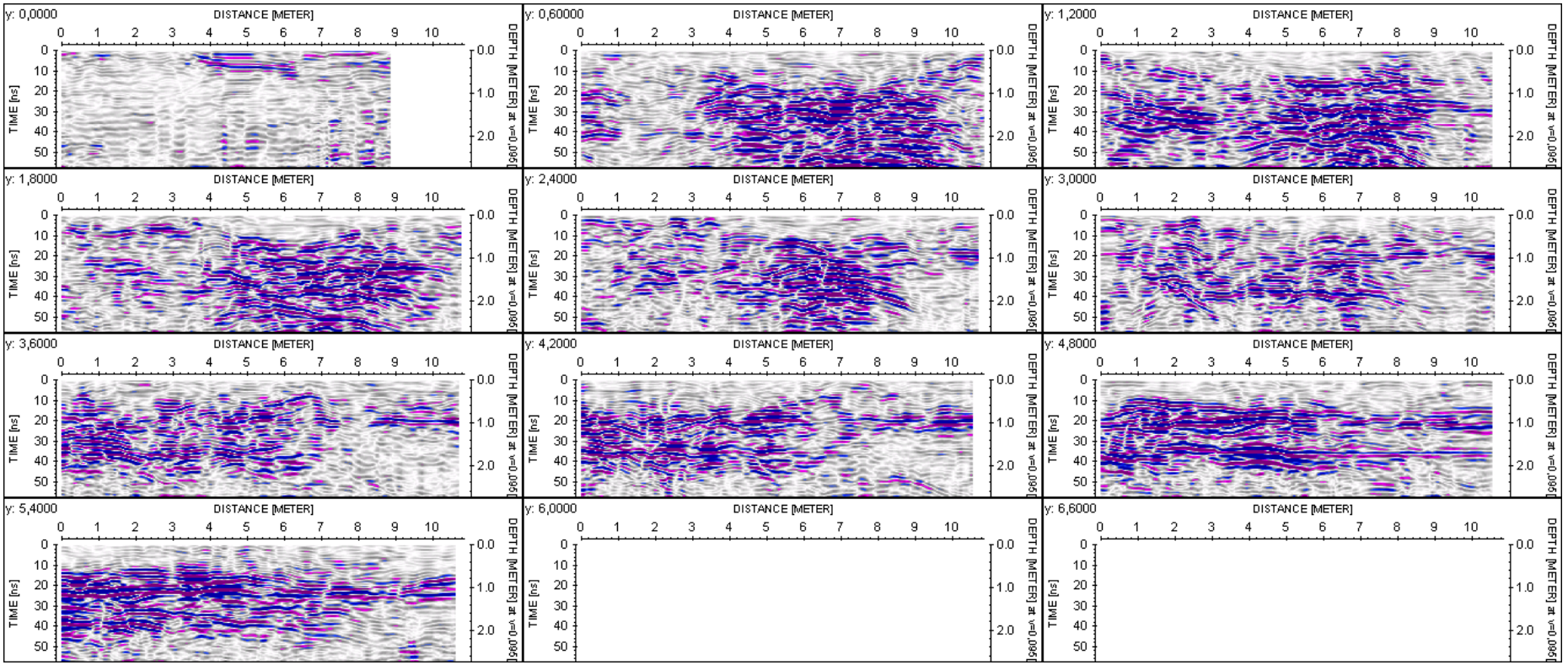

Figure C. 11: Y-cuts of block -2B, S-N direction using a 270 MHz antenna

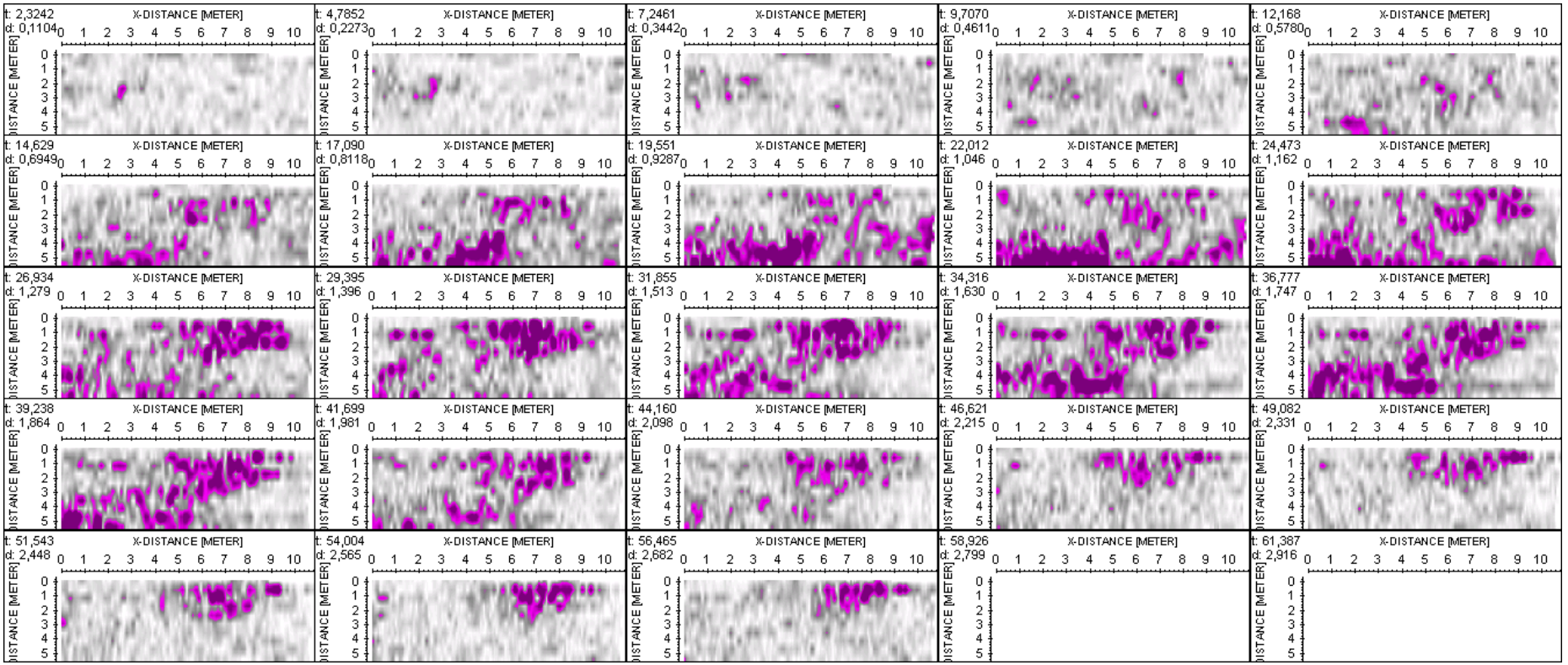

Figure C. 12: Time cuts of block -2B, S-N direction using a 270 MHz antenna

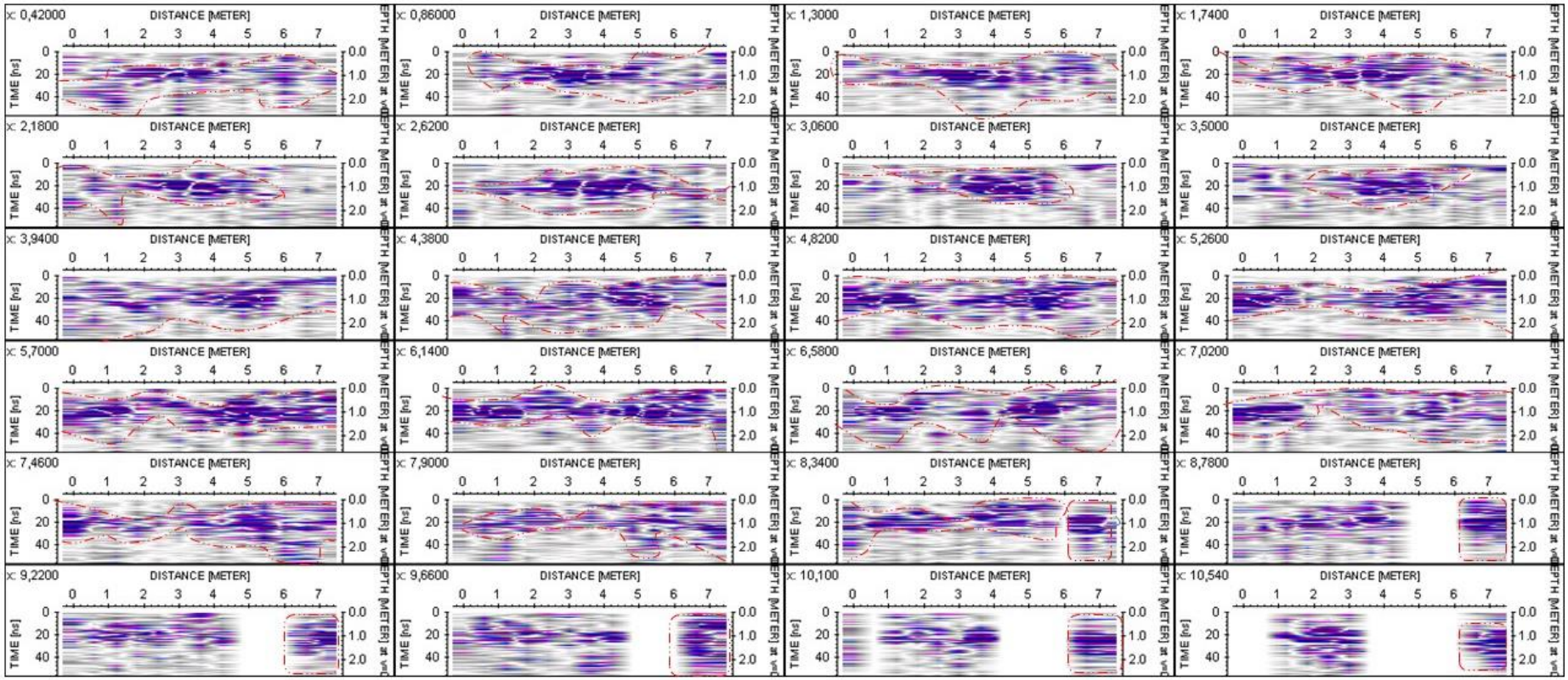

Figure C. 13: X-cuts of block -1B, S-N direction using a 270 MHz antenna

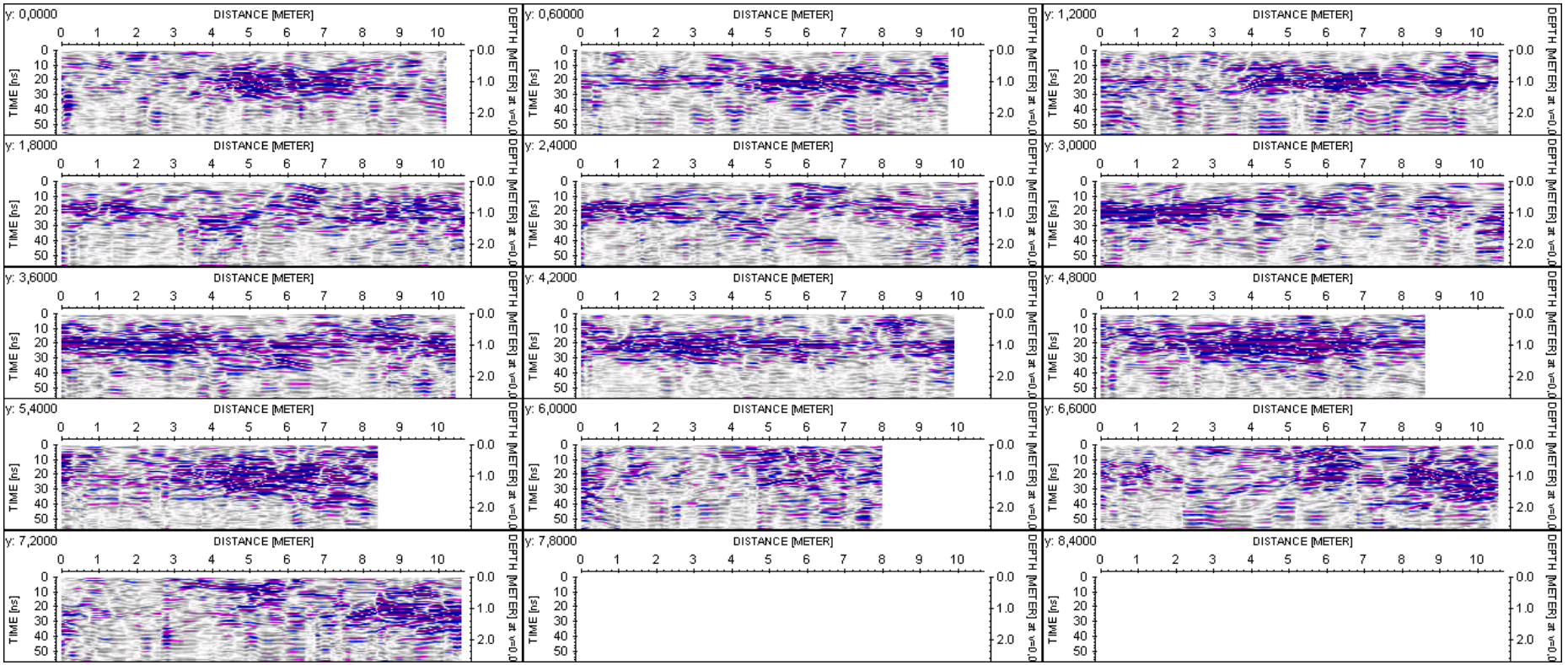

Figure C. 14: Y-cuts of block -1B, S-N direction using a 270 MHz antenna

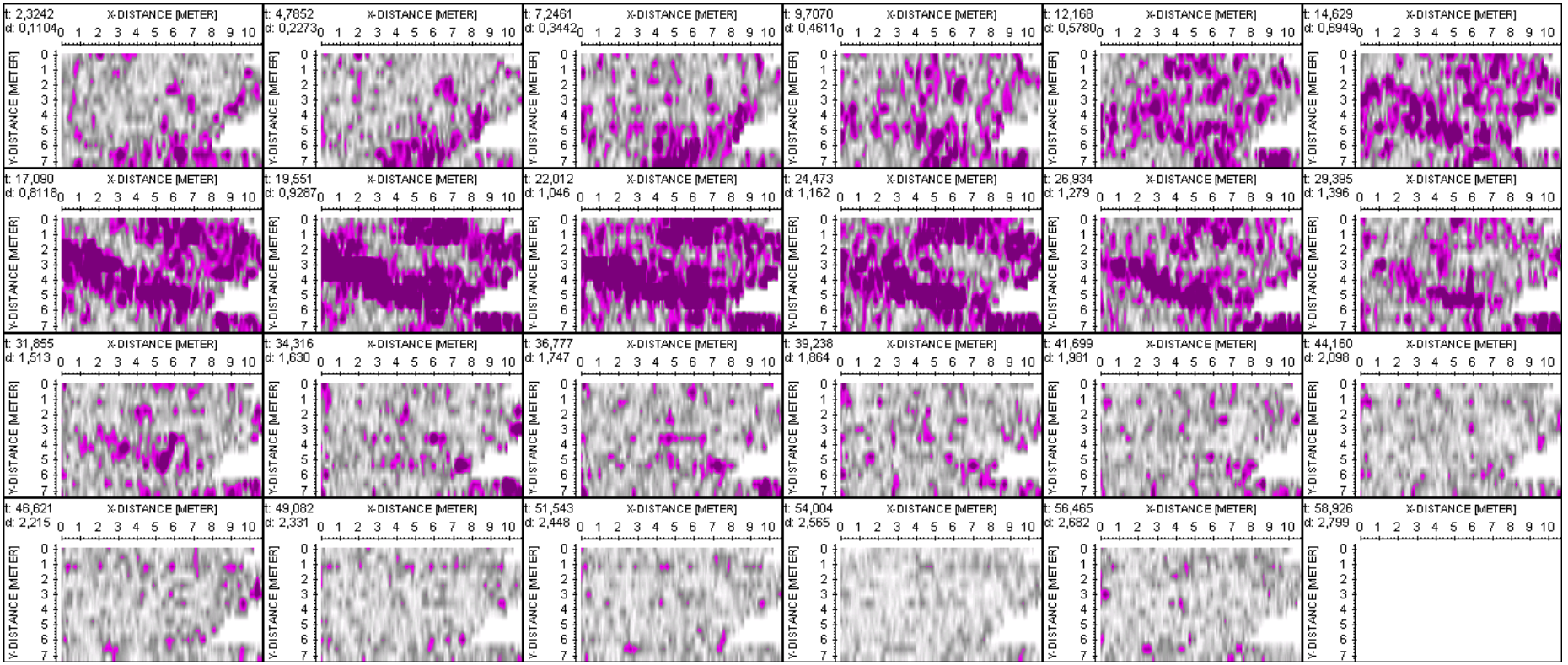

Figure C. 15: Time cuts of block -1B, S-N direction using a 270 MHz antenna

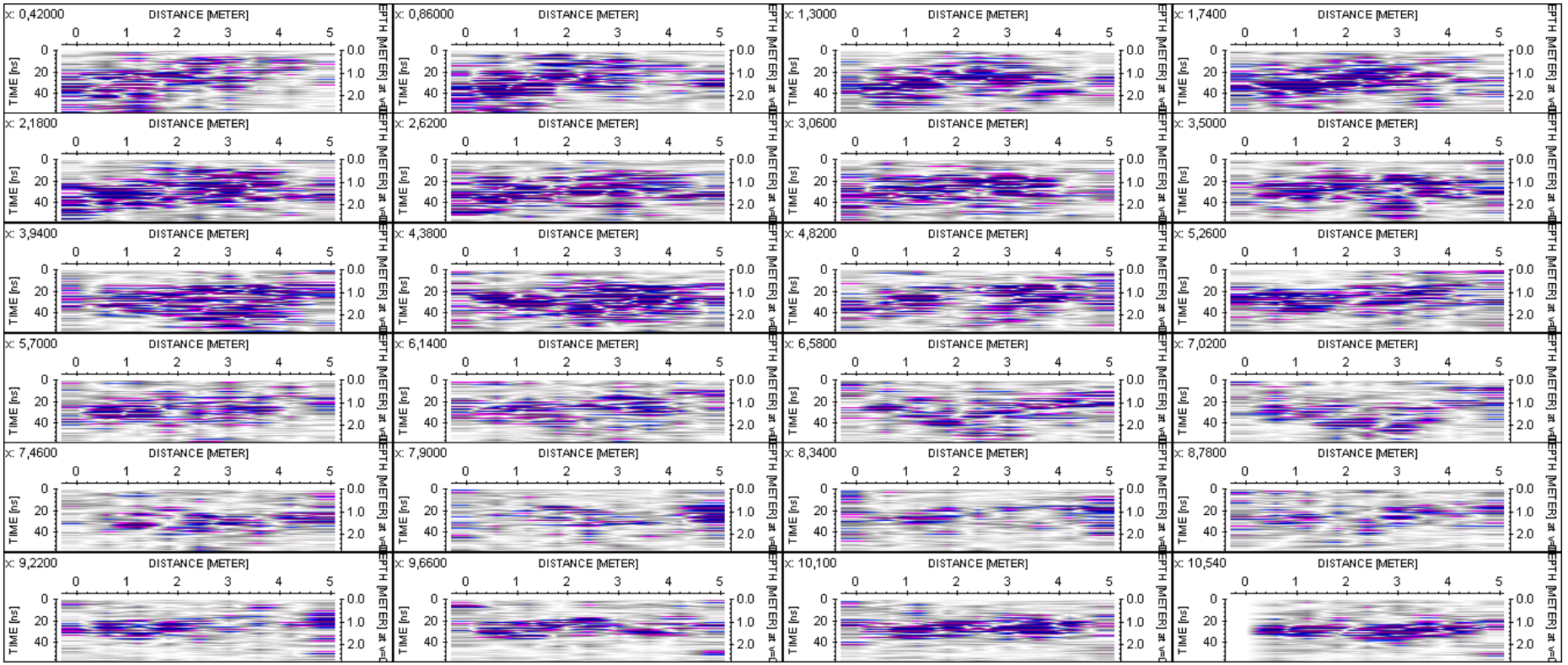

Figure C. 16: X-cuts of block -4C, S-N direction using a 270 MHz antenna

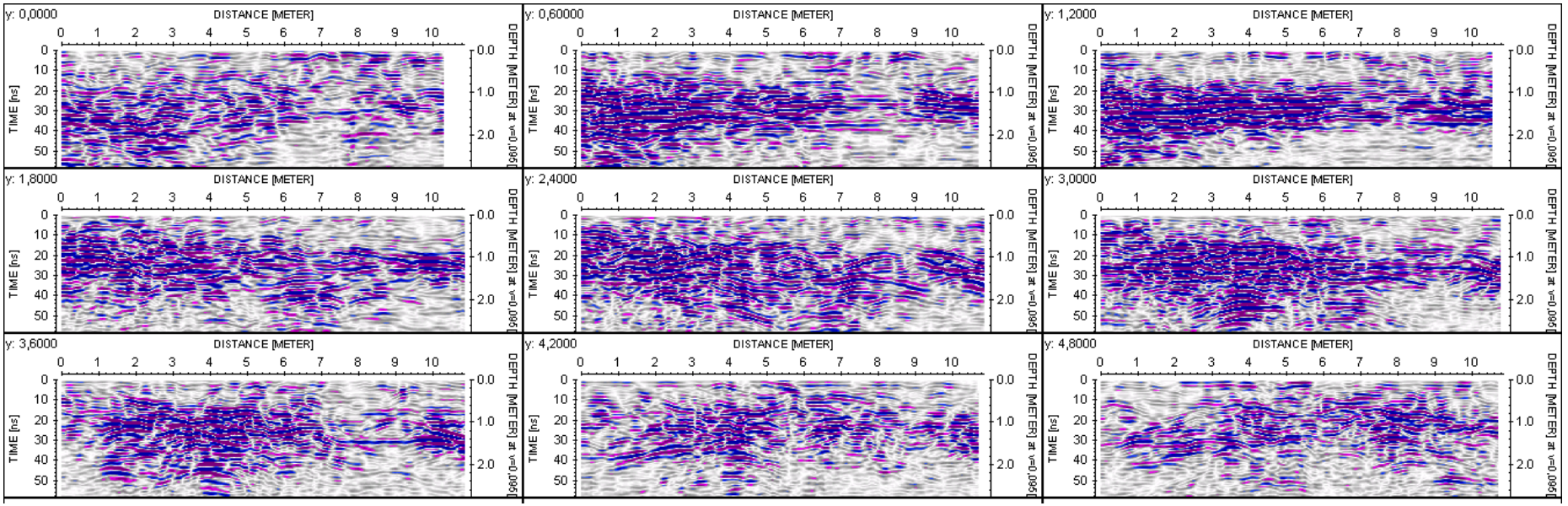

Figure C. 17: Y-cuts of block -4C, S-N direction using a 270 MHz antenna

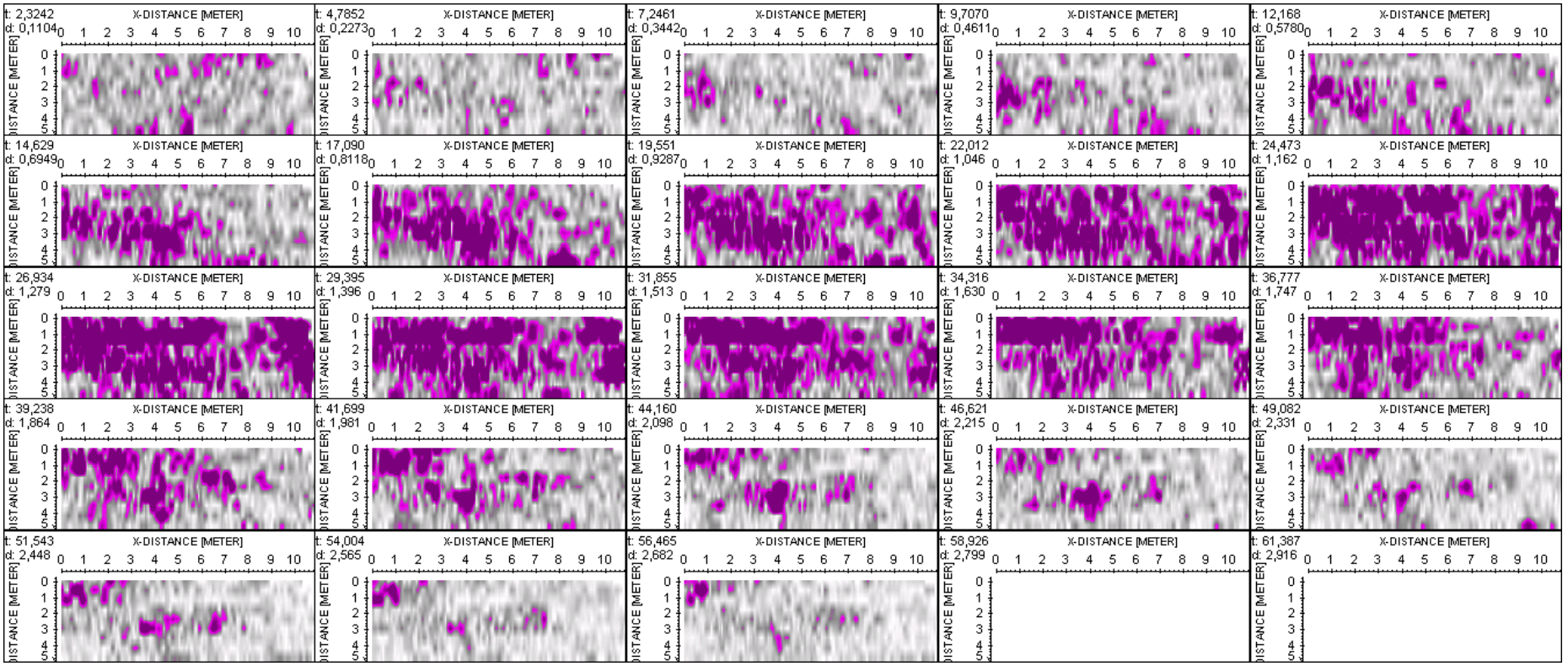

Figure C. 18: Time cuts of block -4C, S-N direction using a 270 MHz antenna

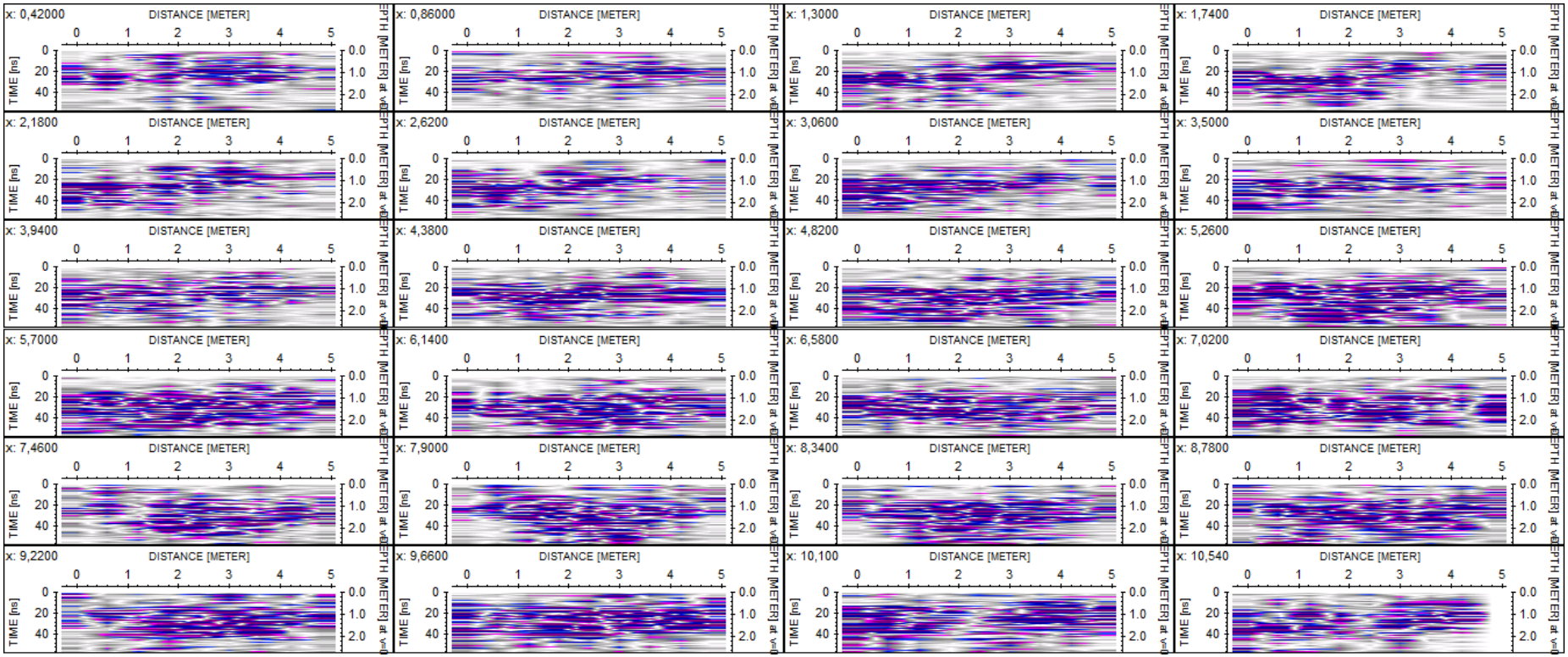

Figure C. 19: X-cuts of block -5C, S-N direction using a 270 MHz antenna

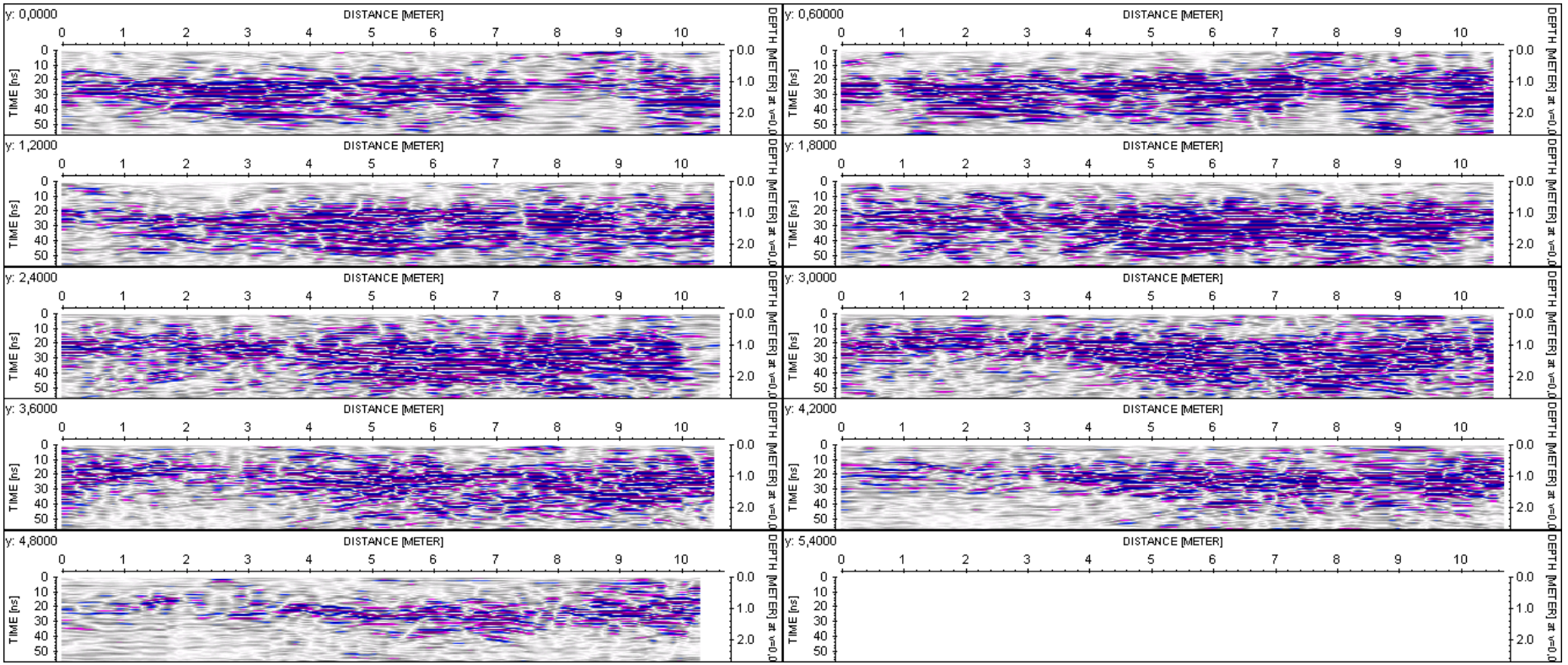

Figure C. 20: Y-cuts of block -5C, S-N direction using a 270 MHz antenna

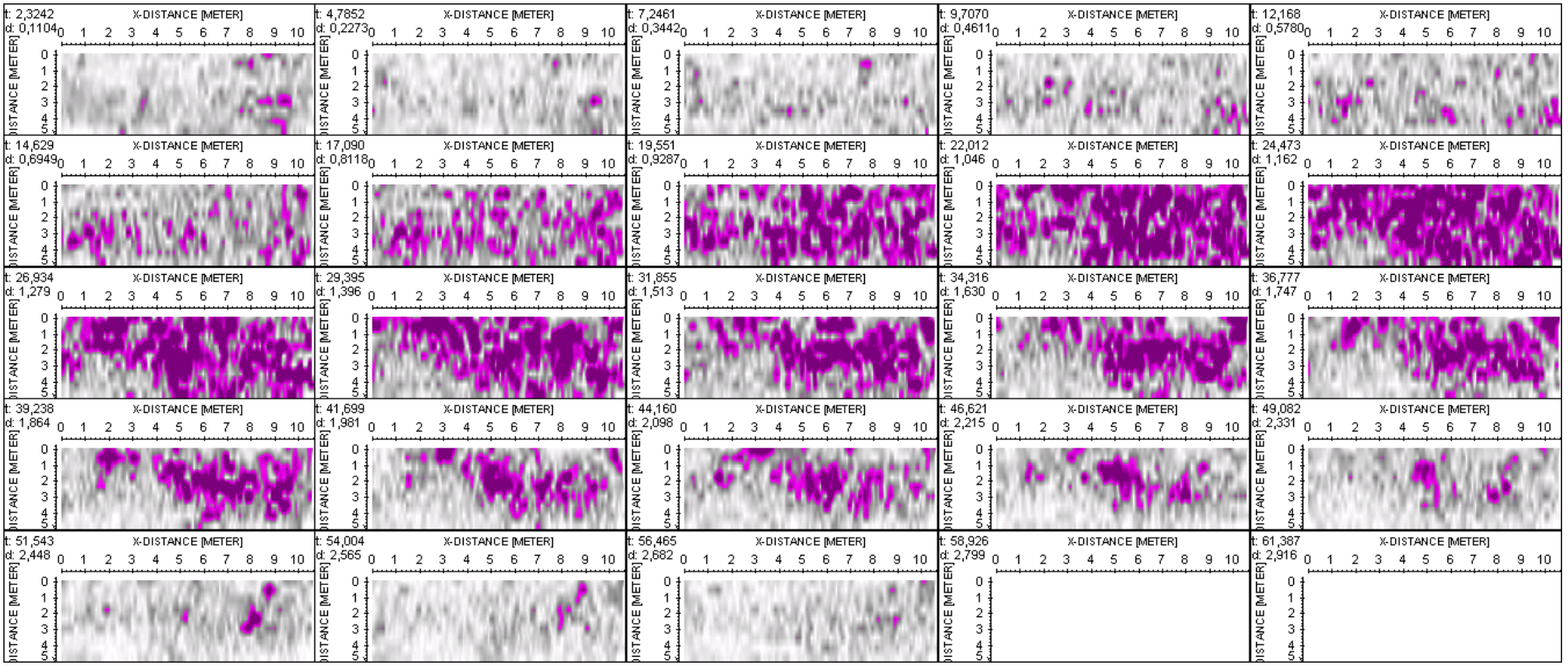

Figure C. 21: Time cuts of block -5C, S-N direction using a 270 MHz antenna

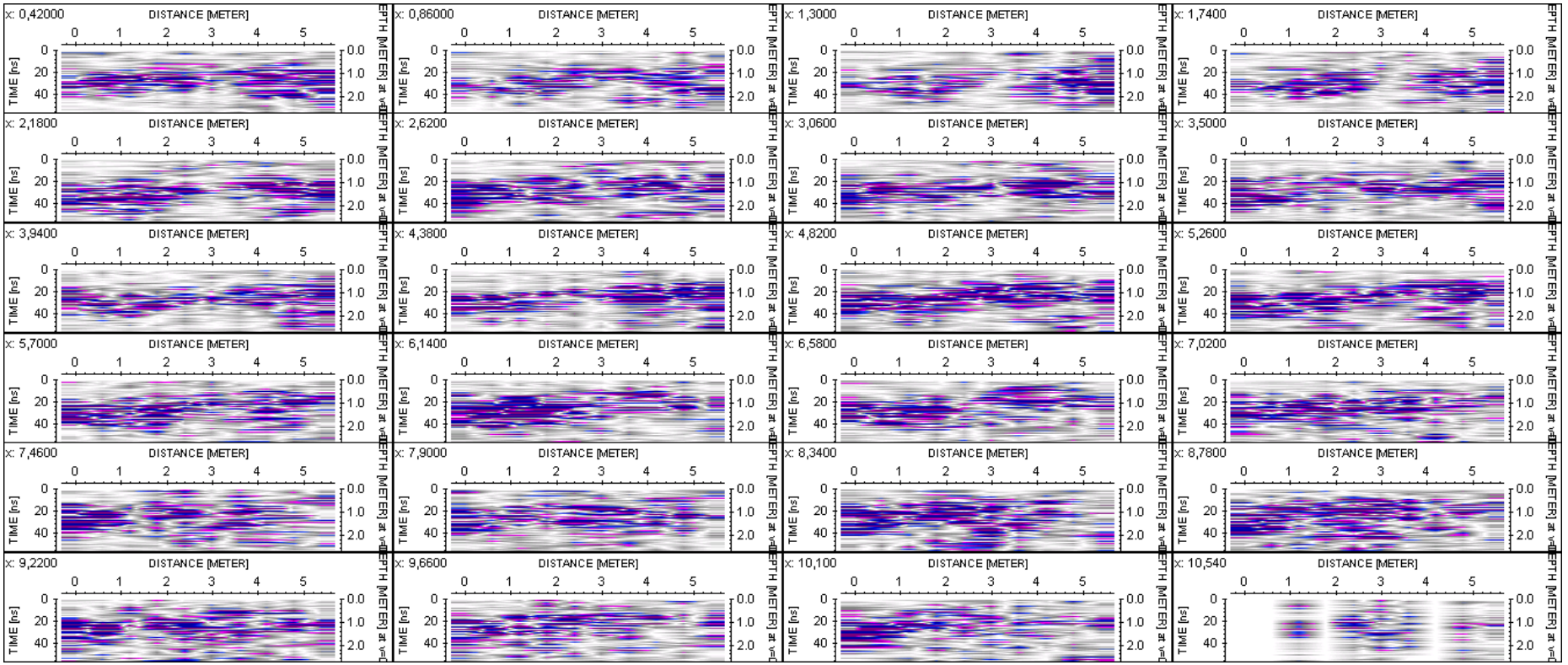

Figure C. 22: X-cuts of block -6C, S-N direction using a 270 MHz antenna

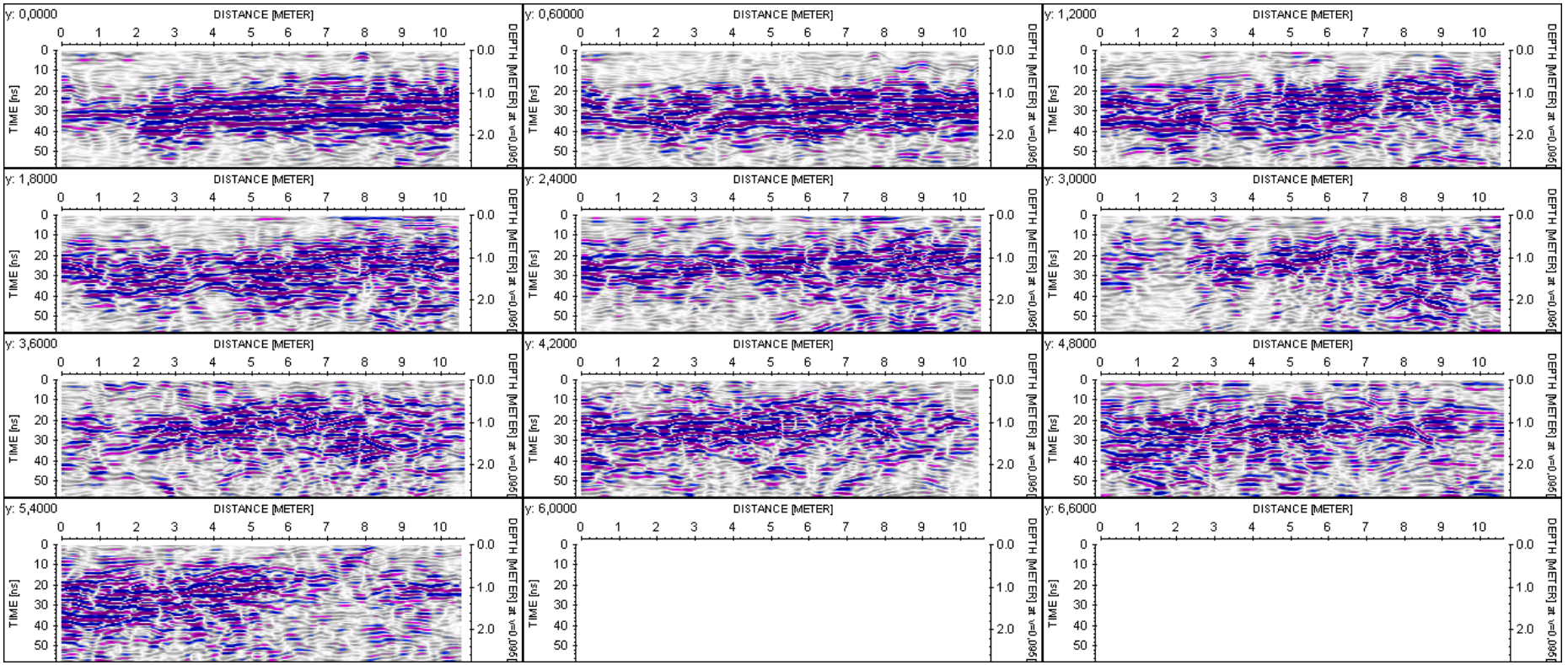

Figure C. 23: Y-cuts of block -6C, S-N direction using a 270 MHz antenna

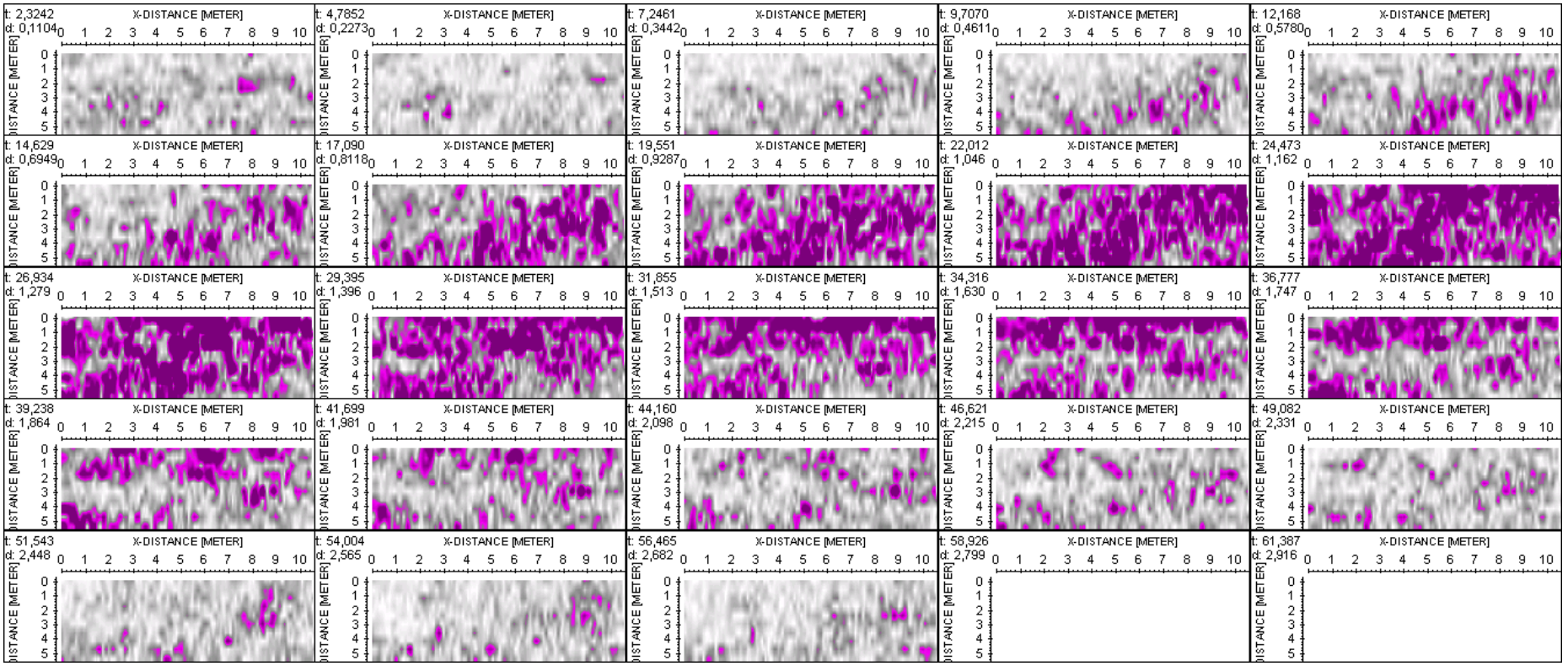

Figure C. 24: Time cuts of block -6C, S-N direction using a 270 MHz antenna

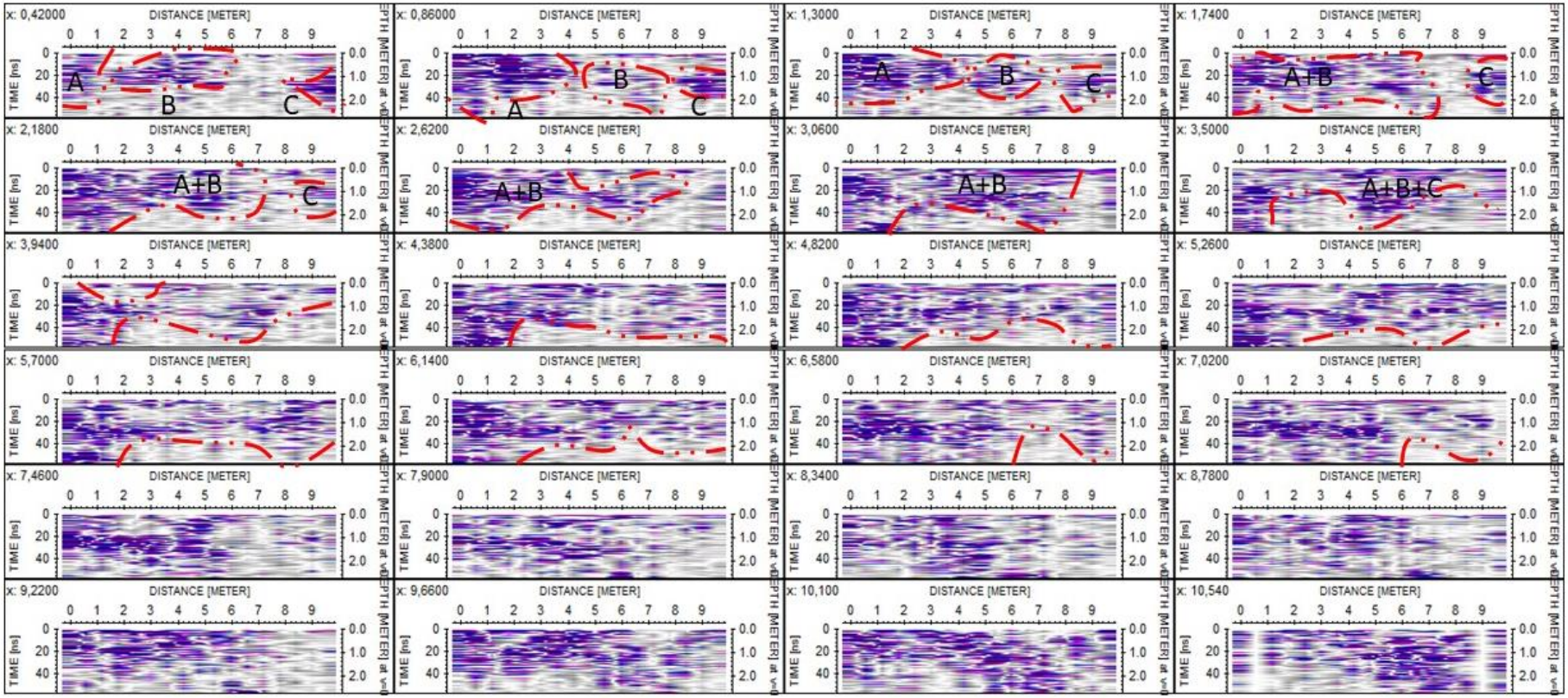

Figure C. 25: X-cuts of block -2A´, W-E direction using a 270 MHz antenna

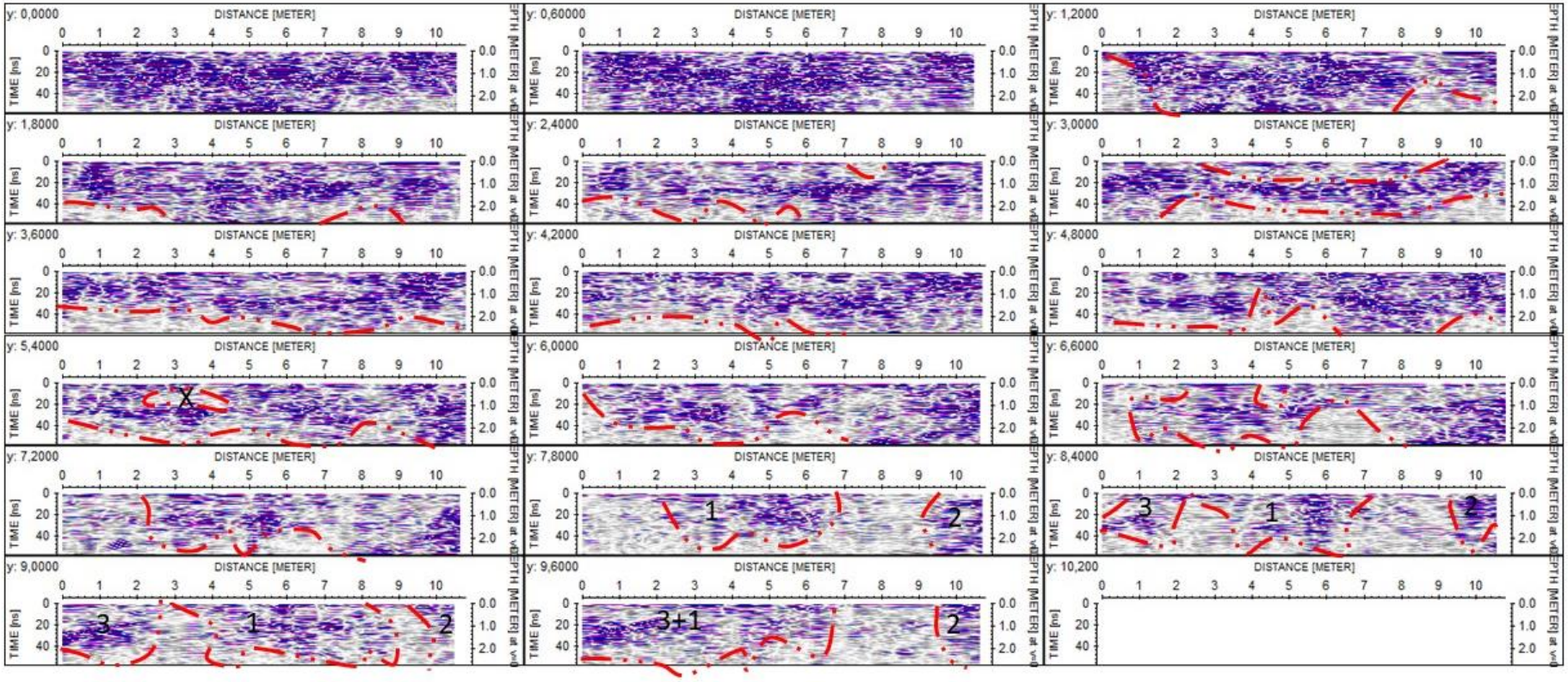

Figure C. 26: Y-cuts of block -2A´, W-E direction using a 270 MHz antenna

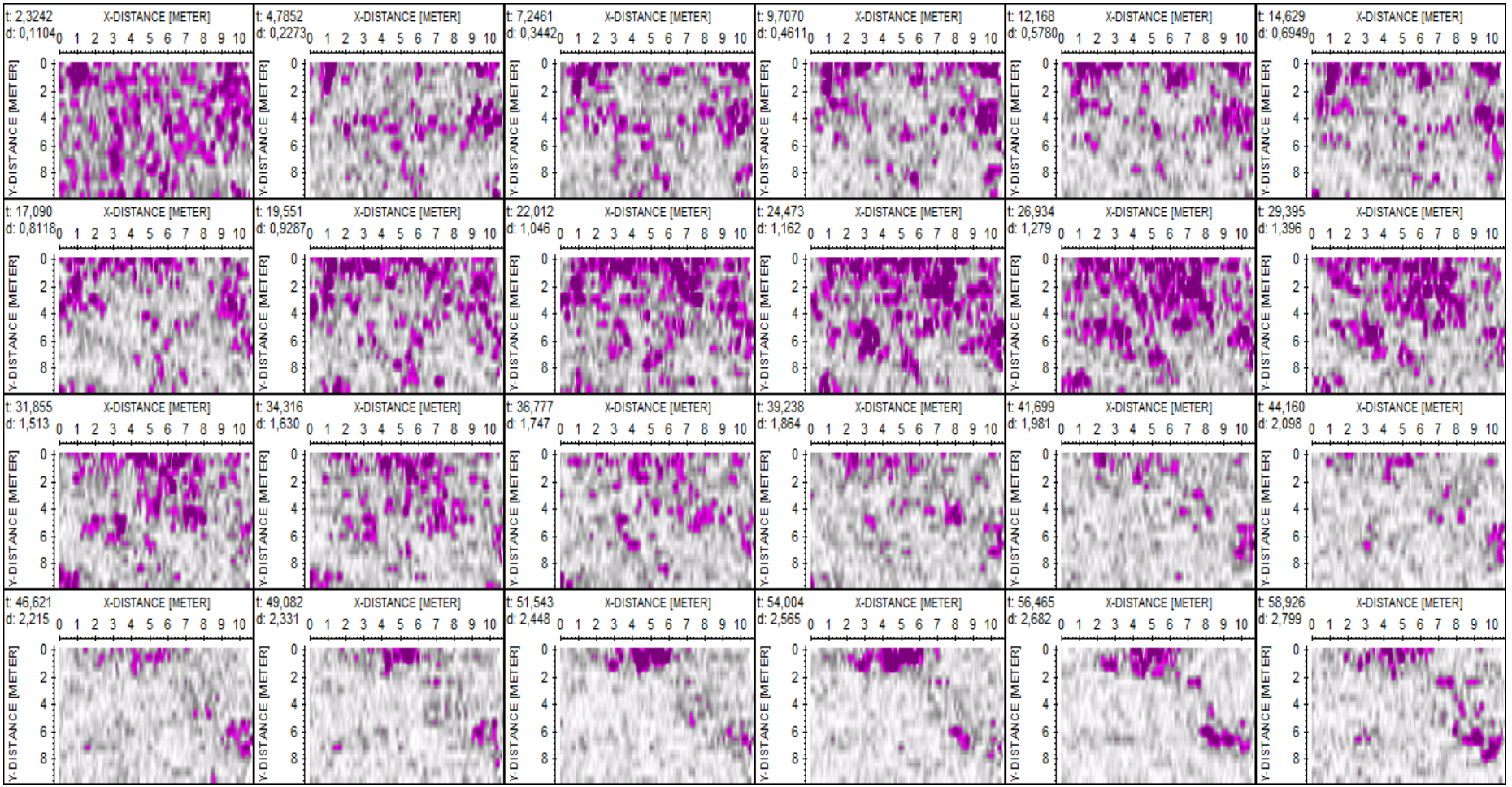

Figure C. 27: Time cuts of block -2A´, W-E direction using a 270 MHz antenna

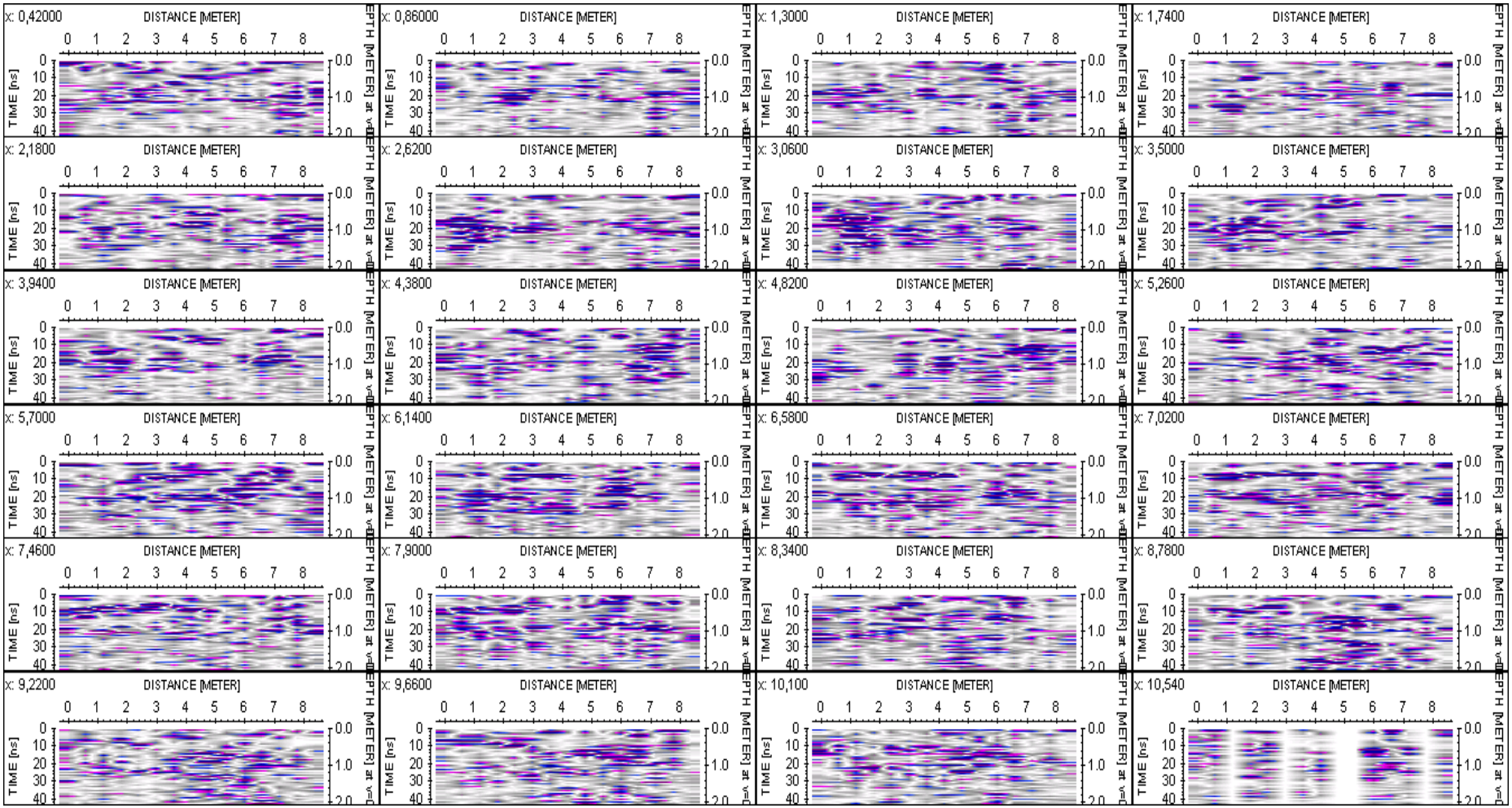

Figure C. 28: X-cuts of block -3A´, S-N direction using a 270 MHz antenna

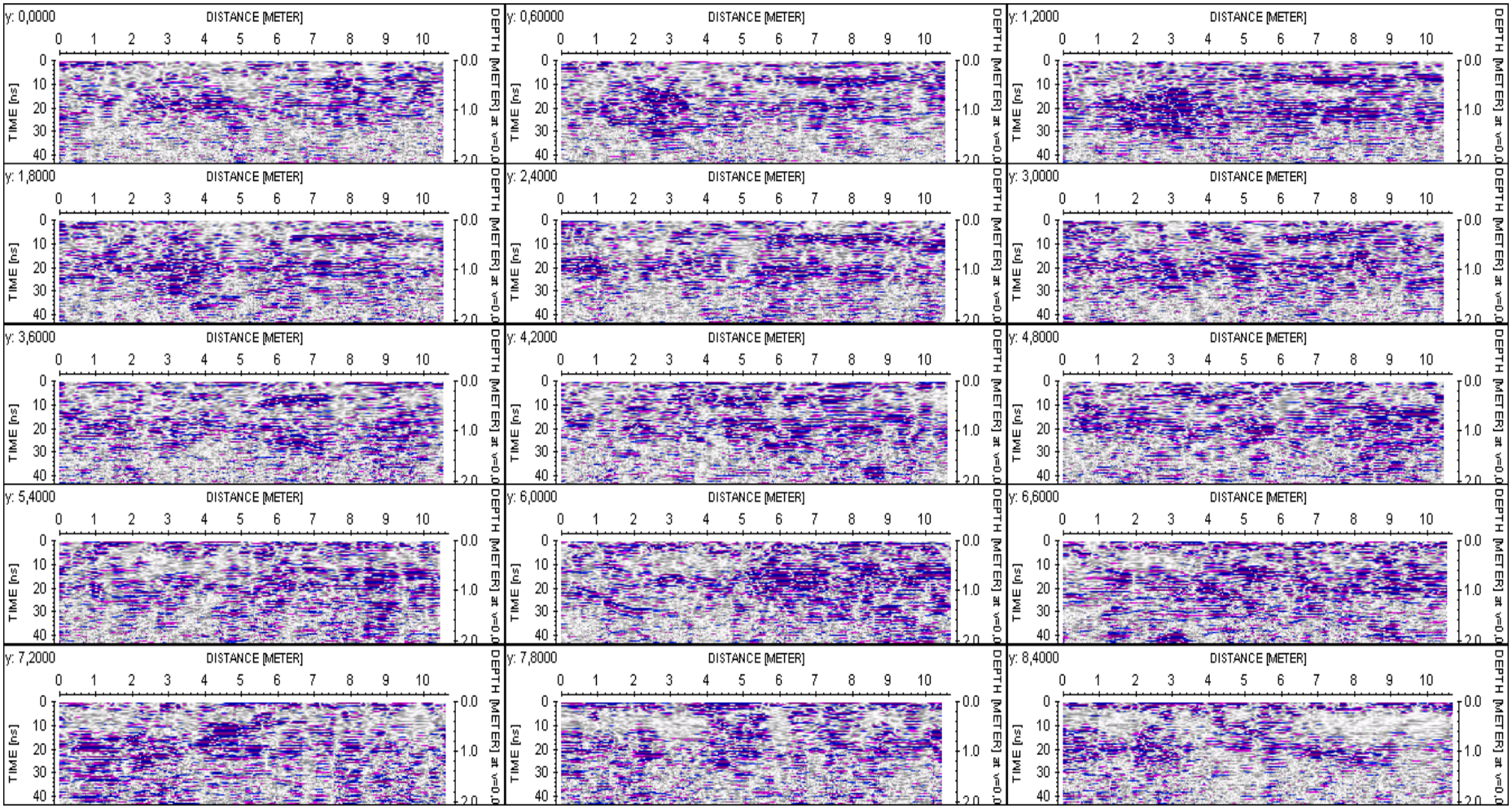

Figure C. 29: Y-cuts of block -3A´, S-N direction using a 270 MHz antenna

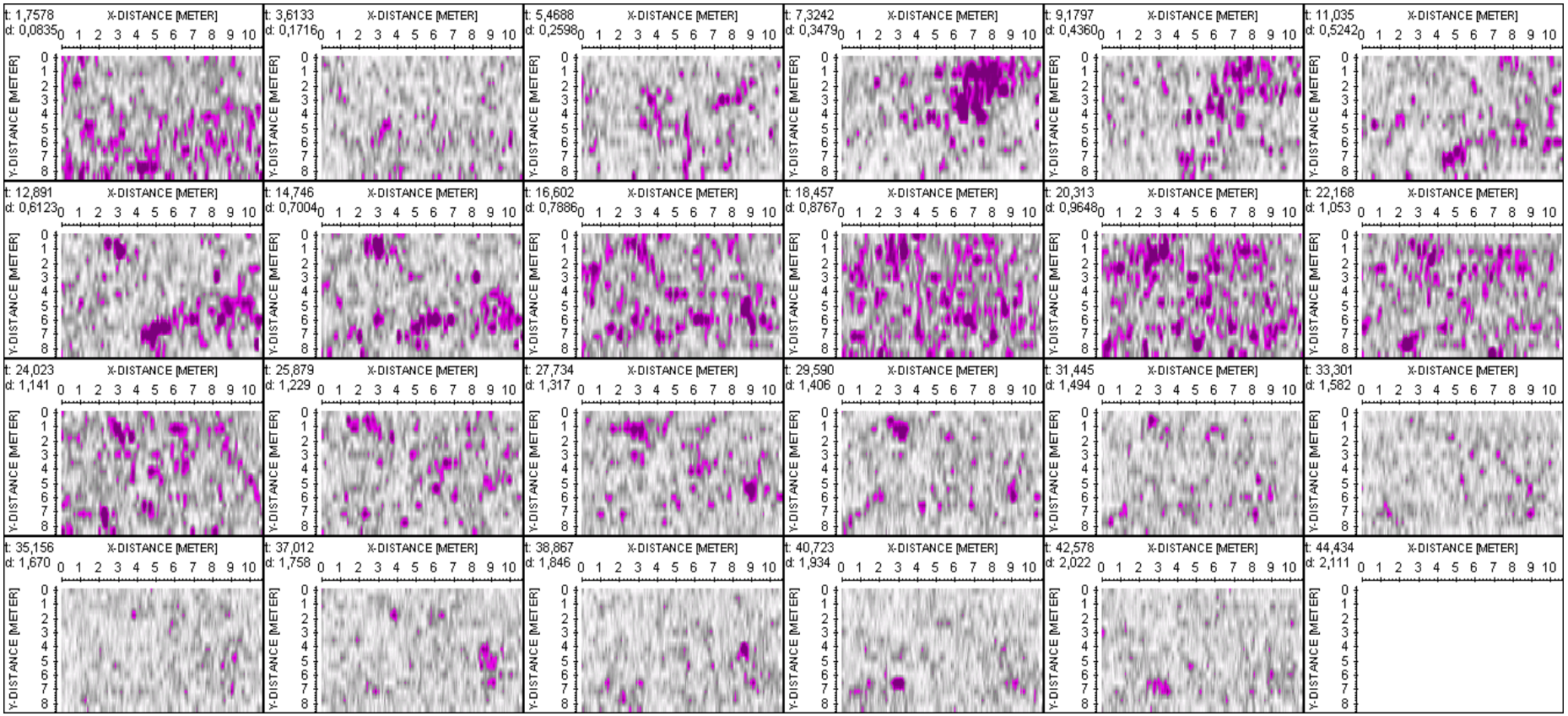

Figure C. 30: Time cuts of block -3A´, S-N direction using a 270 MHz antenna

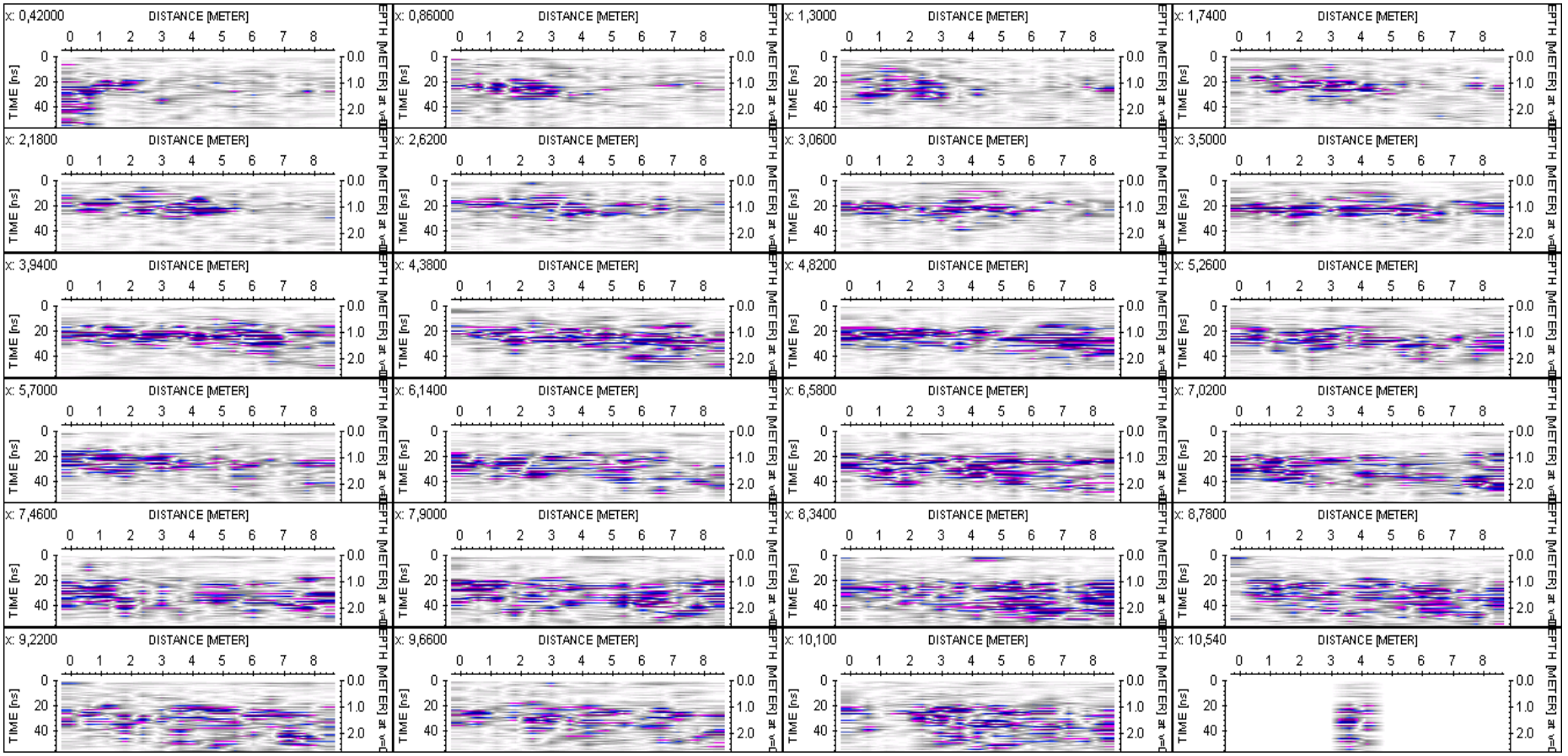

Figure C. 31: X-cuts of block +7D´, S-N direction using a 270 MHz antenna

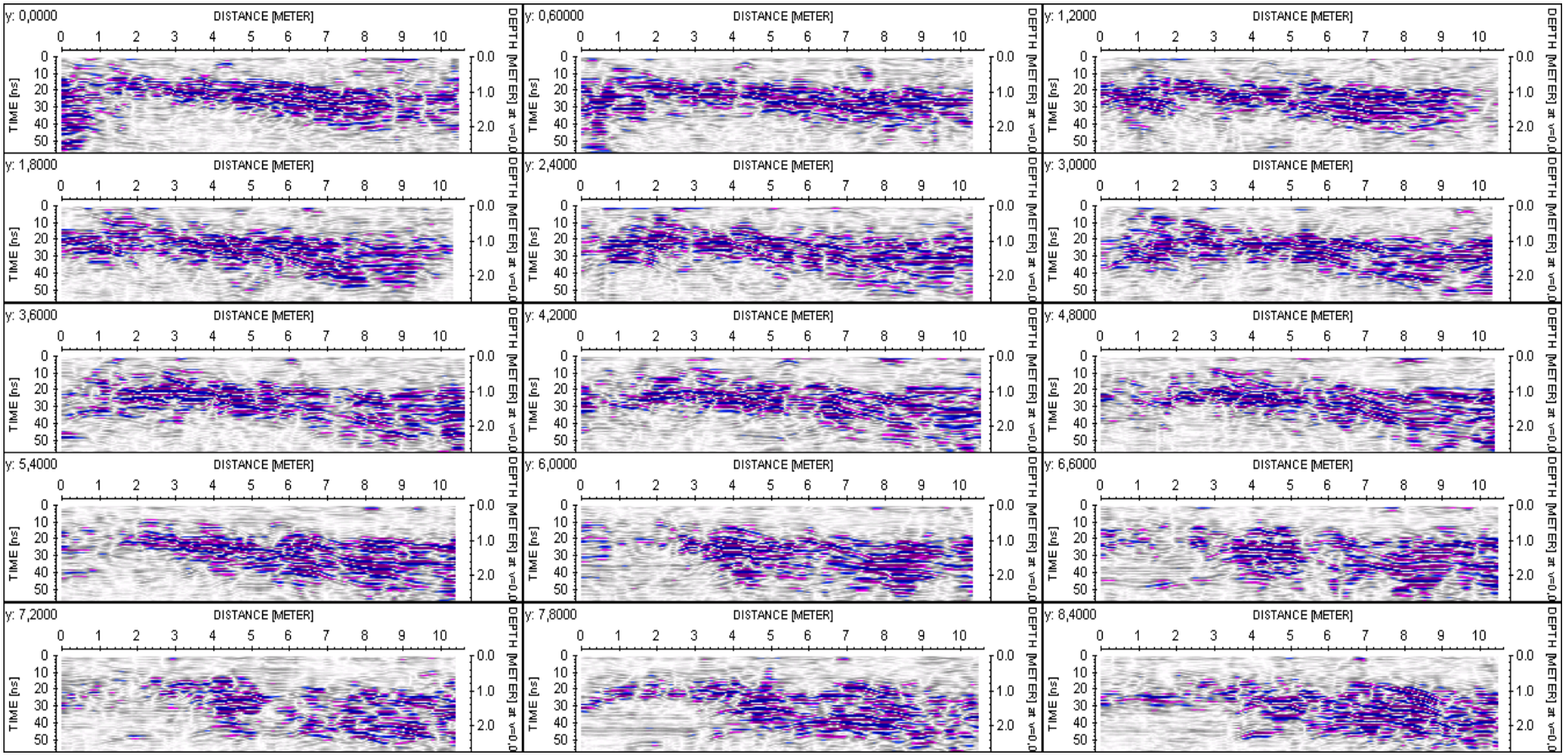

Figure C. 32: Y-cuts of block +7D´, S-N direction using a 270 MHz antenna

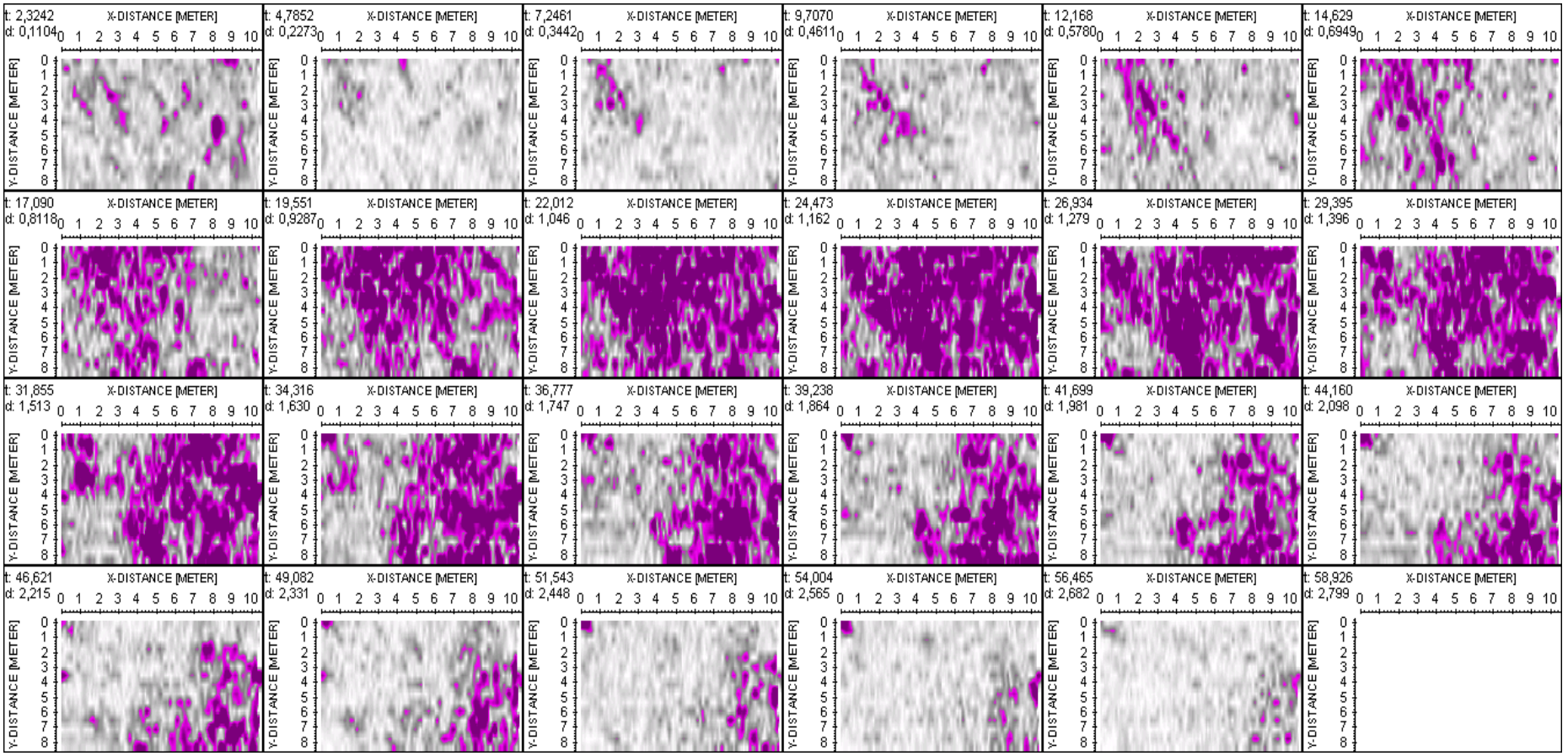

Figure C. 33: Time cuts of block +7D´, S-N direction using a 270 MHz antenna